Geology and petrology of the Catface porphyry Cu-Mo deposit, Vancouver Island, and linkages to the Paleogene Cascade Arc

by

Colin Michael Smith
B.Sc., University of British Columbia, 2007

A Thesis Submitted in Partial Fulfillment of the
Requirements for the Degree of

MASTER OF SCIENCE

in the School of Earth and Ocean Science

© Colin Michael Smith, 2012
University of Victoria

All rights reserved. This thesis may not be reproduced in whole or in part, by photocopy or other means, without permission of the author

Supervisory Committee

Geology and petrology of the Catface porphyry Cu-Mo deposit, Vancouver Island, and linkages to the Paleogene Cascade Arc

by

Colin Michael Smith
B.Sc., University of British Columbia, 2007

Supervisory Committee

Dr. Dante Canil (School of Earth and Ocean Sciences)
Co-Supervisor

Dr. Stephen Rowins (School of Earth and Ocean Sciences, British Columbia Geological Survey)
Co-Supervisor

Dr. Stephen Johnston (School of Earth and Ocean Sciences)
Departmental Member

Dr. Kathryn Gillis (School of Earth and Ocean Sciences)
Departmental Member

Abstract

Supervisory Committee

Dr. Dante Canil (School of Earth and Ocean Sciences)
Co-Supervisor

Dr. Stephen Rowins (School of Earth and Ocean Sciences, British Columbia Geological Survey)
Co-Supervisor

Dr. Stephen Johnston (School of Earth and Ocean Sciences)
Departmental Member

Dr. Kathryn Gillis (School of Earth and Ocean Sciences)
Departmental Member

The geology, petrology and geochemistry of Catface porphyry Cu (Mo-Au) deposit, located on the west coast of Vancouver Island are examined in detail. Detailed core logging and sampling was carried out to characterize the geometry and identity of different intrusive phases and alteration styles prevalent during the emplacement and formation of the deposit, as well as their geochemical affinity. Early- and late-stage potassic alteration is identified, as well as main-stage sodic-calcic and calcic-sodic alteration. Four distinct Paleogene intrusive phases vary from quartz diorite to granodiorite in composition. The rocks are broadly calc-alkaline, weakly peraluminous to moderately metaluminous, and have typical arc geochemical affinity.

The timing of emplacement and mineralization is constrained by U-Pb and Re-Os geochronology at 40.4-41.4 Ma and 40.9 ±0.2 Ma, respectively. All four Paleogene Catface intrusive phases were emplaced close in time with a direct temporal correlation to mineralization. The chalcopyrite- and pyrite-bearing miarolitic cavities in the Halo Porphyry intrusive, combined with U-Pb and Re-Os dates suggest this intrusive phase is the most likely source of mineralizing fluids. The intrusions were emplaced at depths of less four kilometers in the crust, as evidenced by the presence of miarolitic cavities and confirmed through amphibole-plagioclase thermobarometry, which record conditions of 615–700 °C and <200 MPa.

The lack of primary anhydrite and hematite, and the presence of pyrrhotite in the ore system indicate a reduced magmatic-hydrothermal event. The SO_3 contents in apatites are <450 ppm, indicative of a degassed and/or sulphate-free (reduced) magma. The assemblage K-feldspar-quartz-biotite-ilmenite yields oxygen fugacities (fO_2) which are 0.5 to 3.0 log units below the quartz-fayalite-magnetite (QFM) buffer at an assumed pressure of 300 MPa; orders of magnitude more reduced than typical porphyry deposits.

Parental magmas to the Catface deposit were either derived from intrinsically-reduced mantle, or more typical oxidized arc magma that was subsequently reduced during ascent and emplacement. Further isotopic work is required to determine which process contributed to the reduction of these magmas in an arc setting. Nevertheless, recognition of reduced porphyry-related magmatism on west-central Vancouver Island is of similar age to that of North Fork (~36.8-38.9 Ma) deposit in Washington suggesting a consanguinity of reduced magmatism with the Paleogene Cascade arc.

Table of Contents

Supervisory Committee ii

Abstract iii

Table of Contents iv

List of Tables vii

List of Figures viii

Acknowledgments xii

Dedication xiii

CHAPTER 1 - Introduction

1.1 Introduction 1

1.2 Thesis Objectives 5

1.3 Methods and Approach 5

CHAPTER 2 - Geology

2.1 Introduction 8

2.2 Regional Geology 8

2.3 Catface Deposit Geology 10

2.3.1 Karmutsen Basalt 14

2.3.2 Westcoast Complex Diorite 17

2.3.3 Island Plutonic Suite 22

2.3.4 Cliff and Halo Porphyry 22

2.3.5 Catface Intrusion 28

2.3.6 ADP Dykes 28

2.3.7 Hecate Bay Quartz Diorite....33

2.4 Mineralization....33

2.4.1 Vein and Alteration Paragenesis....38

2.4.2 Assay Data Compilation....44

2.5 Conclusions....44

CHAPTER 3 - Geochronology

3.1 Introduction....53

3.2 U-Pb Geochronology....53

3.3 Re-Os Geochronology....56

3.4 Conclusions....60

CHAPTER 4 - Geochemistry and Mineral Chemistry

4.1 Introduction....61

4.2 Geochemistry....62

4.2.1 Major Elements....62

4.2.2 Trace Elements....66

4.3 Mineral Chemistry....66

4.3.1 Amphibole....66

4.3.2 Plagioclase....70

4.3.3 K-Feldspar....70

4.3.4 Biotite....70

4.3.5 Fe-Ti Oxide....72

4.3.6 Apatite....72

4.4 Thermobarometry....72

4.4.1 Al-in-Hornblende Barometry.....75

4.4.2 Amphibole-Plagioclase Thermometry.....76

4.4.3 Results.....76

4.5 Oxybarometry.....79

4.5.1 Results.....80

4.6 Conclusions.....80

CHAPTER 5 - Discussion

5.1 Geology and Emplacement of the Catface Deposit.....84

5.1.1 Alteration.....86

5.2 Evidence for Reduced Magmas Forming the Catface Deposit.....88

5.3 Generation of Reduced Porphyry Copper Deposit Magma in an Arc Setting.....90

CHAPTER 6 - Summary

6.1 Conclusions.....95

6.2 Future Work.....95

Bibliography.....97

Appendix.....see attached file (Smith_Colin_MSc_Appendix)

List of Tables

Table 1. Summary of Geochronological Results from the Catface Porphyry Deposit.....58

Table 2. Estimated Pressures and Temperatures for Catface Porphyry Deposit Samples from Al-in-Hornblende and Amphibole-Plagioclase Thermobarometry.....78

Table 3. Calculated fO_2's at 300 MPa from Biotite-Ilmenite Assemblages at the Catface Porphyry Deposit.....82

Table A1. Digitized Core Logs for Drill Holes from the Cliff Zone of the Catface Porphyry Deposit.....Appendix (see attached file: Smith_Colin_MSc_Appendix)

Table A2. Petrographic Summary of Rocks the Cliff Zone of the Catface Porphyry Deposit .....Appendix (see attached file: Smith_Colin_MSc_Appendix)

Table A3. Petrographic Summary of Veins Styles and Alteration from the Catface Porphyry Deposit.....Appendix (see attached file: Smith_Colin_MSc_Appendix)

Table A4. U-Pb Geochronological Data for Drill Core and Outcrop Samples from the Catface Porphyry Deposit.....Appendix (see attached file: Smith_Colin_MSc_Appendix)

Table A5. Re-Os Geochronological Data for Drill Core Samples from the Catface Porphyry Deposit.....Appendix (see attached file: Smith_Colin_MSc_Appendix)

Table A6. Major and Trace Element Geochemical Data for Samples from the Catface Porphyry Deposit.....Appendix (see attached file: Smith_Colin_MSc_Appendix)

Table A7. Mineral Chemical Data from Electron Microprobe Analyses for Catface Porphyry Deposit Rocks….....Appendix (see attached file: Smith_Colin_MSc_Appendix)

Table A8. Thermobarometric Data and Calculations for the Catface Deposit and the Echo Lake Intrusion.....Appendix (see attached file: Smith_Colin_MSc_Appendix)

Table A9. Analytical Data and Calculations for Biotite-Ilmenite Oxybarometry for Samples form the Catface Porphyry Deposit…….Appendix (see attached file: Smith_Colin_MSc_Appendix)

List of Figures

Figure 1. Locations and ages of Paleogene magmatism and volcanism of the Pacific Northwest, and positions of significant magmatic arcs.....2

Figure 2. Location map of the Catface and North Fork Porphyry Deposits, Echo Lake intrusion and positions of significant magmatic arcs.....3

Figure 3. Simplified regional geology of southern Vancouver Island showing the locations of Paleogene intrusions.....6

Figure 4. Simplified stratigraphic section of southern Vancouver Island.....9

Figure 5. Geology map of the Catface Porphyry Deposit showing locations of drill holes assessed in this study, cross section line A-A', ore zones, structural data, and outcrop U-Pb geochronology samples.....12

Figure 6. Cross section of Catface Porphyry Deposit Cliff Zone showing locations and types of samples collected from drill core.....13

Figure 7. Hand sample of porphyritic Karmutsen basalt with phenocrysts of plagioclase feldspar.....15

Figure 8. Thin section photographs of Karmutsen basalt.....16

Figure 9. Hand sample of Karmutsen basalt displaying biotite-rich hornfels.....18

Figure 10. Hand sample of pyrrhotite grains in Karmutsen basalt.....19

Figure 11. Hand sample of Westcoast Complex diorite sampled from outcrop at the Catface porphyry deposit.....20

Figure 12. Thin section photographs of Westcoast Complex diorite.....21

Figure 13. Hand sample from drill core with basaltic and dioritic xenoliths in Island Plutonic Suite.....23

Figure 14. Hand sample of granodiorite from the Island Plutonic Suite.....24

Figure 15. Thin section photographs of Island Plutonic Suite granodiorite.....25

Figure 16. Hand samples of Cliff and Halo porphyry quartz diorites.....26

Figure 17. Microphotographs of chalcopyrite- and pyrite-bearing miarolitic cavities in Halo Porphyry.....27

Figure 18. Thin section photographs of Cliff Porphyry quartz diorite.....29

Figure 19. Hand sample of Catface Intrusion quartz diorite.....30

Figure 20. Thin section photographs of Catface Intrusion quartz diorite.....31

Figure 21. Hand sample of ADP granodiorite.....32

Figure 22. Thin section photographs of ADP granodiorite.....34

Figure 23. Hand sample of Hecate Bay quartz diorite sampled from outcrop.....35

Figure 24. Thin section photographs of Hecate Bay quartz diorite.....36

Figure 25. Hand sample of Catface Intrusion quartz diorite illustrating disseminated and vein-hosted Cu mineralization.....37

Figure 26. Summary of paragenetic sequence of alteration and mineralization at the Catface porphyry deposit.....39

Figure 27. Hand sample examples of Stage 1 mineralization and alteration showing Cu and Mo mineralization in quartz stockwork associated with albite-actinolite alteration.....40

Figure 28. Thin section photographs of Stage 1 mineralization and alteration showing Cu and Mo mineralization and presence of secondary albite-actinolite.....41

Figure 29. Hand sample examples of Stage 2 mineralization and alteration showing Cu and Mo mineralization in quartz stockwork with actinolite-albite alteration.....42

Figure 30. Thin section photographs of Stage 2 mineralization and alteration showing Cu mineralization in a quartz vein associated with secondary actinolite.....43

Figure 31. Hand sample examples of Stage 3 mineralization and alteration showing quartz-chalcopyrite-pyrite veins associated with selvages of secondary biotite.....45

Figure 32. Thin section photographs of Stage 3 mineralization and alteration showing Cu mineralization associated with secondary biotite.....46

Figure 33. Hand sample examples of Stage 4 mineralization showing crosscutting relationship to earlier Stage 3 veins.....47

Figure 34. Thin section photographs of Stage 4 mineralization showing sulphide stringer veins.....48

Figure 35. Representative scale for relative fracture intensity based on number of fractures per unit length of drill core.....49

Figure 36. Cross-section of Catface porphyry deposit Cliff Zone showing association of Cu and Mo grades with relative fracture intensity.....50

Figure 37. Average Cu and Mo grades versus relative fracture intensity for selected drill holes in the Catface porphyry deposit Cliff Zone.....51

Figure 38. Hand samples submitted for Re-Os in molybdenite geochronology from the Catface porphyry deposit.....54

Figure 39. Concordia diagrams for U-Pb in zircon geochronology.....55

Figure 40. Summary of U-Pb and Re-Os ages for samples from the Catface porphyry deposit with error bars representing analysis uncertainties.....57

Figure 41. Comparison of ages for intrusive phases at the Catface porphyry deposit with the Mt. Washington and Clayoquot-Flores Island Suites and North Fork porphyry deposit.....59

Figure 42. Total alkalis versus silica (TAS) plot for Paleogene Catface deposit rocks compared with samples from North Fork, Echo Lake and other Vancouver Island magmatic suites.....63

Figure 43. K_2O versus SiO_2 diagram showing Paleogene Catface deposit rocks compared with North Fork and Echo Lake samples, and other Paleogene igneous rocks from Vancouver Island.....64

Figure 44. SiO_2 versus ASI (Aluminum Saturation Index) diagram for Paleogene Catface deposit rocks compared with North Fork and Echo Lake samples, and other Paleogene igneous rocks from Vancouver Island.....65

Figure 45. Chondrite-normalized spidergram plot for Paleogene Catface deposit rocks compared with igneous rocks from North Fork and other Paleogene igneous rocks from Vancouver Island.....67

Figure 46. Sr/Y versus Y (ppm) diagram for Paleogene Catface deposit rocks compared with North Fork and Echo Lake samples, and other Paleogene igneous rocks from Vancouver Island.....68

Figure 47. Amphibole classification diagram for samples from the Catface porphyry deposit and Echo Lake intrusion.....69

Figure 48. Comparison of core and rim compositions in plagioclase feldspars from Paleogene Catface deposit rocks.....71

Figure 49. Sulphur (SO_3) concentrations in apatites of Catface porphyry deposit compared with those at Echo Lake and those associated with strongly oxidized porphyry copper deposits.....73

Figure 50. Sulphur (SO_3) versus Cl in weight percent for apatites from Paleogene Catface rocks, plotted against data from Echo Lake and oxidized porphyry deposit apatites, with the approximate position of the Nickel-Nickel-Oxide (NNO) oxygen buffer.....74

Figure 51. Pressures and temperatures estimated from Al-in-hornblende barometry and amphibole-plagioclase thermometry for samples from Catface and Echo Lake with uncertainties to 1 standard deviation.....77

Figure 52. Temperature-fO_2 estimates at 300 MPa from biotite-ilmenite oxybarometry for samples from three intrusive phases of the Catface deposit. Also shown is the temperature range estimated from Catface amphibole-plagioclase thermometry, and fO_2 estimates for North Fork rocks and typical magnetite-series granites.....81

Figure A1. Precision of geochemical analyses based on %difference of sample CS10-18 and CS10-18(duplicate).....Appendix

Figure A2. Accuracy of geochemical analyses based on %difference of analysis to STD SO-18 and STD Oreas45Ca.....Appendix

Acknowledgments

I would like to send my sincere gratitude to Dante for his unwavering support throughout my time in Victoria. Dante's technical expertise is exceptional and his down-to-earth character enabled me to never lose sight of the bigger picture. I am very fortunate to have had Dante as a supervisor, mentor and friend. I would like to equally thank Steve Rowins, whom I've known since undergraduate studies as UBC. His passion and excitement for mineral deposits is unparalleled, and Steve's breadth of experience in the exploration industry, public sector and academia has been invaluable to my academic pursuits. I would also like to thank Imperial Metals Corp. and Jim Miller-Tait for the dedicated financial, logistical, and technical support throughout this project. Funding provided by the Ministry of Energy and Mines and University of Victoria was an essential foundation supporting the analytical and field work components of this thesis, and a student grant provided by Geoscience BC was of great importance to supplement living costs. I would like to also thank Julianne Madsen for sharing her geochemical data, as well as Mati Raudsepp and Edith Czech for their assistance with the electron microprobe at UBC. It is my pleasure to also recognize the many people behind the scenes whose efforts truly made this a world-class experience: Allison Rose, Kimberly Smith-Jones, Terry Russell, Kathleen Chrétien, David Nelles, Duncan Johannessen, Jody Spence, Steve Fellows, and many more. Lastly, none of this would have been possible without the love and support of my family and friends.

Dedication

To my amazing family:

Dad, your spirit shines in every moment of my life, and always will. Mom, your courage, wisdom and passion inspires me to be a better person every day. Meghan, the purity of your soul and the magic in your spirit is supernatural.

I am truly blessed to share life with all of you.

Chapter 1
INTRODUCTION

1.1 Introduction

Porphyry Cu (Mo-Au) deposits are the most globally significant source of copper, accounting for 50-60% of world production and 40% of Canadian production (Sinclair, 2007). These deposits also account for nearly all global Mo production, and represent significant sources of Au, Ag and Sn. Porphyry Cu (Mo-Au) deposits are high-tonnage, low-grade (0.2 to >1% Cu) ore systems containing from tens of millions to billions of tonnes of ore. Globally, these deposits are concentrated in discrete, linear, metallogenic provinces associated with arcs. Most porphyry deposits throughout Canada and the world are associated with Mesozoic and Cenozoic orogenic belts, although major deposits are also found in Paleozoic and Precambrian terranes (Sinclair, 2007). Within these metallogenic provinces, porphyry copper deposits develop in close proximity to epizonal intrusions, which are the source of fluids, metals, and heat required to drive ore-forming hydrothermal circulation and mineralization.

The eastern margin of the Pacific Basin experienced extensive arc-related magmatism and associated porphyry-style mineralization during the Paleogene (Madsen, 2004; Madsen et al., 2006), and it has long been suspected that a genetic link exists between Paleogene porphyry deposits in the Central Cascades of Washington and those in southwestern British Columbia and Vancouver Island (McDougall, 1976; Hollister, 1978) (Figure 1). To test this consanguinity, the Catface porphyry Cu (Mo-Au) deposit ("Catface") on west-central Vancouver Island is studied in detail and compared with the North Fork porphyry Cu-Au deposit in the Cascades of Washington (Figure 2). North Fork is part of a suite of porphyry

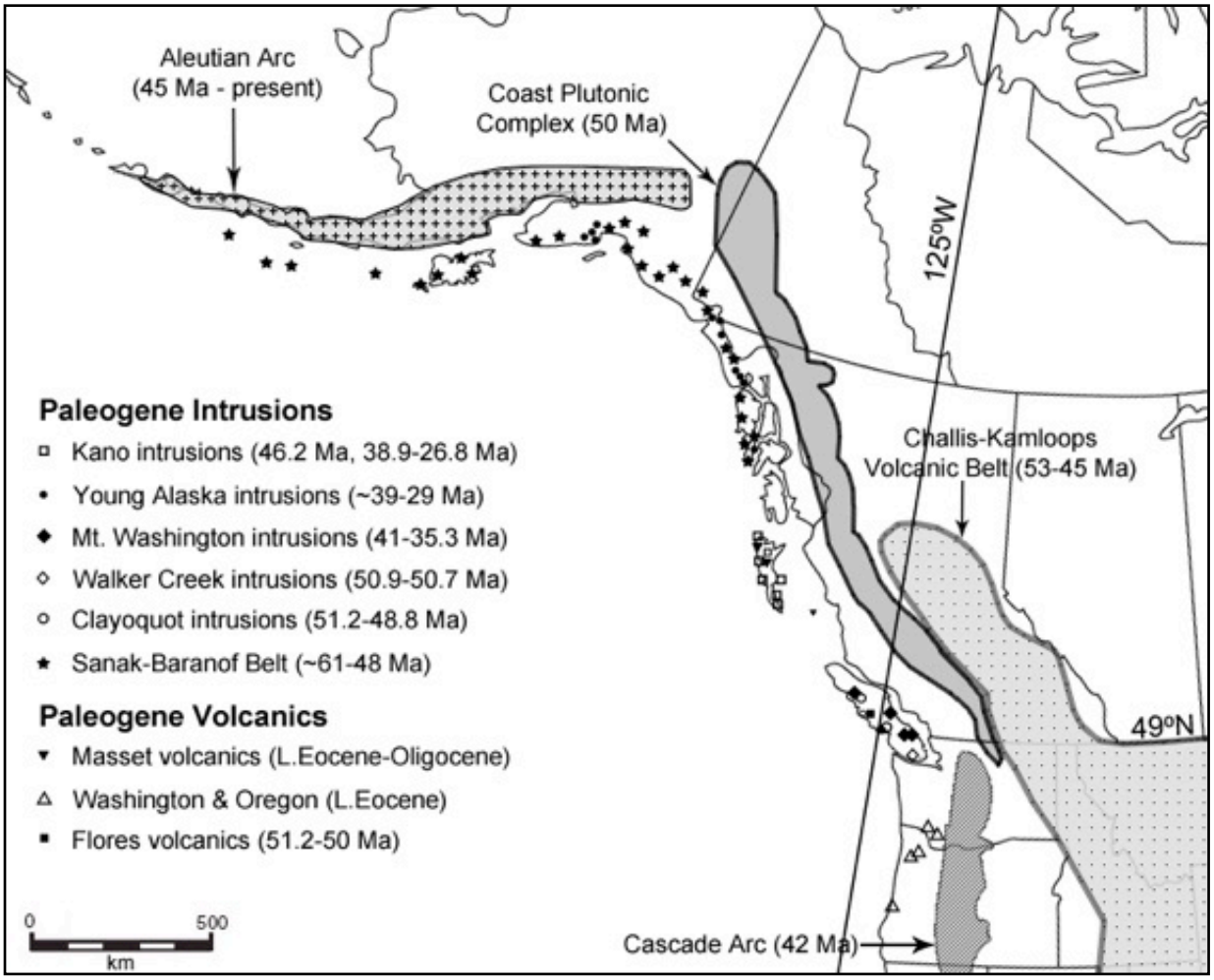

Figure 1: Map of Pacific Northwest showing locations of Paleogene magmatism of the Pacific Northwest and positions of significant magmatic arcs (after Madsen, 2004).

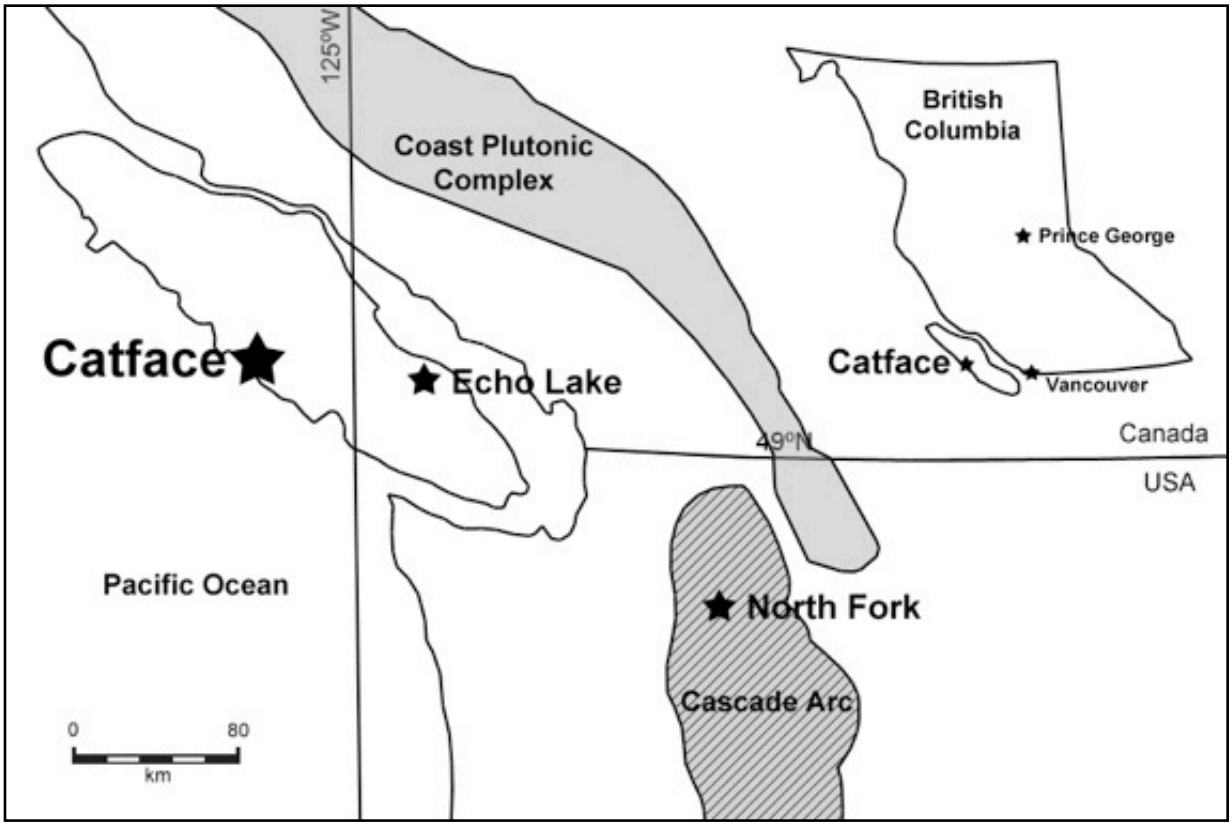

Figure 2: Location of Catface and North Fork porphyry deposits, the barren Paleogene Echo Lake pluton, and position of significant Paleogene arcs.

copper deposits that are Late Eocene (38.9-36.8 Ma) in age (Smithson, 2004). Muller and Carson (1969) report a K-Ar in biotite age for Catface deposit rocks of 48 ±12 Ma. More modern geochronology applied to the Catface deposit could assess its relationship to other Paleogene magmatic suites on Vancouver Island and in the Cascades.

Porphyry deposits are defined as either classically oxidized porphyry copper deposits or reduced porphyry copper deposits on the basis of pluton mineralogy and the mineralogical features of the ores and associated alteration assemblages. The classic oxidized porphyry copper deposit model involves ore fluids that are relatively oxidized, with oxygen fugacities (fO_2) ranging between the hematite-magnetite (HM) and nickel-nickel oxide (NNO) oxygen buffers at the temperatures associated with mineralization (Burnham and Ohmoto, 1980; Rowins, 2000a, 2000b). Oxidized porphyries host significant amounts of primary magnetite, hematite, and sulphate minerals (i.e. anhydrite), and there is a strong association of porphyry deposits with oxidized I-type granitoids (Burnham and Ohmoto, 1980). In contrast, numerous porphyry Cu (Mo-Au) systems show evidence of having formed from relatively reduced ore fluids with fO_2's less than or equal to the quartz-fayalite-magnetite (QFM) oxygen buffer. These reduced porphyry copper deposit systems lack primary hematite and sulphate minerals, typically host abundant hypogene pyrrhotite, and show an association with reduced I-type, ilmenite-bearing granitoids (Rowins, 2000a, 2000b; Smithson, 2004; Smithson and Rowins, 2004). The North Fork Cu-Au deposit exemplifies a reduced porphyry copper deposit with magma fO_2's ranging from one log unit above to one log unit below the quartz-fayalite-magnetite oxygen buffer (QFM ±1) (Smithson, 2004). These redox conditions explain the presence of primary pyrrhotite and the absence of hypogene sulphate and primary hematite at the deposit.

1.2 Thesis Objectives

The similar timing of magmatism between North Fork and the Mt. Washington suite intrusions on Vancouver Island provides support to the proposal that the "reduced" Cascade porphyry Cu-Au belt extends to the northwest from Washington into southwestern British Columbia and Vancouver Island. The objective of this thesis is to investigate whether magmatism and associated porphyry-style mineralization in Paleogene rocks on Vancouver Island is the northern extension of the Cascade magmatic arc in Washington. This potential genetic linkage is investigated in a geological, geochronological, geochemical and petrological investigation of the Catface deposit, located 12 km NNW of Tofino, on the west coast of Vancouver Island (Figure 2 and Figure 3). These new data are combined with ancillary data from mineral exploration on the Catface deposit to determine: (1) the age of intrusions and mineralization, (2) the style of mineralization, (3) the redox state (oxidized vs. reduced) and depth of emplacement of the magmas and hydrothermal system, and (4) the geochemical or age relationships to other Paleogene magmatism in the Pacific Northwest.

1.3 Methods and Approach

The fieldwork was conducted over six weeks in the summer of 2010, and one week in the summer of 2011. Most of the field work was focused on the Catface deposit. The field area is an active exploration site, owned and operated by Catface Copper Mining Ltd., a subsidiary of Imperial Metals Corp. Access to the site was achieved via water taxi from a camp near the Ahousaht First Nations Reserve on Flores Island. Movement about the exploration site was facilitated by active and reactivated logging roads.

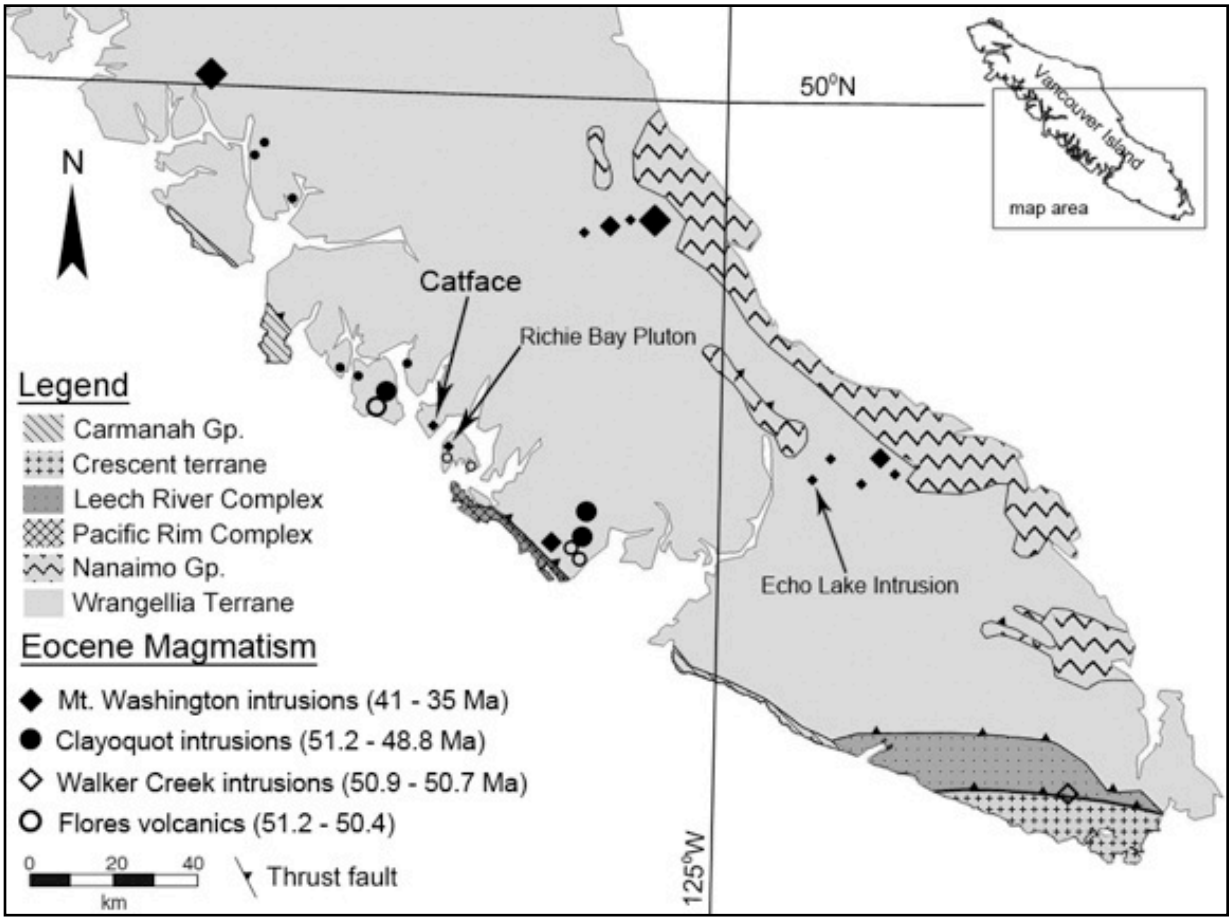

Figure 3: Simplified regional geology of southern Vancouver Island showing locations of Paleogene intrusions (rendered from Madsen, 2004).

At Catface, a total of 1633 meters of core was logged and sampled in detail from four holes drilled in 2008. The cores were logged meter-by-meter, characterizing lithology, alteration, structure, mineralization, fracture intensity, and percentage quartz veins (or "stockwork"). Over 160 core samples were collected. Of the 160 samples, 14 were selected for whole rock and trace element analysis, 20 were selected for petrographic work, and nine were selected for geochronology. Of the 20 samples selected for petrographic work, seven were chosen for electron microprobe (EMP) analysis for mineral chemistry. The Echo Lake intrusion, with an age of 38 Ma (Madsen, 2004; Madsen et al., 2006), located 30 km east of Catface was also sampled in outcrop for comparisons to Catface and North Fork (Figure 2 and Figure 3).

Chapter 2
GEOLOGY

2.1 Introduction

In this chapter, the regional geology of Vancouver Island is reviewed, as a background for the details of the Catface deposit geology based on drill core descriptions. The drill core was examined in detail for the characterization of rock types, intrusive contacts, mineralization styles, and alteration assemblages. Assay data for Cu and Mo in each drill hole compiled by Imperial Metals (1057 samples) were incorporated to examine any trends in with the detailed geology. Hydrothermal alteration at Catface is interpreted predominately on a qualitative basis, using mineral assemblages, as geochemical analyses (described in Chapter 2.4 and 2.4.1) were focused on characterizing representative, unaltered examples of each rock type.

2.2 Regional Geology

Rocks of Vancouver Island are a part of the Insular belt of the Canadian Cordillera (Monger, 1997). Most of Vancouver Island is underlain by the Wrangellia Terrane, extending from south-central Alaska, through southwestern Yukon, Haida Gwai, and to southern Vancouver Island (Jones et al., 1977). On Vancouver Island, Devonian island arc volcanic and plutonic rocks of the Sicker Group are the basement of Wrangellia (Figure 3 and Figure 4). Overlying the Sicker Group are Permian carbonates and epiclastic rocks of the Buttle Lake Formation, followed by the Triassic Vancouver Group, comprised of a thick (6km) section of subaqueous and subaerial basaltic volcanics known as the Karmutsen Formation (Nixon et al., 1993). Conformably overlying the Karmutsen is a thin (30-300m) succession of limestone referred to as the Quatsino Formation. The uppermost sequence of the Vancouver Group is

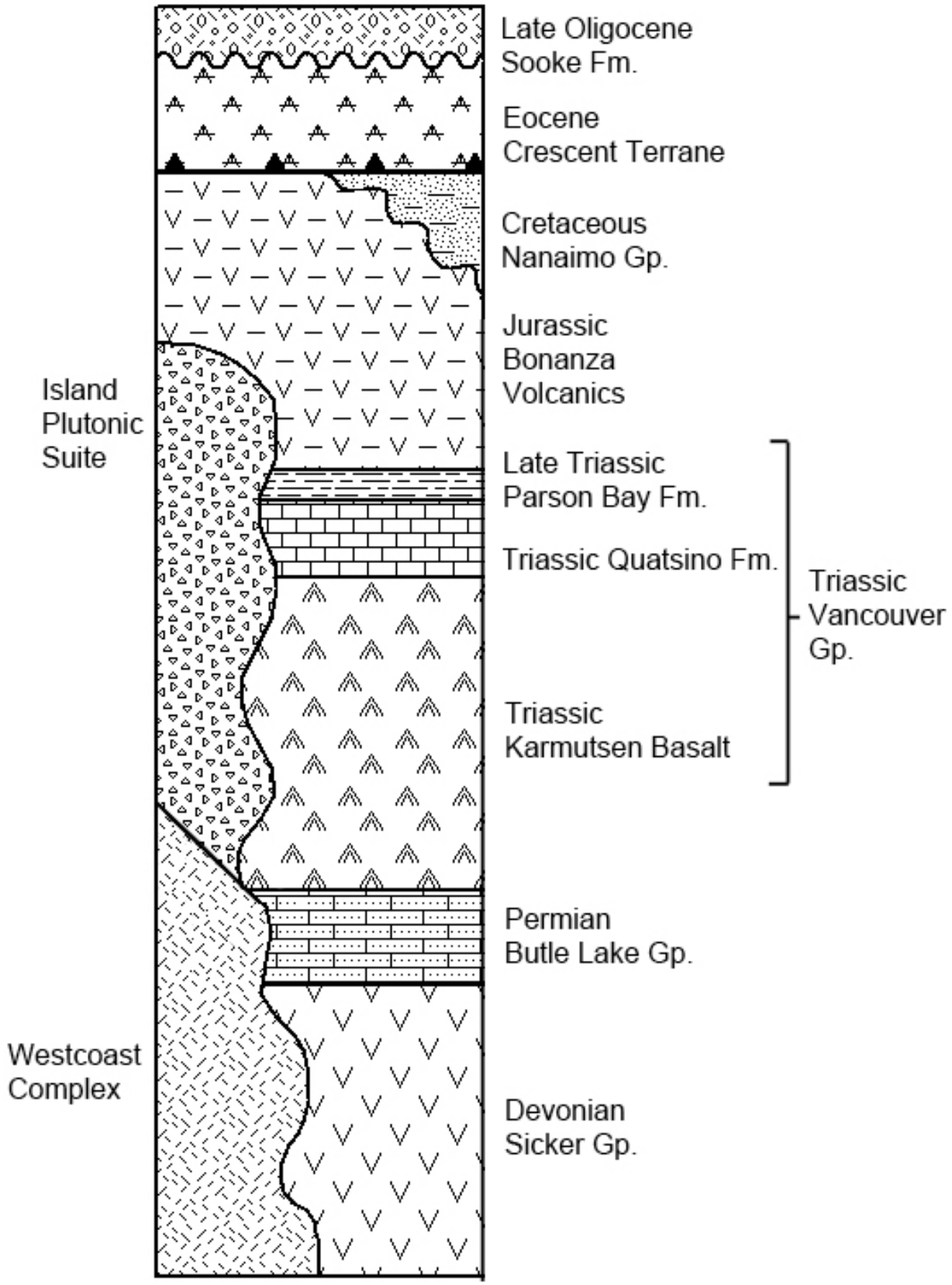

Figure 4: Simplified stratigraphic section of southern Vancouver Island (after Larocque, 2008).

represented by the Parson Bay Formation, a thinly-bedded section of clastic sediments that conformably overlies the Quatsino Formation (Nixon et al., 1995).

The uppermost Vancouver Group (i.e. Parson Bay Formation) is intruded and overlain by island arc igneous rocks of the Jurassic Bonanza Group. This group is divided into three units: the Westcoast Complex, Island Plutonic Suite, and Bonanza Volcanics. The Westcoast Complex represents the deepest unit in the Bonanza Group. The Island Plutonic Suite is a shallower lever plutonic suite (less than 10 km depth), with intrusions ranging in composition from granite to diorite (Nixon and Orr, 2007; Canil and Larocque, 2010). These plutons intrude the Vancouver Group and the Bonanza volcanic package, which is interpreted as the extrusive equivalents of the Westcoast Complex and Island Plutonic Suite (Nixon and Orr, 2007).

On the eastern portion of Vancouver Island, Wrangellia is unconformably overlain by Late Cretaceous sedimentary rocks of the Nanaimo Group (Massey and Friday, 1987). In the Eocene the outboard Crescent terrane was thrust beneath the Pacific Rim and overlying Wrangellia terranes, leading to the formation of the Cowichan Fold and Thrust Belt, which involved the Nanaimo Group and its basement rocks (England and Calon, 1991; Johnston and Acton, 2003). Two distinct pulses of Paleogene magmatism on Vancouver Island are identified by Madsen et al (2006) as the earlier Clayoquot suite (51.2–48.8 Ma) and the later Mt. Washington suite (41.0–35.3 Ma). Clastic sedimentary rocks of the Oligocene Carmanah Group unconformably overlie portions of western and southern Vancouver Island.

2.3 Catface Deposit Geology

The Catface deposit is situated at a northwest trending contact between mafic volcanic rocks of the Upper Triassic Karmutsen Formation and diorite and monzonite of the Jurassic Westcoast Complex and Island Plutonic Suite (Figure 5). Drill cores (Appendix, Table A1)

oriented orthogonal to the strike of the contact intersect all rock units described below and were used to construct a cross section of the deposit (Figure 6). A summary of thin section petrography is included in the Appendix (Table A2 and A3)

Four intrusive phases are recognized at Catface (McDougall, 1976; McDougall and Enns, 1995): (1) porphyritic quartz diorite (Cliff and Halo Porphyries), (2) a phaneritic quartz diorite (Catface Intrusion), (3) late plagioclase-hornblende porphyry dykes (ADP Dyke), and (4) a phaneritic leucocratic quartz diorite (Hecate Bay quartz diorite) southeast of the deposit (Figure 5 and Figure 6). The quartz diorite at the centre of the Catface deposit is similar to the Ritchie Bay pluton described four km southeast with a U-Pb age for zircon of 41 ±1 Ma (Isachsen, 1987). Thus, Paleogene phases of the Catface deposit likely belong to the Mt. Washington Intrusive Suite (Madsen, 2004, Madsen et al., 2006). No clear timing relationships are obvious for the four younger magmatic phases at Catface, potentially suggesting contemporaneous emplacement. Regional faults typically strike northwest and northeast (McDougall, 1976).

Three zones of mineralization are recognized at the Catface deposit: the (main) Cliff Zone, the Irishman Creek Zone, and the Hecate Bay Zone (Figure 5). The Cliff Zone hosts the bulk of the porphyry mineralization at Catface, with an indicated reserve of 56.9 million tonnes averaging 0.40% Cu and an additional inferred resource of 262.4 million tonnes grading 0.38% Cu (Simpson and Chapman, 2009). Copper and Mo mineralization at the Cliff Zone consists of disseminated and fracture-controlled chalcopyrite, bornite, and molybdenite. The Cliff Zone was explored by Falconbridge Ltd. from 1961-1979, including the development of an 857 meter long adit into the core of the deposit. This adit allowed for extensive underground drilling, and provided ore material for bulk sample metallurgical testing (MINFILE 092F 120).

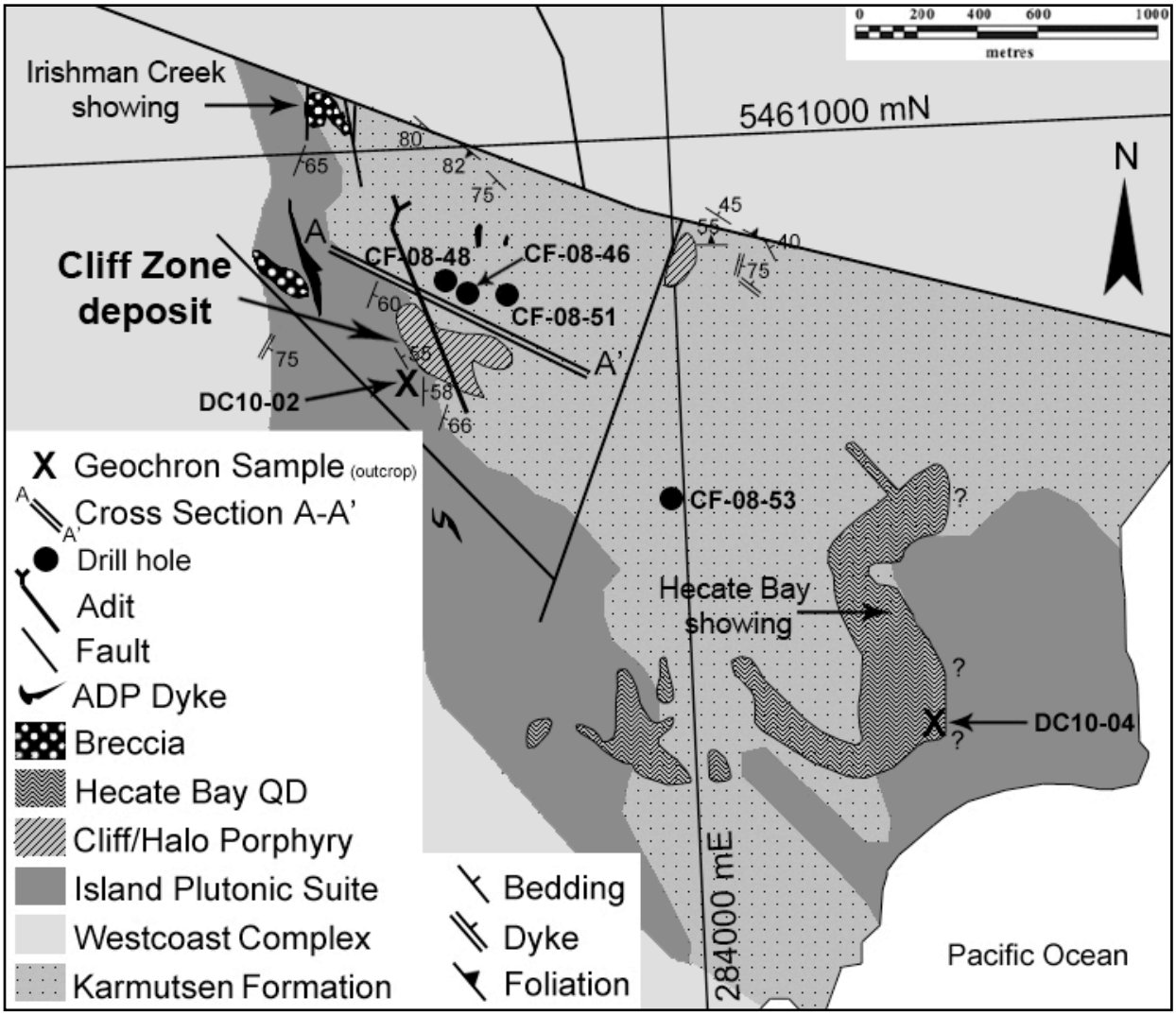

Figure 5: Simplified geology of the Catface porphyry deposit with locations of drill holes used in this study, adit, cross section A-A', and location of main Cliff Zone and Irishman Creek and Hecate Bay showings. Structural data and locations of two outcrop U-Pb samples are also displayed.

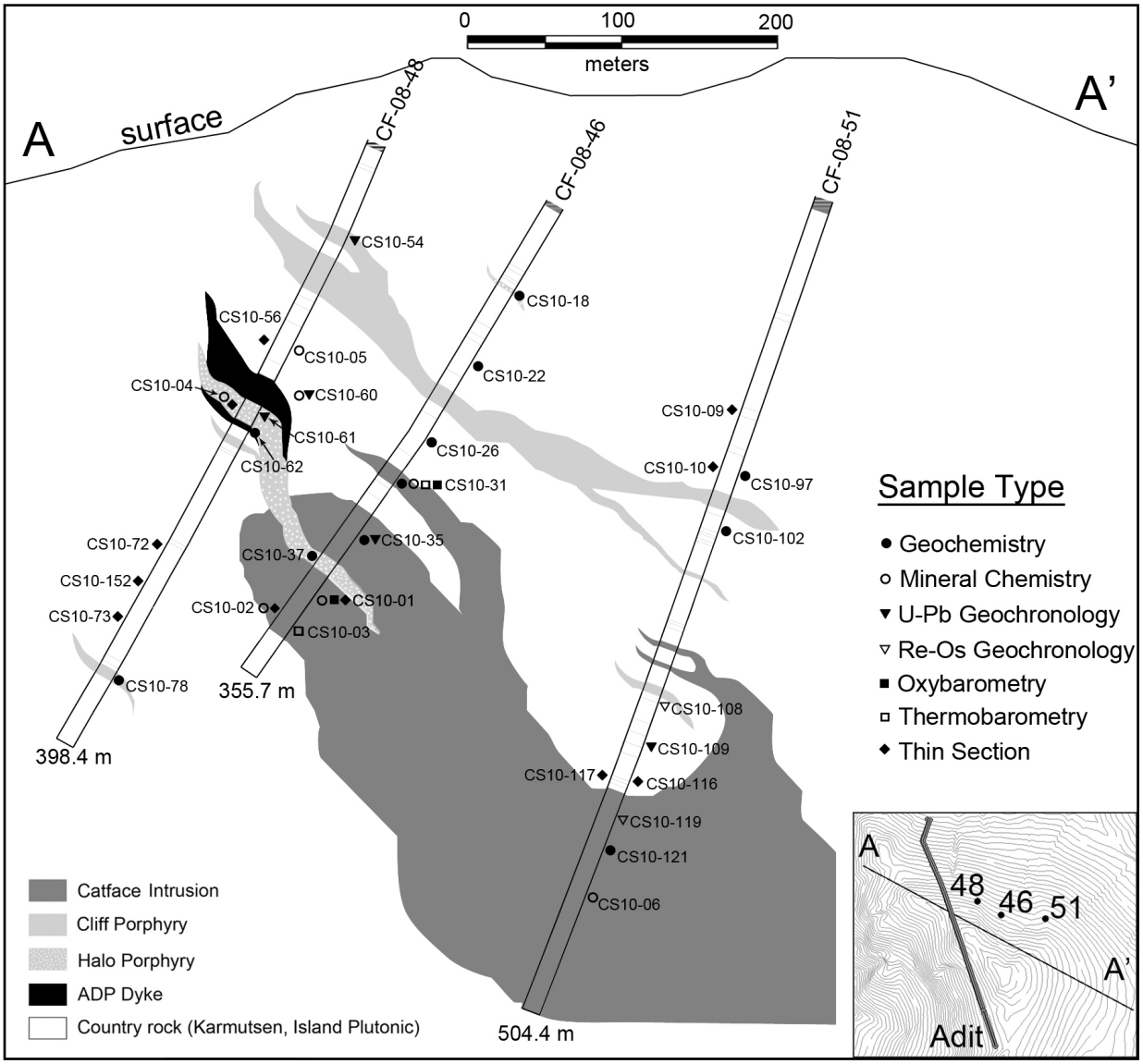

Figure 6: Cross section of Catface porphyry deposit Cliff Zone showing Paleogene intrusive phases and sample locations for geochemistry, mineral chemistry, geochronology, oxybarometry, thermobarometry, and thin section petrography.

The Irishman Creek Zone is situated 900 meters north of the Cliff Zone, and hosts disseminated chalcopyrite, pyrite and minor pyrrhotite mineralization in mafic volcanic rocks and in brecciated quartz monzonite. In addition, sulphide-rich lobes containing abundant magnetite, chalcopyrite, pyrite and pyrrhotite are present (MINFILE 092F 251, 1999). The Hecate Bay Zone is located 2.2 km southeast of the Cliff Zone, where mineralization is associated with the Hecate Bay quartz diorite. Disseminated and fracture-filled mineralization averaging 0.25% Cu is concentrated within the porphyritic core of the Hecate Bay stock; however, elevated grades up to 1.0% Cu have been discovered in copper bearing shear zones that extend several hundred meters outside the main zone (MINFILE 092F 231, 1990).

2.3.1 Karmutsen Basalt

Karmutsen basalt is the oldest rock at the Catface deposit. The basalt is phyric to aphanitic, dark grey-green to black and variably porphyritic to glomerocrystic (10-30% phenocrysts) (Figure 7 and Figure 8). Phenocrysts are 90-100% plagioclase; characterized by subhedral 1-3 mm crystals, and rare subhedral 0.5-1 mm lath-to-wedge shaped amphibole phenocrysts are present. The groundmass consists of quartz and feldspar, with lesser amphibole. Trace opaque minerals include fine-grained primary magnetite, and secondary pyrite, chalcopyrite, ±molybdenite, ±pyrrhotite, ±bornite, and ±rutile. Moderate to strong sericitization and local silicification associated with late microscopic fractures is observed in plagioclase crystals, and amphiboles display weak chloritization and secondary biotite replacement. Pervasive biotite (hornfels), characterized as secondary by being fine grained and ‘shreddy’, is localized near contacts with felsic intrusions and veins, giving the rock a distinctive brown colour in hand sample (Figure 9). Chloritization overprints secondary biotite, commonly associated with mineralization. Secondary azurite and malachite are observed replacing Cu

Figure 7: Sample from drill core of porphyritic Karmutsen basalt with phenocrysts of plagioclase feldspar.

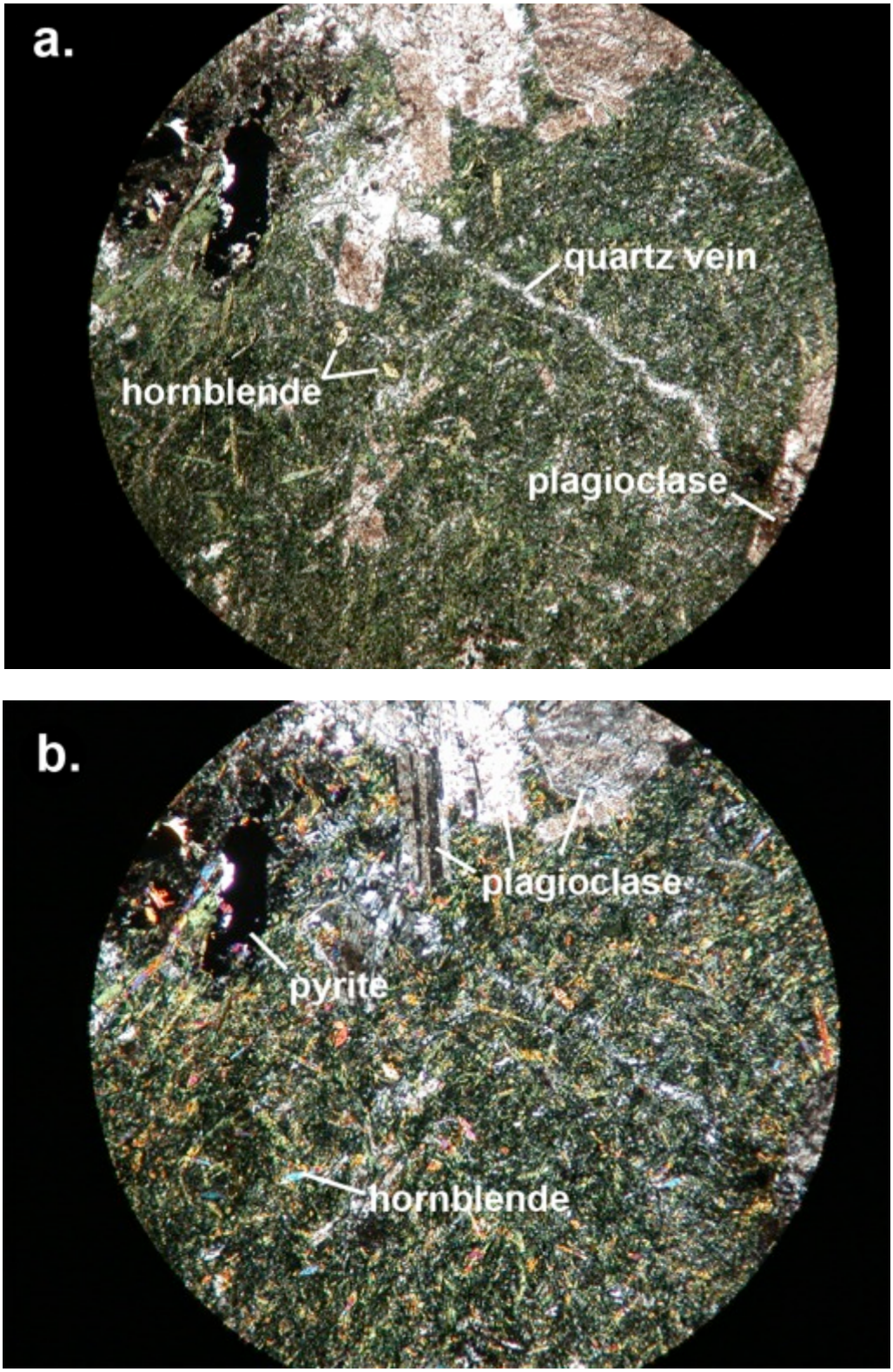

Figure 8: Thin section photographs of Karmutsen basalt in PPL (a) and XPL (b) showing late silicification, secondary pyrite mineralization, and strongly sericitized plagioclase feldspars (field of view is 4 millimeters).

sulphide fracture surfaces, and pyrrhotite occurs as discrete grains up to 0.7 cm in diameter in distal regions of the deposit (Figure 10).

2.3.2 Westcoast Complex Diorite

Diorite of the Jurassic Westcoast Complex is exposed along the west and south coast of Catface Peninsula (Figure 5). The diorite intrudes the Karmutsen basalt, hosting partially assimilated angular volcanic fragments (McDougall, 1976). The diorite is equigranular, medium-grained (1-2.5 mm diameter crystals), medium to dark grey and melanocratic, with hornblende comprising 50 to 60% of the modal mineralogy as 1-3 mm long subhedral laths (Figure 11 and Figure 12). Unzoned, subhedral, 1-2.5 mm plagioclase feldspars make up 40% of the rock. The remaining felsic minerals include 0-5% subhedral orthoclase feldspar with moderate sericitization, and 5-10% anhedral, finer-grained (1 mm diameter) quartz, with well-developed sutured grain boundaries and rare strained lattices. Rare biotite is observed, and accessory primary apatite, zircon and titanite grains account for <1% of the rock. Opaque minerals comprise roughly 1% of the rock, including primary magnetite and ilmenite, and secondary pyrite, chalcopyrite, ±molybdenite, and ±bornite. Moderate to strong sericitization is present in plagioclase, and most primary hornblendes and biotites are partially altered to chlorite. Hydrothermal alteration is concentrated in zones of elevated fracturing intensity, quartz stockwork, and mineralization. Secondary albite and actinolite are commonly associated with mineralized quartz veins, and rare late chlorite-epidote (clinozoisite) veinlets are locally abundant. Secondary biotite is observed overprinting primary crystals as shreddy, fine-grained clusters.

Figure 9: Sample from drill core of Karmutsen basalt displaying patchy (brown) biotite-rich hornfels, commonly developed near contacts with crosscutting felsic intrusions.

Figure 10: Hand sample from drill core of pyrrhotite grains (~1 cm in diameter) in Karmutsen basalt.

Figure 11: Hand sample of Westcoast Complex diorite sampled from outcrop at the Catface porphyry deposit.

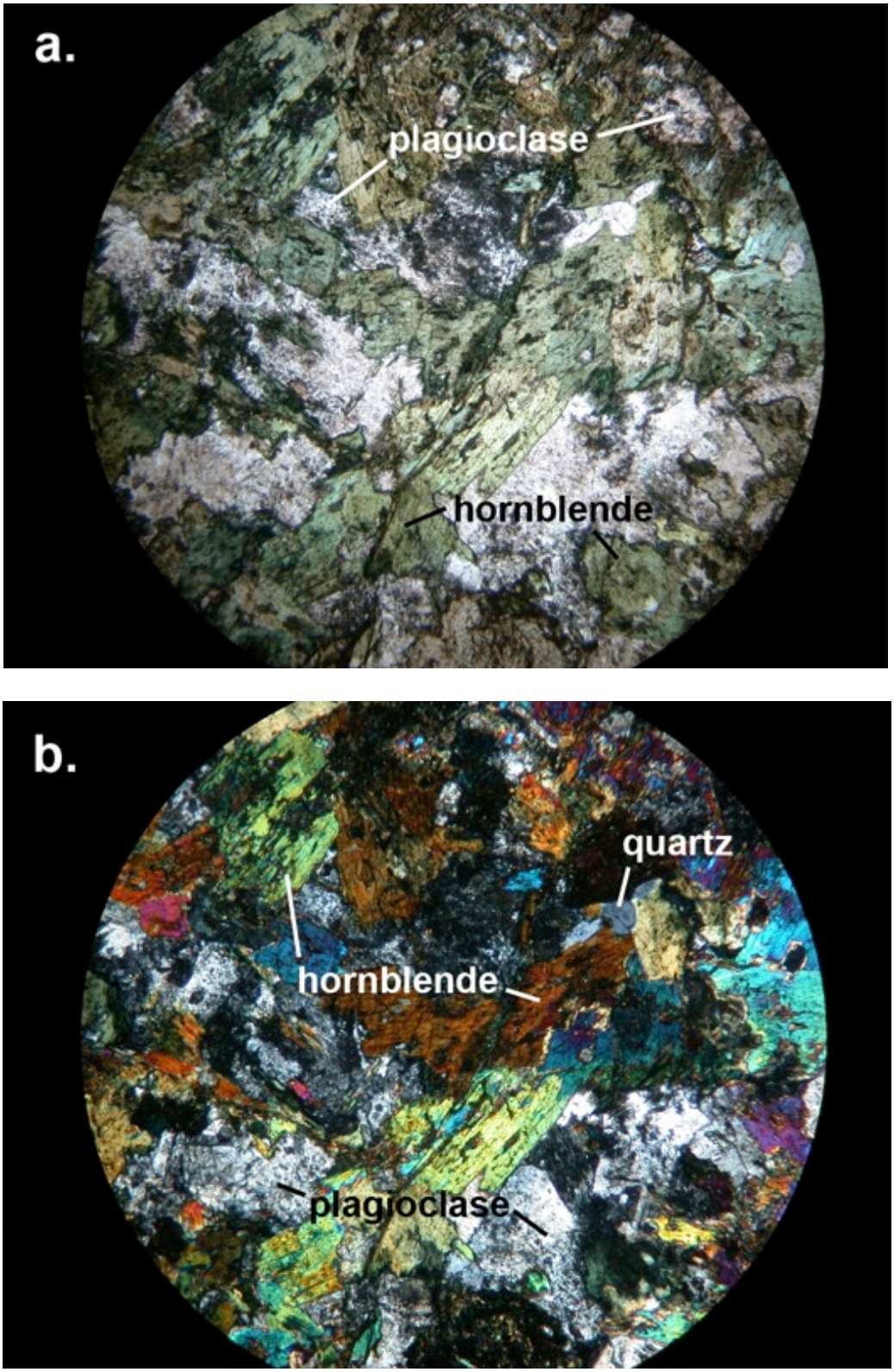

Figure 12: Thin section photographs of Westcoast Complex diorite in (a) PPL and (b) XPL showing moderate chloritization of hornblende and sericitization of plagioclase feldspars (field of view is 4 millimeters).

2.3.3 Island Plutonic Suite

Coarse-grained quartz monzonite of the Jurassic Island Plutonic Suite is well exposed on the central west-sloping face of the mountain where it outcrops for ~3 km (McDougall, 1976). The rock is a creamy white-grey and contains numerous mafic volcanic xenoliths (Figure 13). Plagioclase comprises 55-56% of the rock, and occurs as 2-4 mm long, subhedral tablets. Some plagioclase crystals are poikilitic to fine-grained acicular amphibole (likely actinolite). Subhedral to anhedral 1-3 mm diameter quartz crystals make up 15-25% of the rock, and anhedral orthoclase feldspar and biotite comprise 5-15% (Figure 14). Strong sericitization is present in feldspars, and primary biotites, characterized by coarse grain sizes, are commonly overgrown by secondary (fine-grained and shreddy) biotites (Figure 15). Trace quantities of primary zircon, apatite and titanite are present, and opaque minerals including primary ilmenite and magnetite, and secondary pyrite, chalcopyrite, ±pyrrhotite, ±molybdenite, ±bornite.

2.3.4 Cliff and Halo Porphyry

The Cliff and Halo Porphyry intrusions crosscut the Triassic and Jurassic rocks and outcrop for ~700 meters along a cliff exposure (Figure 5). Emplacement of these porphyries was strongly controlled by pre-existing structures and contacts associated with the Island Plutonic Suite. The Cliff and Halo Porphyries are medium-grey porphyritic quartz diorites. The Halo phase is distinguished by being more altered and containing limonitic halos (Figure 16) around 1-4 mm chalcopyrite and pyrite-bearing clusters interpreted as miarolitic cavities (Figure 17). McDougall (1976) identifies the Cliff Porphyry as lenticular, dyke-like bodies, whereas the Halo Porphyry forms less elongate intrusions. Weakly aligned, subhedral hornblendes ranging from 0.5-2 mm in size make up 35-65% of the phenocryst population. The remaining phenocrysts comprise sub-to-anhedral, 0.5-3 mm long plagioclase and rare

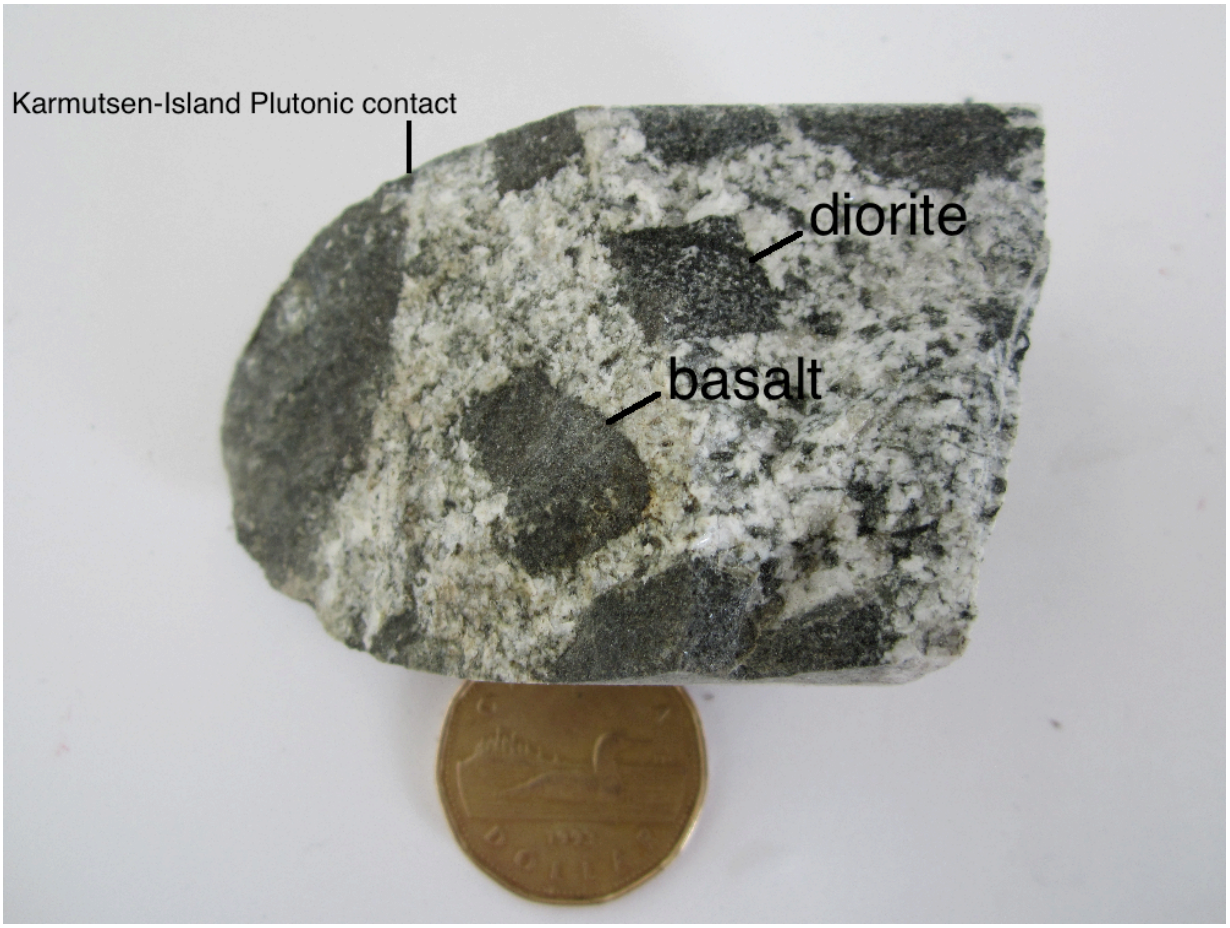

Figure 13: Hand sample from drill core with basaltic and dioritic xenoliths in Island Plutonic Suite.

Figure 14: Hand sample of granodiorite from the Island Plutonic Suite illustrating its distinctive coarse-grained texture and creamy-white appearance.

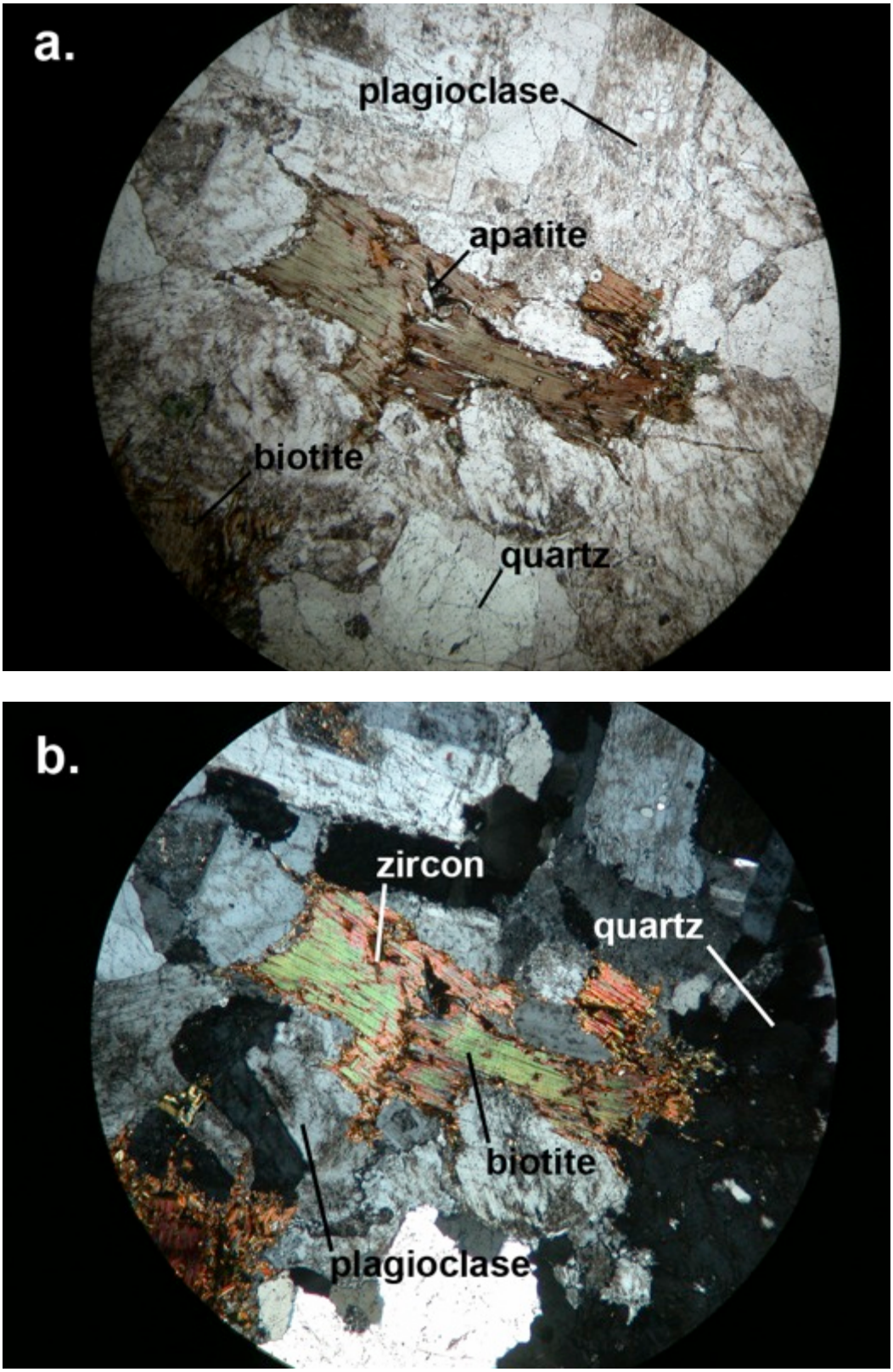

Figure 15: Thin section photographs of granodiorite from the Island Plutonic Suite in (a) PPL and (b) XPL, showing a ~2 millimeter primary (chloritized) biotite crystal rimmed by finer-grained secondary biotites (field of view is 4 millimeters).

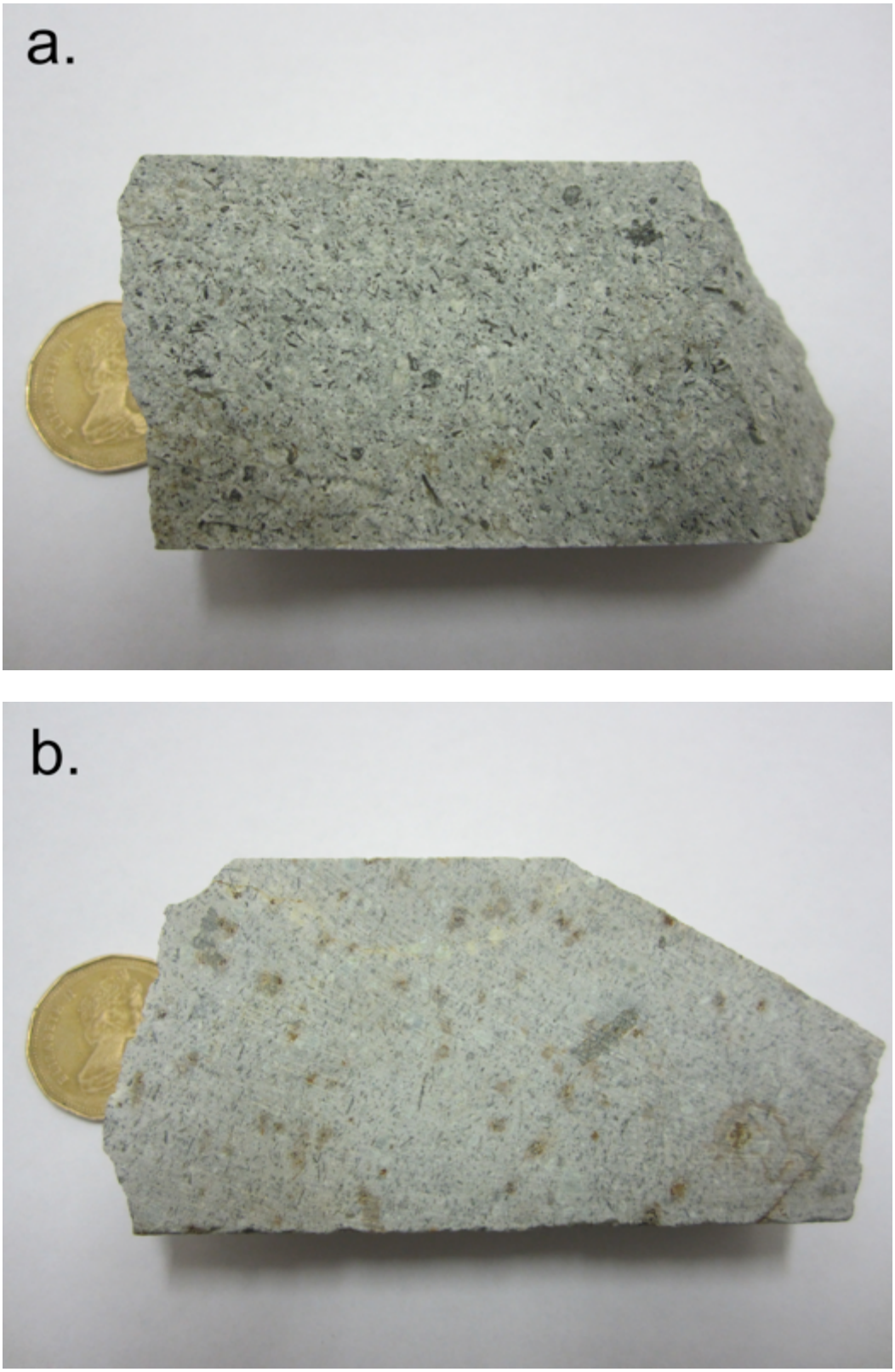

Figure 16: Hand samples of (a) Cliff Porphyry and (b) Halo Porphyry. Note the similarity of texture but the more bleached appearance and presence of limonitic alteration halos around sulphide mineralization in the Halo Porphyry.

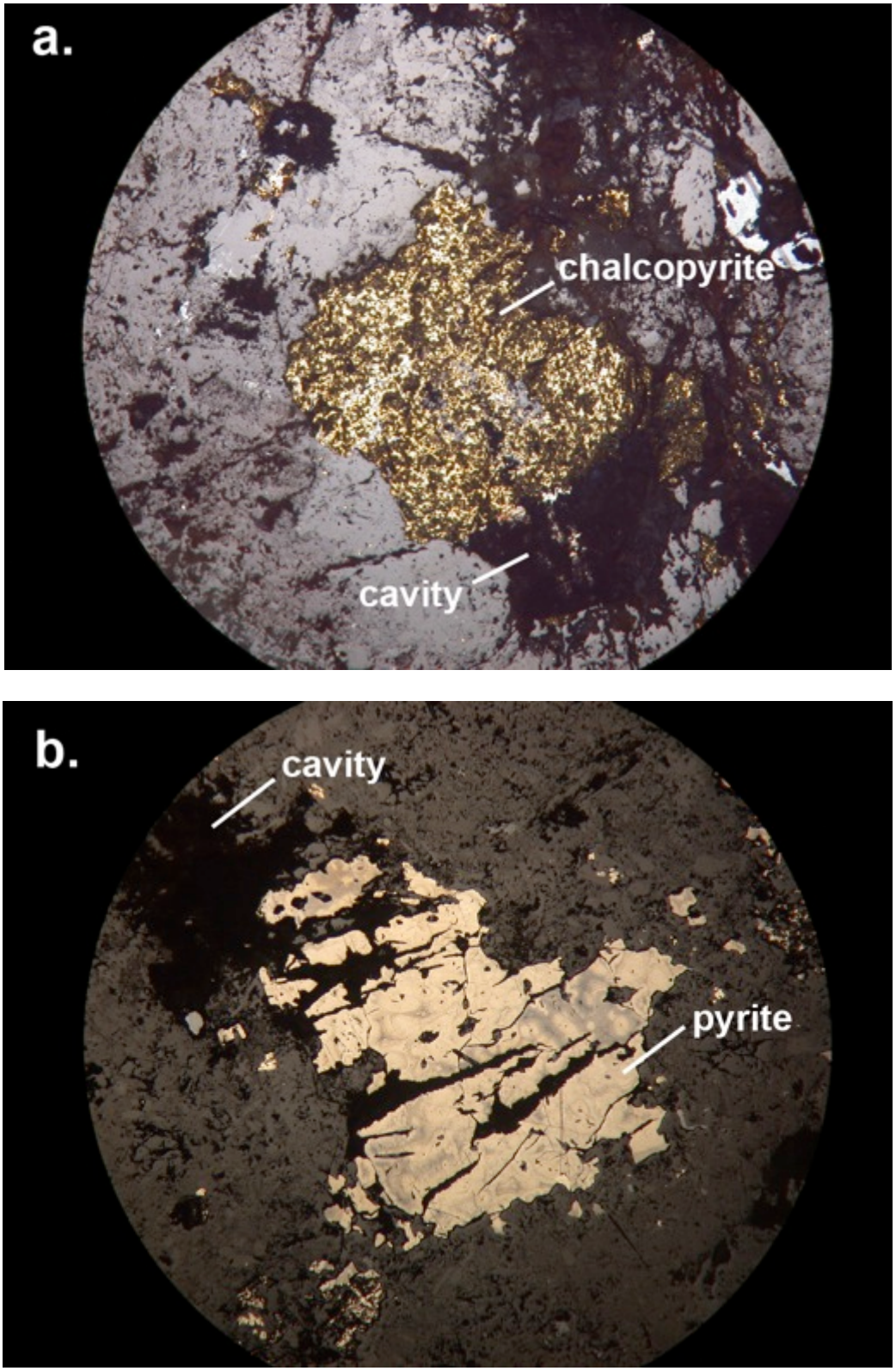

Figure 17: Microphotographs of sulphide-bearing (a. chalcopyrite; b. pyrite) miarolitic cavities in Halo Porphyry in reflected light (field of view is 4 millimeters).

orthoclase (Figure 18). The groundmass is composed of plagioclase, quartz, and lesser amphibole, with accessory zircon, apatite and titanite. Opaque minerals include primary ilmenite, magnetite, and disseminated secondary pyrite, chalcopyrite, pyrrhotite, ±molybdenite, and ±bornite.

2.3.5 Catface Intrusion

The Catface Intrusion is a fresh, medium-grained, light grey, equigranular to sub-equigranular quartz diorite intruding as a bulbous body at least 140 meters in thickness (Figure 19 and Figure 20). The rock is composed of approximately 40-60% subhedral plagioclase crystals 1-3 mm in size with oscillatory zoning. Subhedral 1-2 mm quartz crystals comprise 10-20% of the rock, and orthoclase makes up roughly 2 to 5% of the Catface Intrusion. Biotite is the most abundant mafic phase, with subhedral crystals ranging 0.5-2 mm in size of both primary (larger discrete crystals) and secondary (fine-grained, shreddy overgrowths) origin. Anhedral amphibole (hornblende) crystals 1-2 mm in size are observed. Primary accessory apatite, zircon, titanite, ilmenite and magnetite are identified, as well as secondary pyrite, chalcopyrite, ±molybdenite, and ±bornite.

2.3.6 ADP Dykes

The ADP Dykes represent volumetrically minor intrusions at Catface that trend northerly to northwesterly for ~1500 meters within the Island Plutonic Suite monzonite (Figure 5). The dykes are chocolate brown-purple porphyritic quartz diorite to granodiorite with 20-30% phenocrysts ranging 1-3 mm in size in a highly altered fine-grained matrix (Figure 21). Phenocrysts are composed of 60-80% sub-to-anhedral plagioclase and 20-40% amphibole. Most plagioclase phenocrysts are pervasively sericitized; however, ~30% of the feldspars are fresh with well-developed oscillatory zoning. The chloritized groundmass is composed of 60%

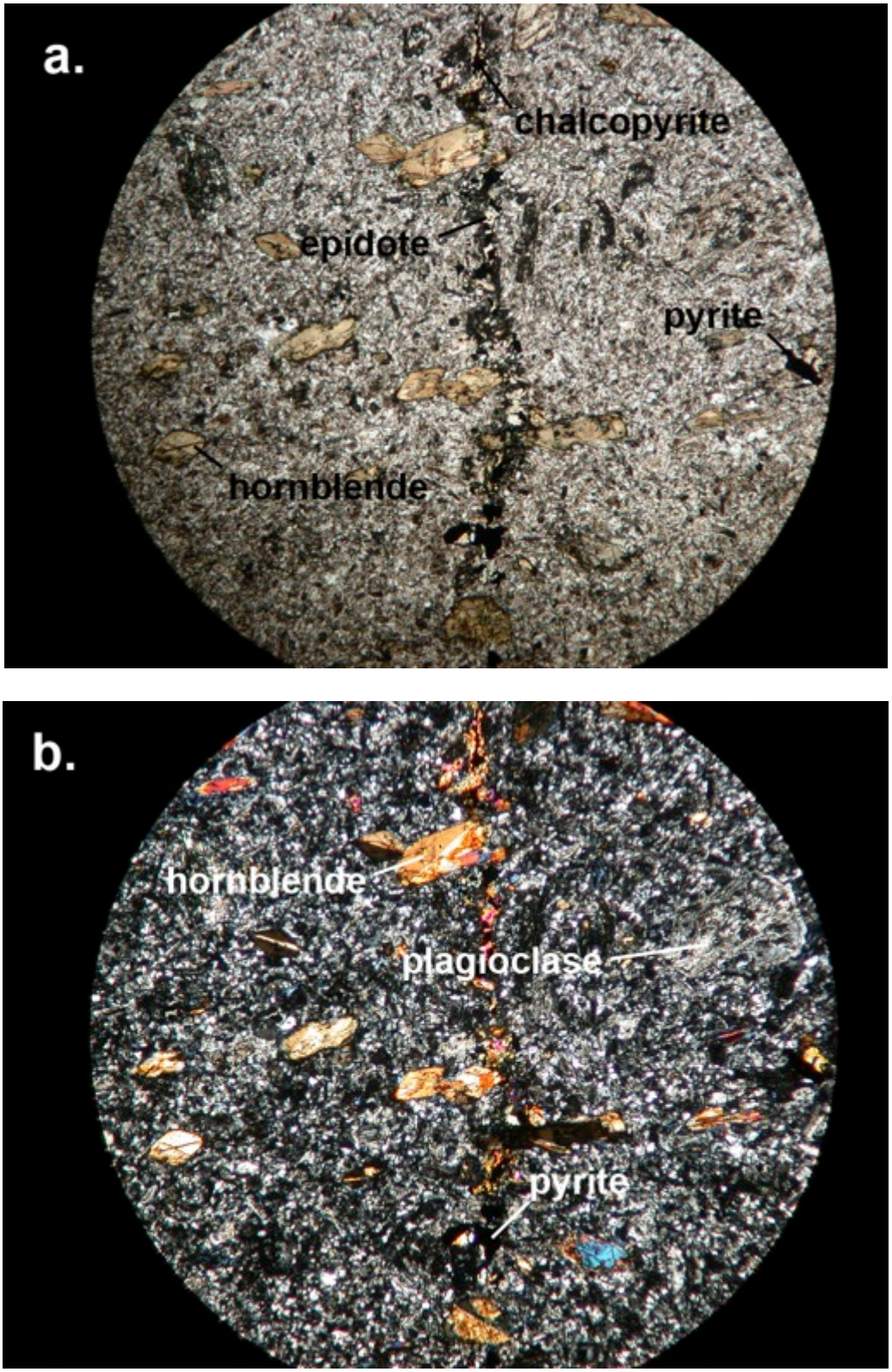

Figure 18: Thin section photographs of Cliff Porphyry in (a) PPL and (b) XPL with weakly aligned hornblende phenocrysts and a late, crosscutting epidote veinlet (field of view is 4 millimeters).

Figure 19: Hand sample of Catface quartz diorite phase, illustrating relatively fresh appearance and trace amounts of disseminated sulphides (pyrite, chalcopyrite).

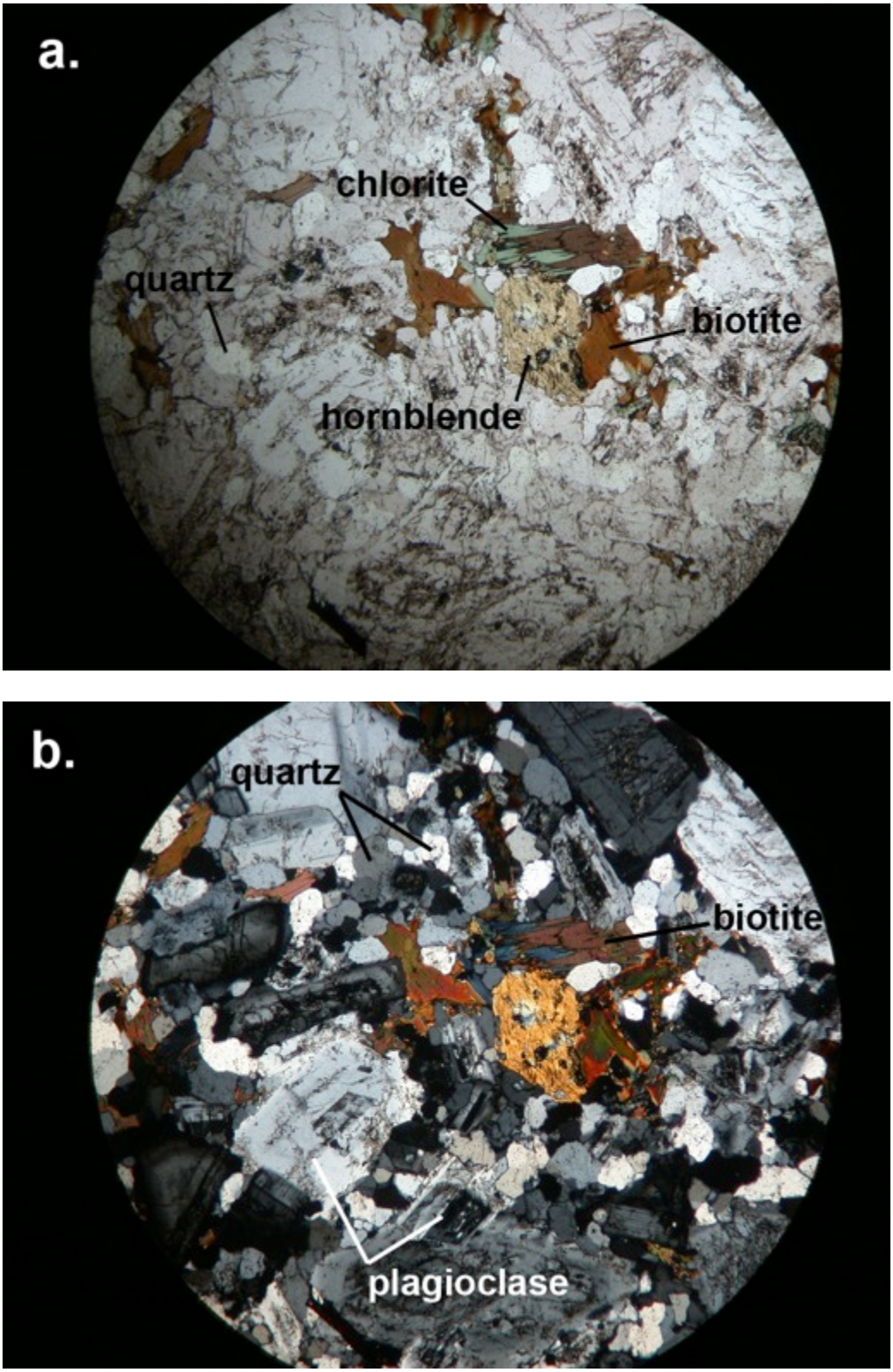

Figure 20: Thin section photographs of Catface quartz diorite in (a) PPL and (b) XPL, illustrating unaltered plagioclase and hornblende, and partially chloritized biotites (field of view is 4 millimeters).

Figure 21: Hand sample of ADP dyke with plagioclase and (lesser) amphibole phenocrysts. This rock is distinguished from Karmutsen basalt by its chocolate-brown to purple groundmass and amphibole phenocrysts.

plagioclase, 20% quartz, 10% biotite, and 10% amphibole, with accessory zircon, apatite ilmenite, magnetite and titanite, and secondary pyrite, chalcopyrite, ±molybdenite, and ±bornite (Figure 22).

2.3.7 Hecate Bay Quartz Diorite

The Hecate Bay quartz diorite is a fresh, medium-grained (1-3 mm wide crystals), equigranular to sub-equigranular rock that intrudes ~2 km southeast of the Cliff Zone (Figure 5 and Figure 23). Hecate Bay phase is composed of 50-60% hornblende, 25-35% plagioclase, 5-10% quartz, and 2-5% potassium feldspar (microcline). Feldspars are fresh to weakly sericitized with oscillatory zonation developed in some crystals, and quartz is typically interstitial and finer-grained (Figure 24). Primary accessory zircon, apatite, titanite, ilmenite and magnetite occur throughout the rock, with <1% secondary pyrite, chalcopyrite, and ±pyrrhotite.

2.4 Mineralization

The primary mineralization style is disseminated and fracture-controlled chalcopyrite with lesser molybdenite, pyrite and bornite (Figure 25). Quartz stockwork is weak to moderate at Catface, and elevated intensity coincides with enhanced grade. Chalcopyrite is the most abundant ore mineral at the Cliff Zone, followed in abundance by bornite, pyrite, molybdenite, pyrrhotite, and chalcocite. McDougall (1976) identified native copper, covellite, idaite, digenite, cuprite, valerite, and tenorite. The secondary copper oxide minerals malachite and azurite are common, whereas chrysocolla is rare.

Chalcopyrite forms rare, discrete blebs in all lithologies, and locally replaces plagioclase and occurs with quartz infilling amygdules in Karmutsen basalt country rock. Bornite formation mimics that of chalcopyrite, but is spatially restricted to the center of the deposit. Rare secondary chalcocite forms “sooty” fracture coatings, which McDougall (1976) interprets to be

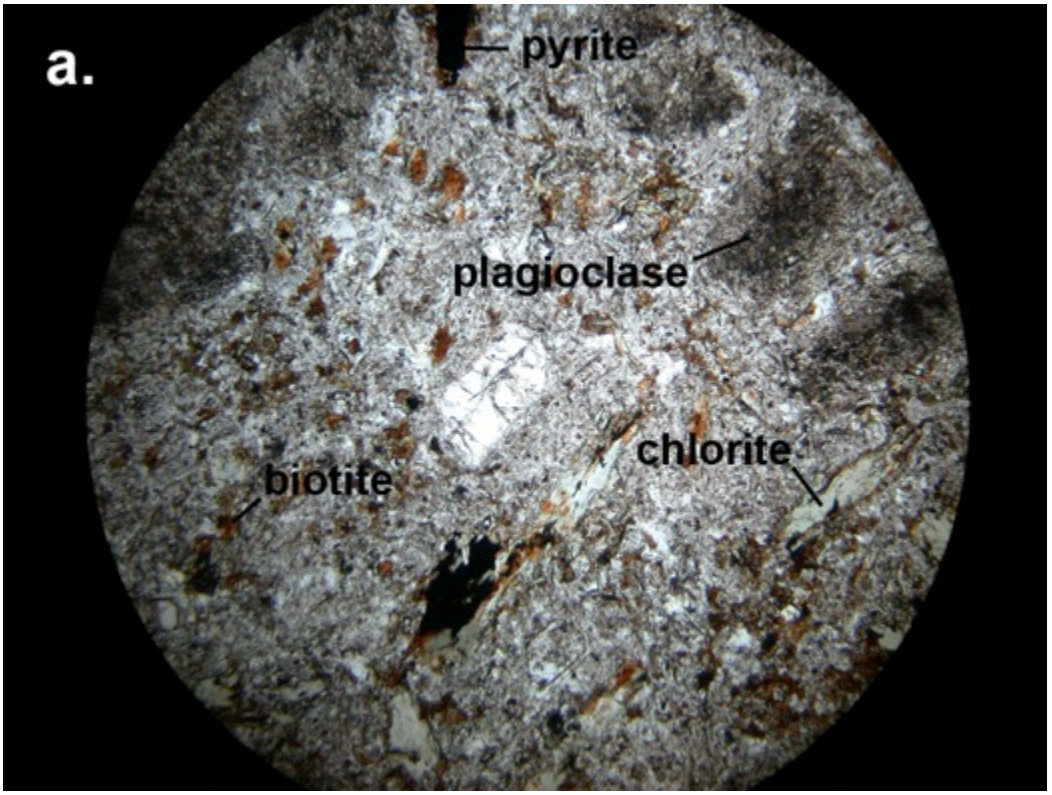

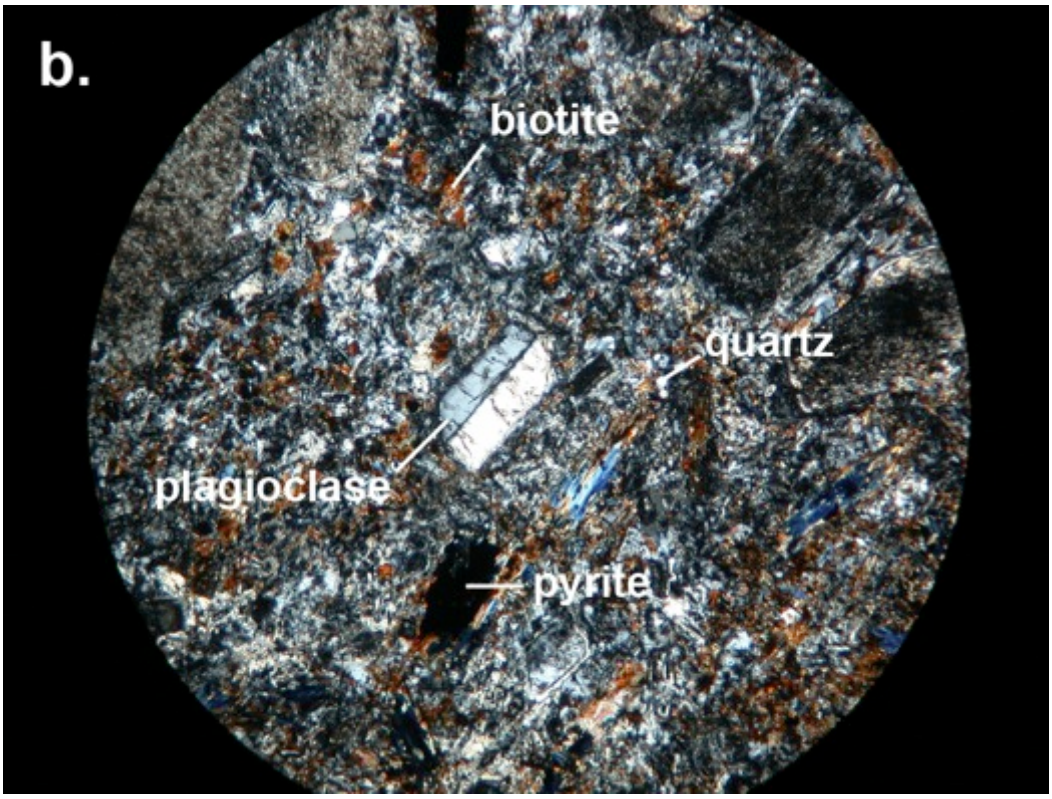

Figure 22: Thin section photographs of ADP dyke in (a) PPL and (b) XPL showing two generations of plagioclase, one of which is pervasively sericitized and the other of which is unaltered (field of view is 4 millimeters).

Figure 23: Hand sample of Hecate Bay quartz diorite sampled from outcrop at the Catface porphyry deposit.

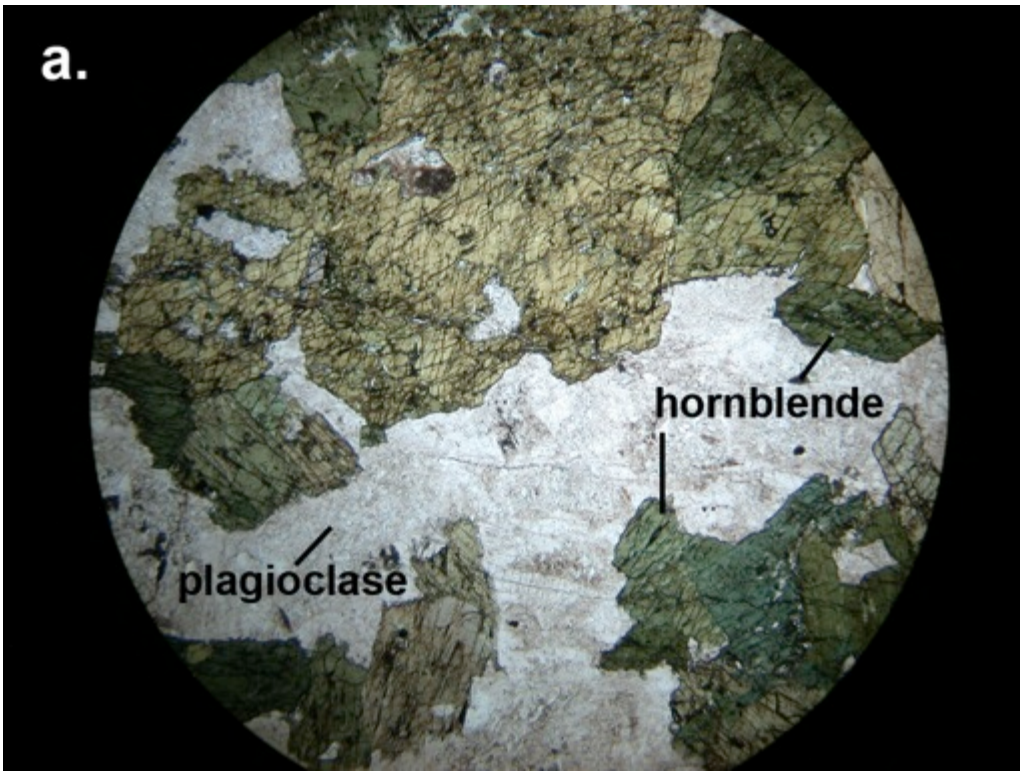

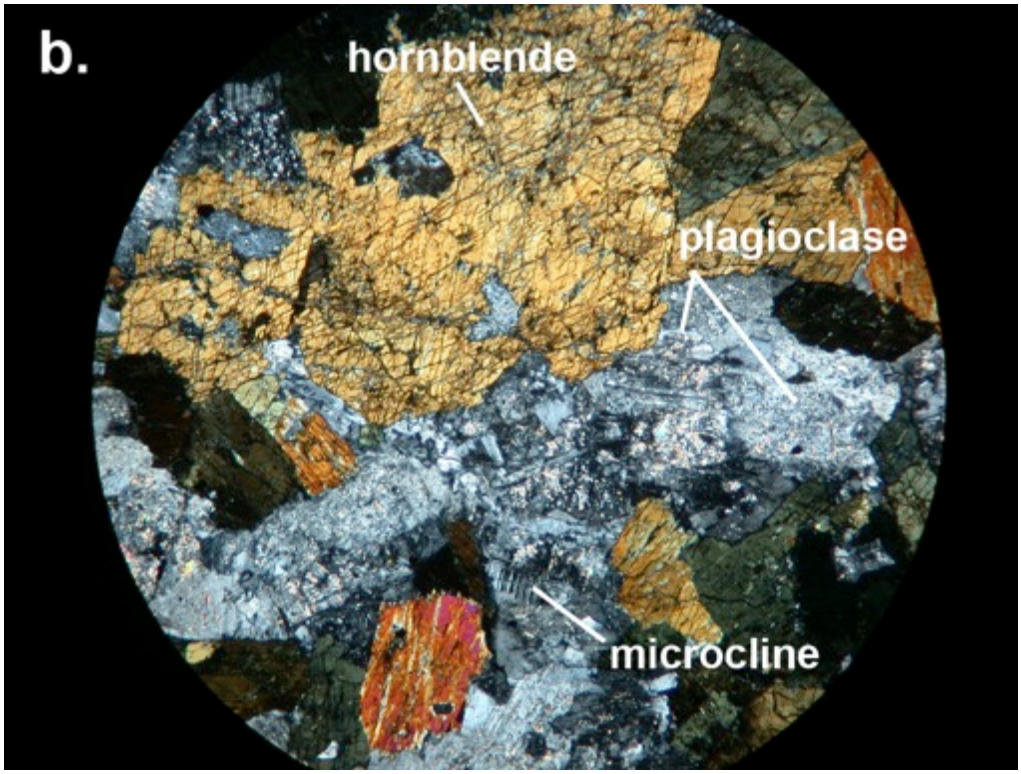

Figures 24: Thin section photographs of Hecate Bay quartz diorite in (a) PPL and (b) XPL illustrating fresh hornblendes and weakly sericitized plagioclase feldspars (field of view is 4 millimeters).

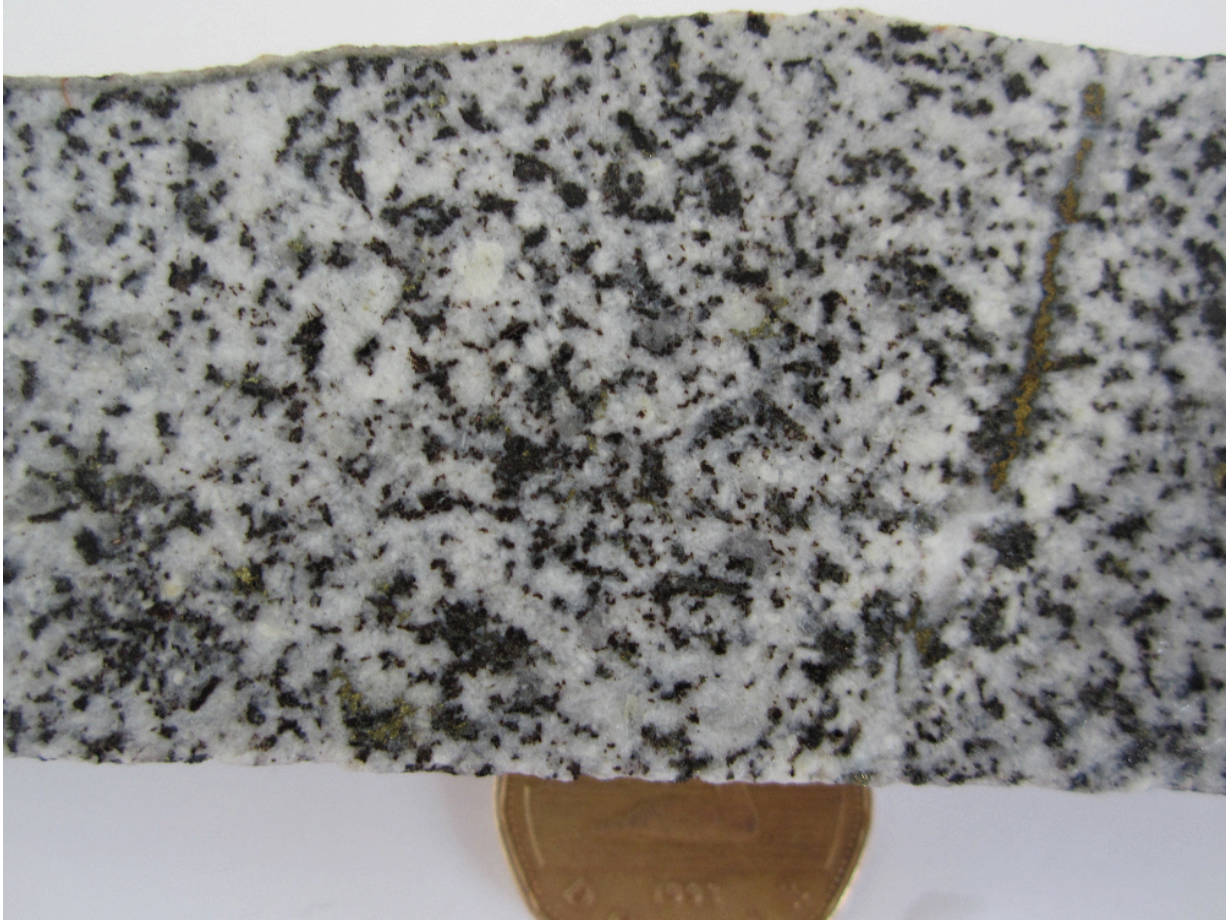

Figure 25: Hand sample of Catface Intrusion quartz diorite illustrating disseminated and vein-hosted Cu mineralization (chalcopyrite-pyrite±bornite).

secondary replacements of chalcopyrite and bornite. Molybdenite mineralization is weak to moderate and occurs as discrete, disseminated flecks, fracture fillings, and rare massive blebs (up to 7 millimetres in diameter) in copper sulphide and quartz stockwork veins. Disseminated and vein-hosted pyrite occurs throughout the deposit. Pyrrhotite is rare in the core of the deposit and occurs as discrete grains up to 1 cm in size in the mafic volcanic rocks (Figure 10). Four stages of mineralization and alteration are described below and summarized in Figure 26. These stages overprint an earlier metamorphic hornfels most commonly observed in the mafic volcanic rocks in the vicinity of younger (Paleogene) intrusions (Figure 9).

2.4.1 Vein and Alteration Paragenesis

Stage 1: The central zone of mineral deposit is dominated by chalcopyrite-bornite-molybdenite veins associated with quartz stockwork (Figure 27). This generation of veins is the most volumetrically abundant, with the abundance of veins correlating with elevated Cu and Mo grades. Copper mineralization is dominant, although Mo mineralization is also present. Alteration minerals include quartz, albite, actinolite and rare scapolite. These hydrothermal minerals occur within veins and as selvages along vein margins (Figure 28).

Stage 2: This mineralization is focused in the core of the deposit and decreases in abundance towards the periphery of the ore-body. Chalcopyrite-molybdenite ±pyrite ±bornite veins commonly crosscut the Stage 1 veins (Figure 29 and Figure 30). Alteration mineralogy consists of quartz, actinolite, albite, and lesser chlorite and scapolite.

Stage 3: The third stage of mineralization has less molybdenite, an absence of bornite and the appearance of pyrrhotite. Pyrite-chalcopyrite ±pyrrhotite ±molybdenite veins with different alteration minerals occur at the margin of the ore system. Selvages of biotite, chlorite and lesser epidote are common along vein margins, and are best developed where the vein is

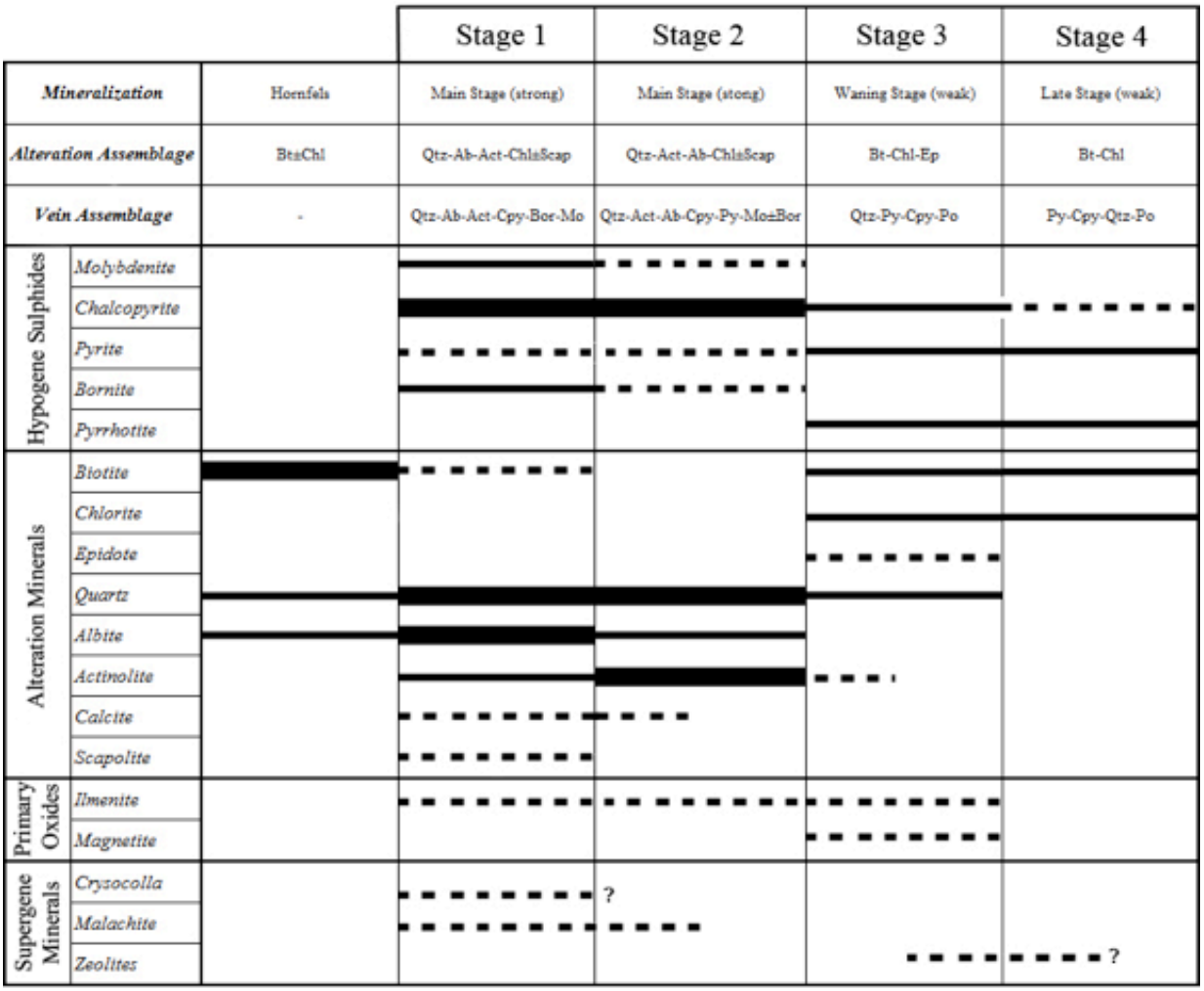

Figure 26: Summary of paragenetic sequence of alteration and mineralization at the Catface porphyry deposit. Widths of solid lines reflect modal abundance of particular mineral: thick solid line ~2-5% and thin solid line ~1-2%. Dashed line indicates a mineral occurrence that is sometimes present. Act – actinolite, Ab – albite, Bor – bornite, Bt – biotite, Cal – calcite, Chl – chlorite, Cpy - chalcopyrite, Ep - epidote, Kfs – K-Feldspar, Mo - molybdenite, Po – pyrrhotite, Qtz - quartz (mineral abbreviations from Kretz, 1985).

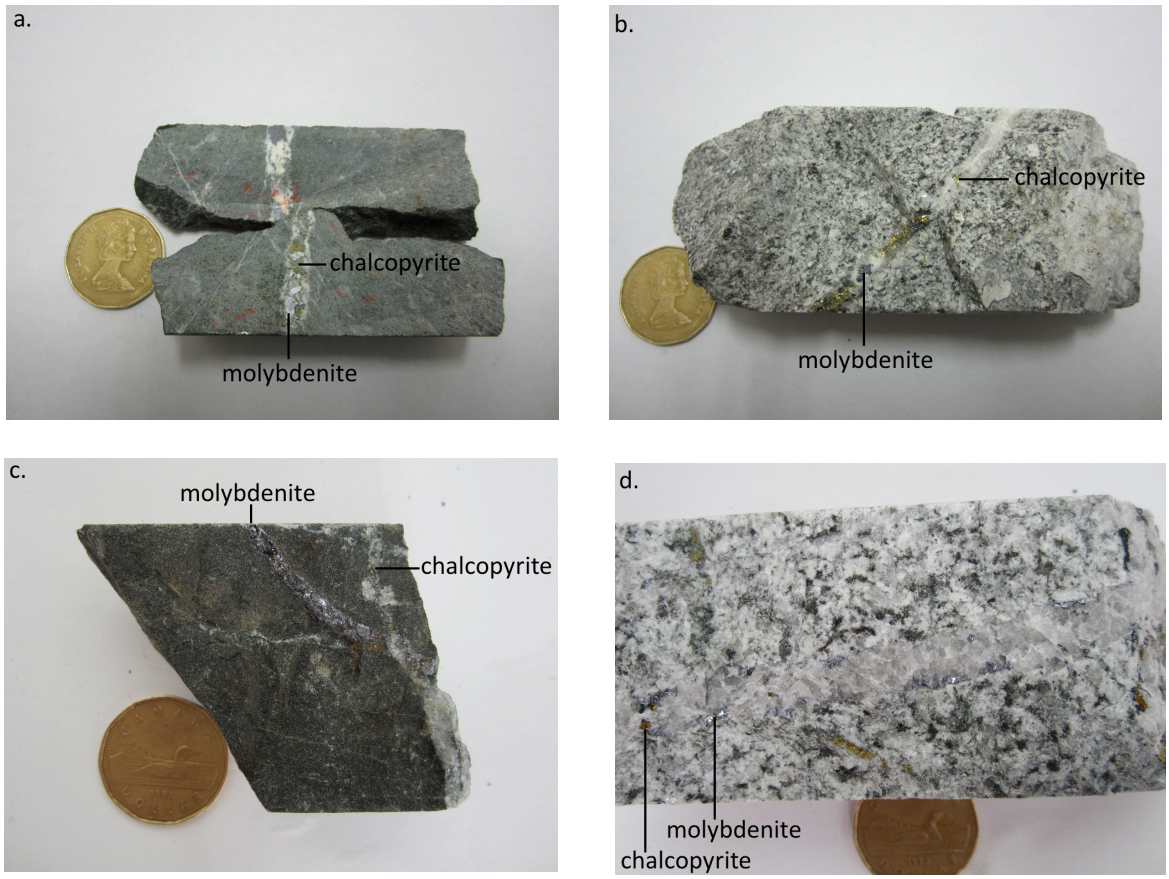

Figure 27: Hand sample examples of stages of mineralization and alteration: (a) Karmutsen basalt with molybdenite blebs up to 6 mm in diameter in an albite-molybdenite-chalcopyrite-actinolite vein, (b) Catface quartz diorite crosscut by a quartz-chalcopyrite-molybdenite-albite vein, (c) Stage 2 quartz-chalcopyrite-actinolite vein crosscut by a Stage 1 vein with massive molybdenite, (d) quartz-chalcopyrite-molybdenite-albite vein in Catface quartz diorite.

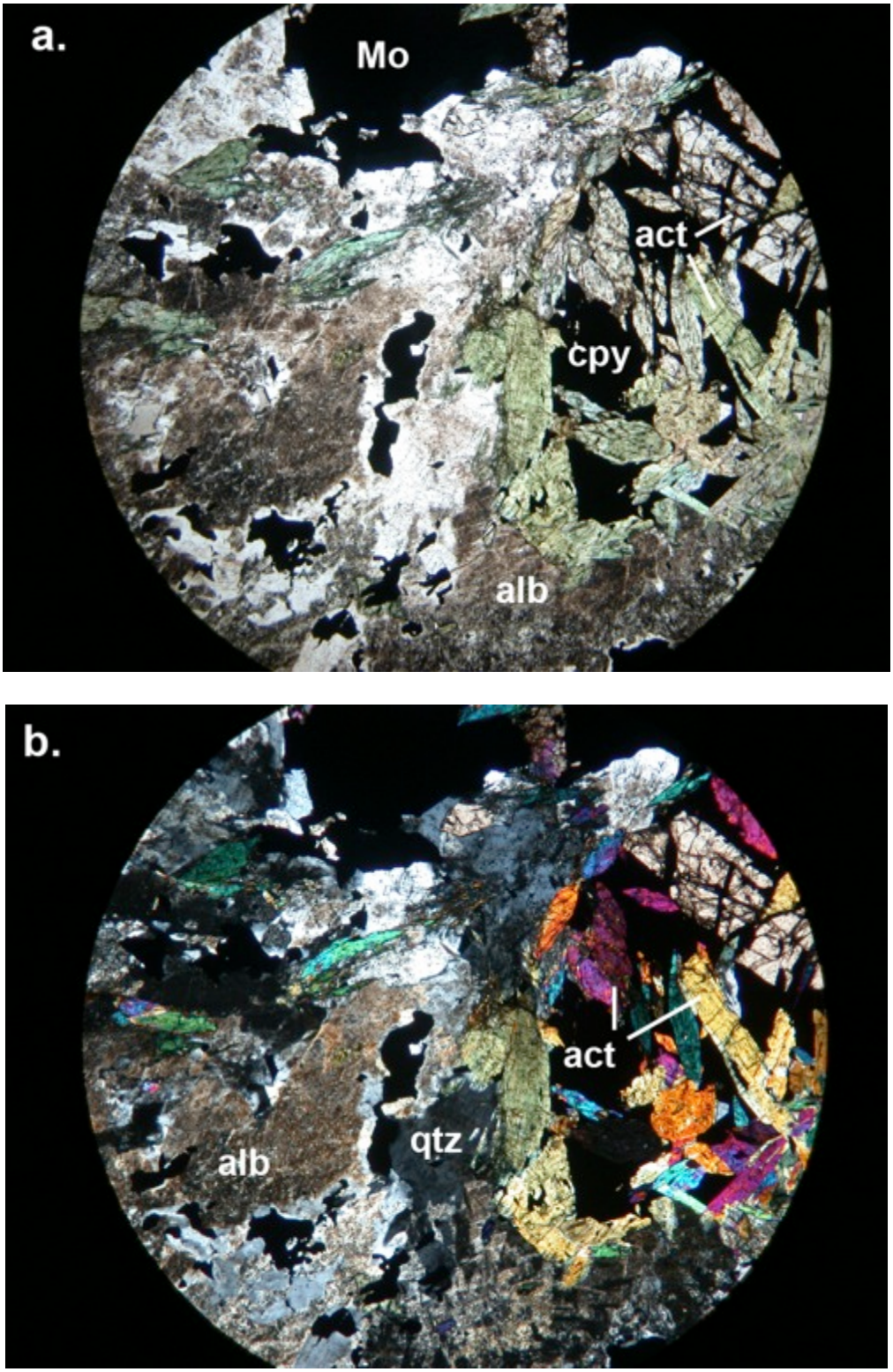

Figure 28: Thin section photographs of Stage 1 mineralization and alteration in (a) PPL and (b) XPL in granodiorite of Island Plutonic Suite (field of view is 4 millimeters).

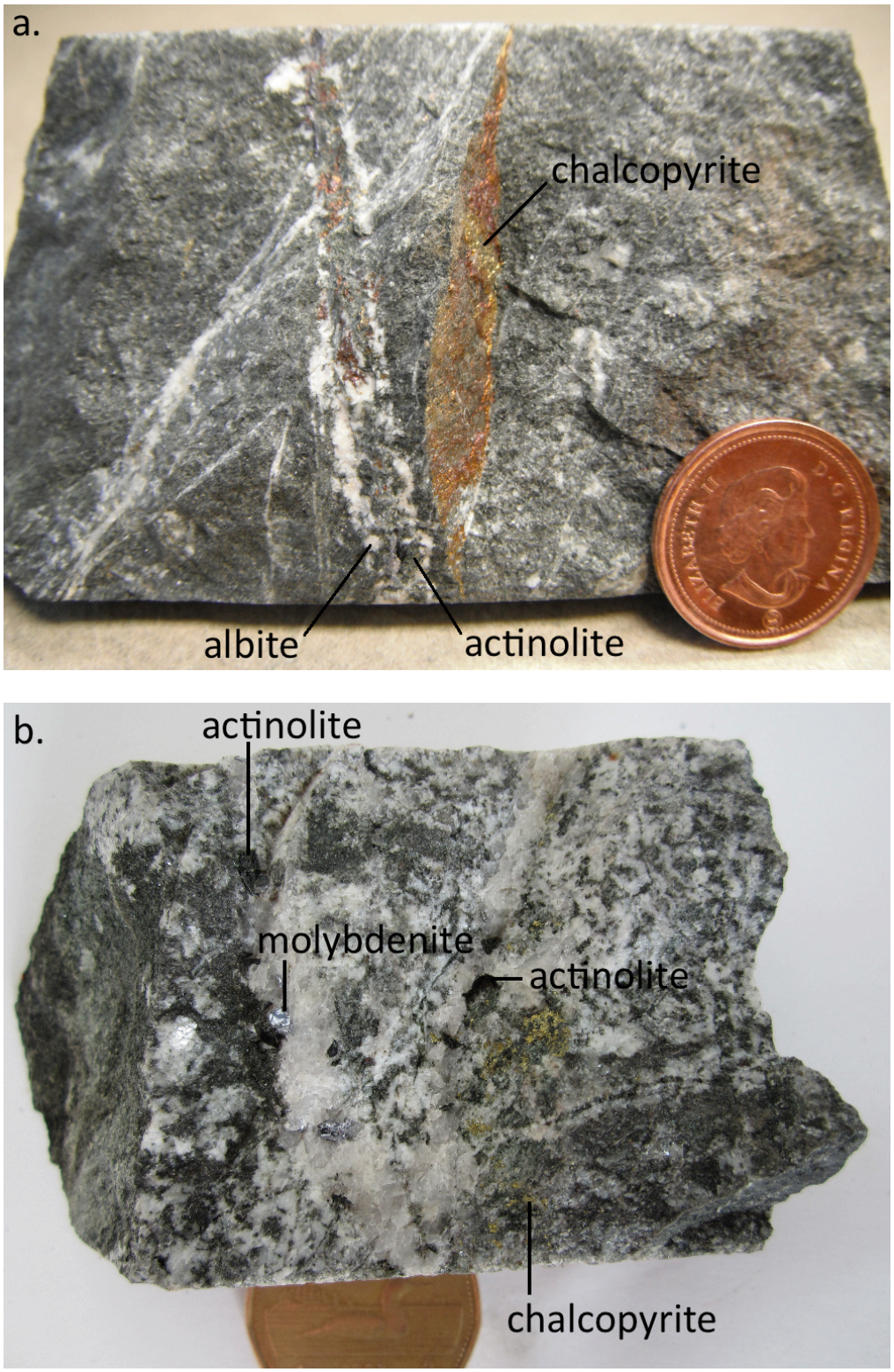

Figure 29: Examples of Stage 2 mineralization in (a) Karmutsen basalt and (b) Catface quartz diorite, characterized by Cu and lesser Mo mineralization (chalcopyrite, molybdenite, ±bornite) and an alteration assemblage of actinolite, albite and minor chlorite.

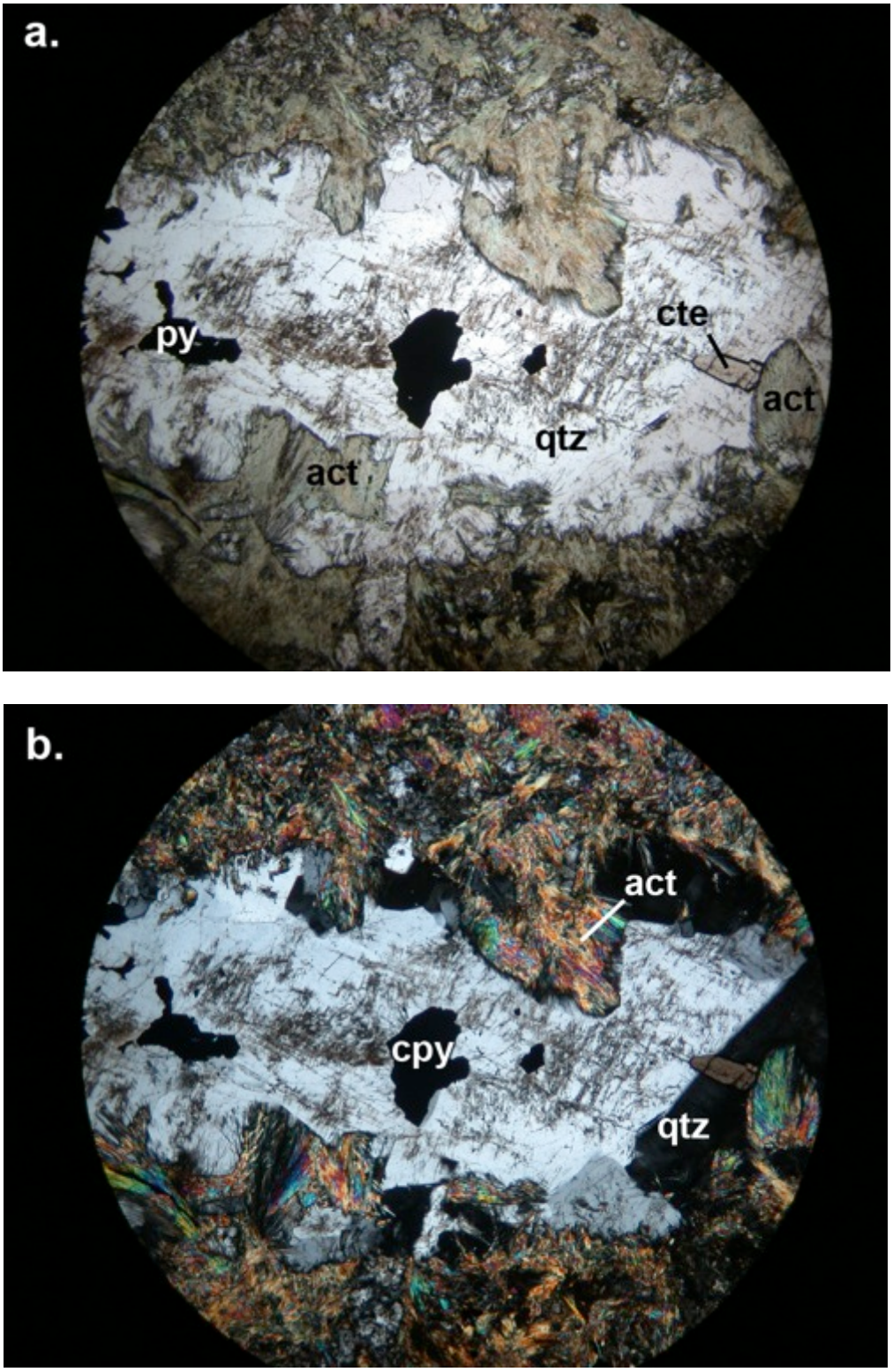

Figure 30: Thin section photographs of Stage 2 mineralization and alteration in (a) PPL and (b) XPL, characterized by Cu mineralization (chalcopyrite) and an alteration assemblage of actinolite and lesser albite and chlorite (field of view is 4 millimeters).

hosted in mafic volcanic rocks (Figure 31 and Figure 32).

Stage 4: The final mineralization is volumetrically minor, crosscuts all other mineralization, and consists of mm to sub-mm scale "stringer" veins of pyrite, chalcopyrite and pyrrhotite with two or more of these phases commonly present (Figure 33 and Figure 34). The stringer veins are present throughout the deposit, although pyrrhotite is restricted to the deposit periphery. Biotite and chlorite are developed at the contact between some veins and wall rocks.

2.4.2 Assay Data Compilation

Copper and Mo grades were obtained throughout the length of each drill core. Fracture intensity was logged based on the number of fractures per unit length of core (Figure 35). Fractures associated with the ore system were distinguished from drilling-related fractures by the presence of mineralization and alteration. Fracture intensity profiles are plotted in cross sectional form with corresponding average Cu and Mo grades for each drill hole (Figure 36). A moderate to strong correlation between fracture intensity and grade is evident for both Cu and Mo, with elevated grades coinciding with isolated faults and/or fault zones. Average Cu and Mo grades were determined for each level of fracture intensity (Figure 37), showing average Cu grades increasing with the degree of fracturing, with a similar but less pronounced relationship for Mo.

2.5 Conclusions

Four phases of magmatism intrude Mesozoic country rocks at the Catface porphyry copper deposit: the Cliff and Halo Porphyries, Catface Intrusion, ADP Dyke, and Hecate Bat Quartz Diorite. Relative and absolute timing(s) of these phases are defined by U-Pb geochronology in Chapter 3. The ore grades, mineralization styles, alteration assemblages, and

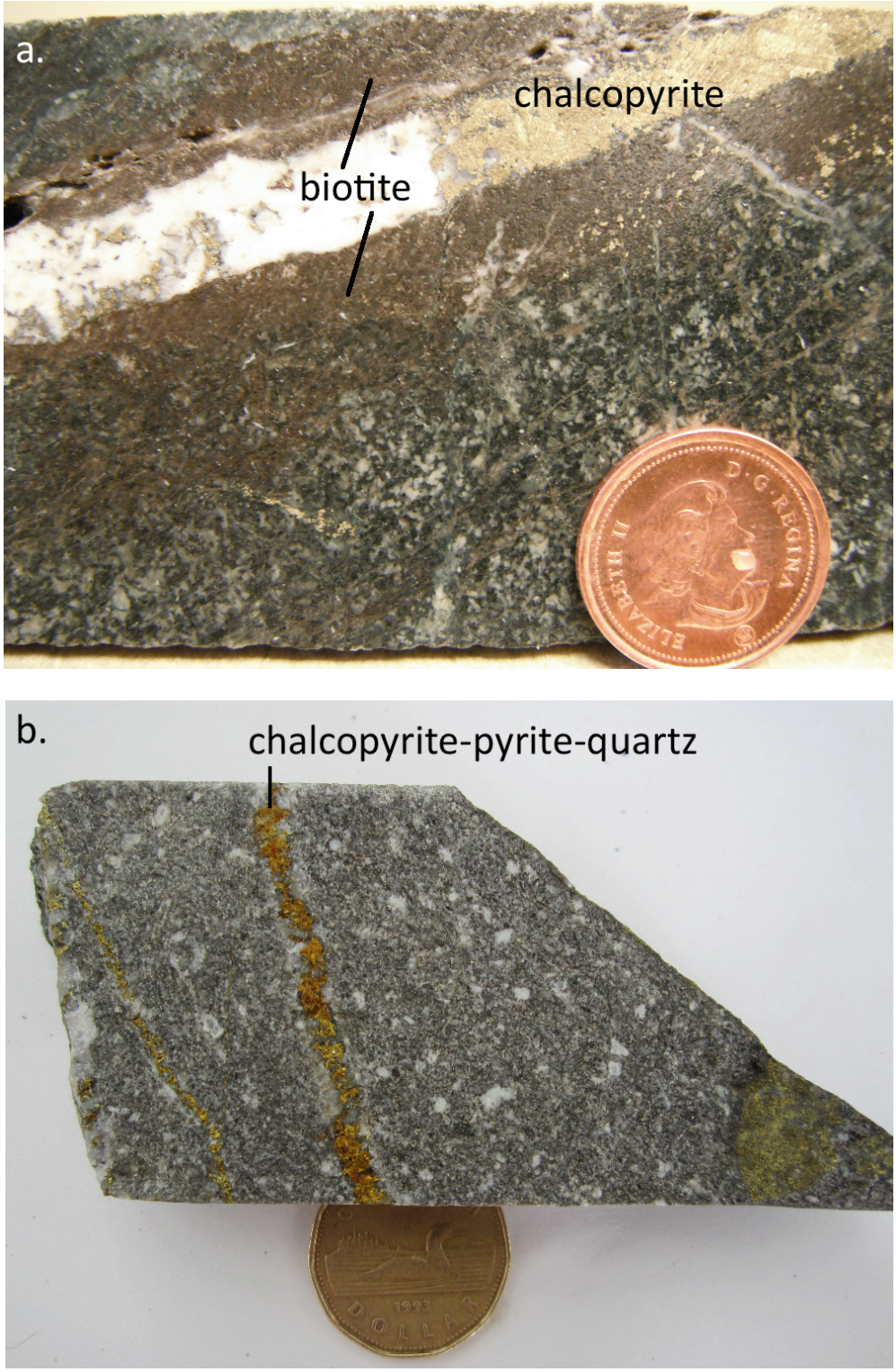

Figure 31: Examples of Stage 3 mineralization and alteration: (a) Westcoast Complex diorite and a chalcopyrite-quartz-albite vein with a 1 cm thick selvage of secondary biotite. Fine-grained pyrrhotite also occurs with chalcopyrite as discrete mm-scale grains. (b) a chalcopyrite-quartz-pyrite vein in ADP dyke.

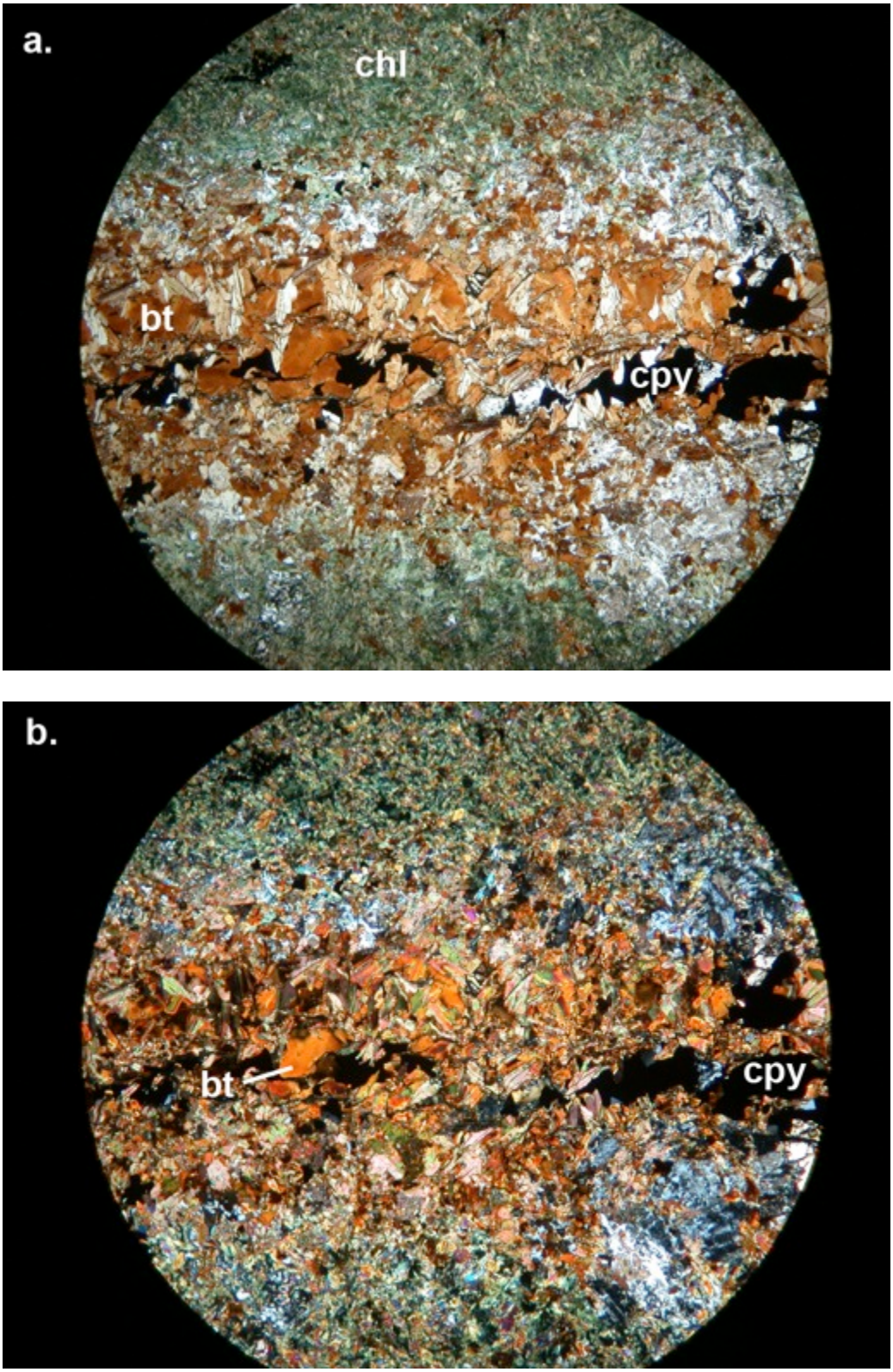

Figure 32: Thin section photographs of Stage 3 mineralization and alteration in (a) PPL and (b) XPL in sample of Karmutsen basalt, showing pervasive growth of secondary biotite along the margins of a chalcopyrite ±pyrrhotite vein (field of view is 4 mm).

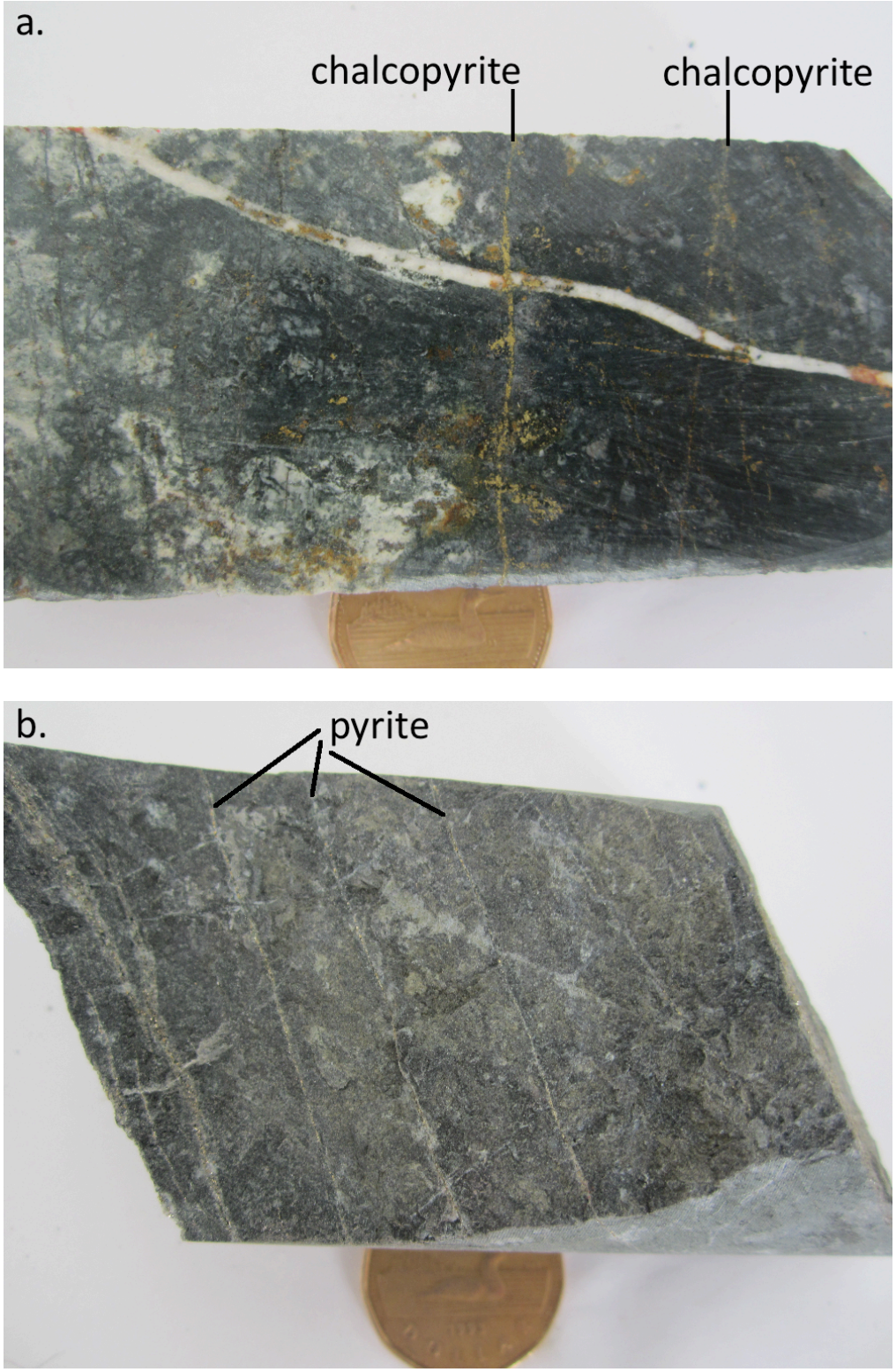

Figure 33: Examples of stages of mineralization and alteration, with (a) Stage 5 chalcopyrite stringers crosscutting a Stage 3 quartz-albite-chalcopyrite vein in sample of altered Karmutsen basalt, (b) several parallel Stage 4 pyrite stringers hosted in Karmutsen basalt.

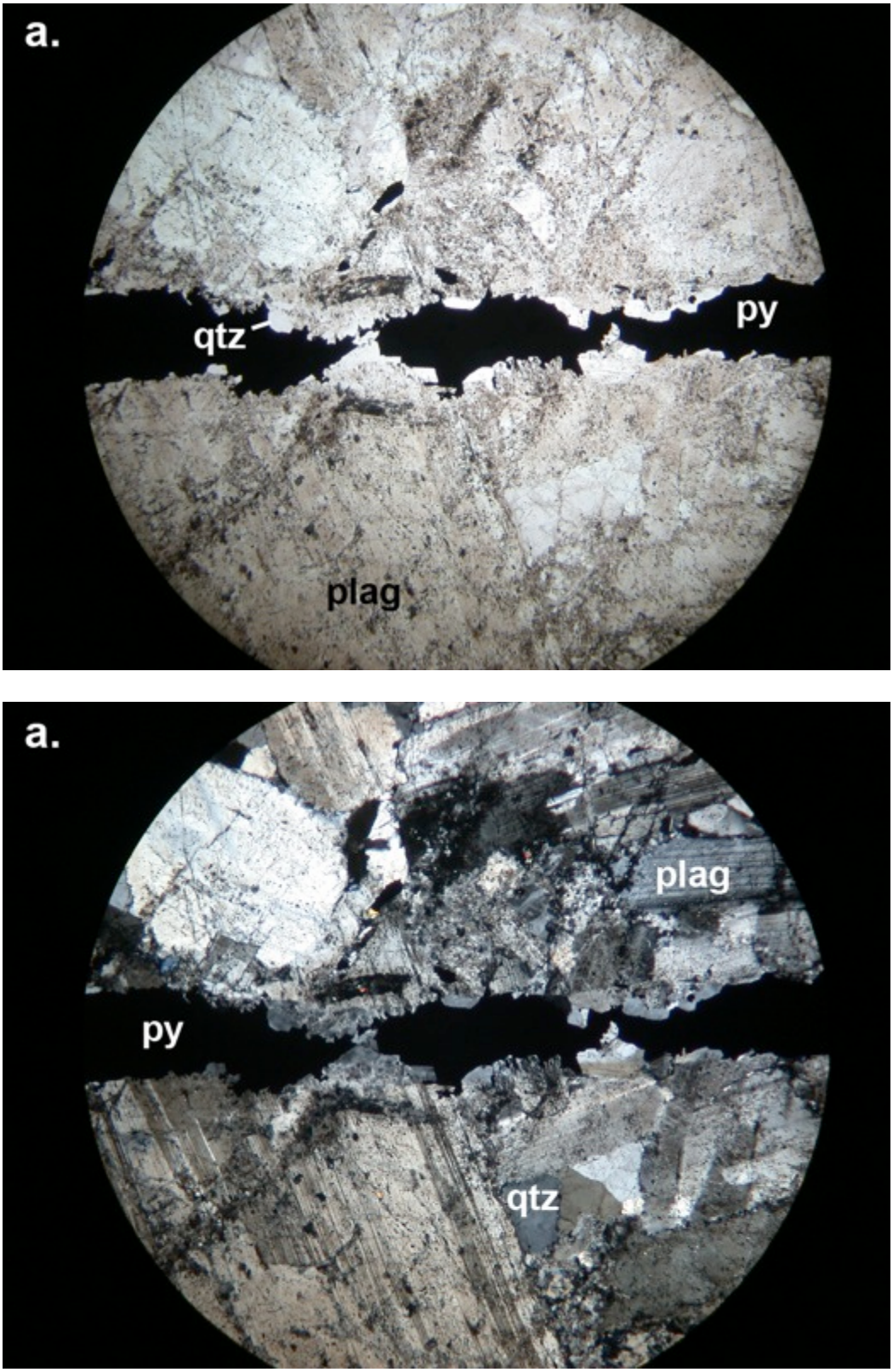

Figure 34: This section photographs of Stage 4 mineralization and alteration in (a) PPL and (b) XPL, characterized by millimeter to sub-millimeter scale sulphide stringer veins (field of view is 4 millimeters).

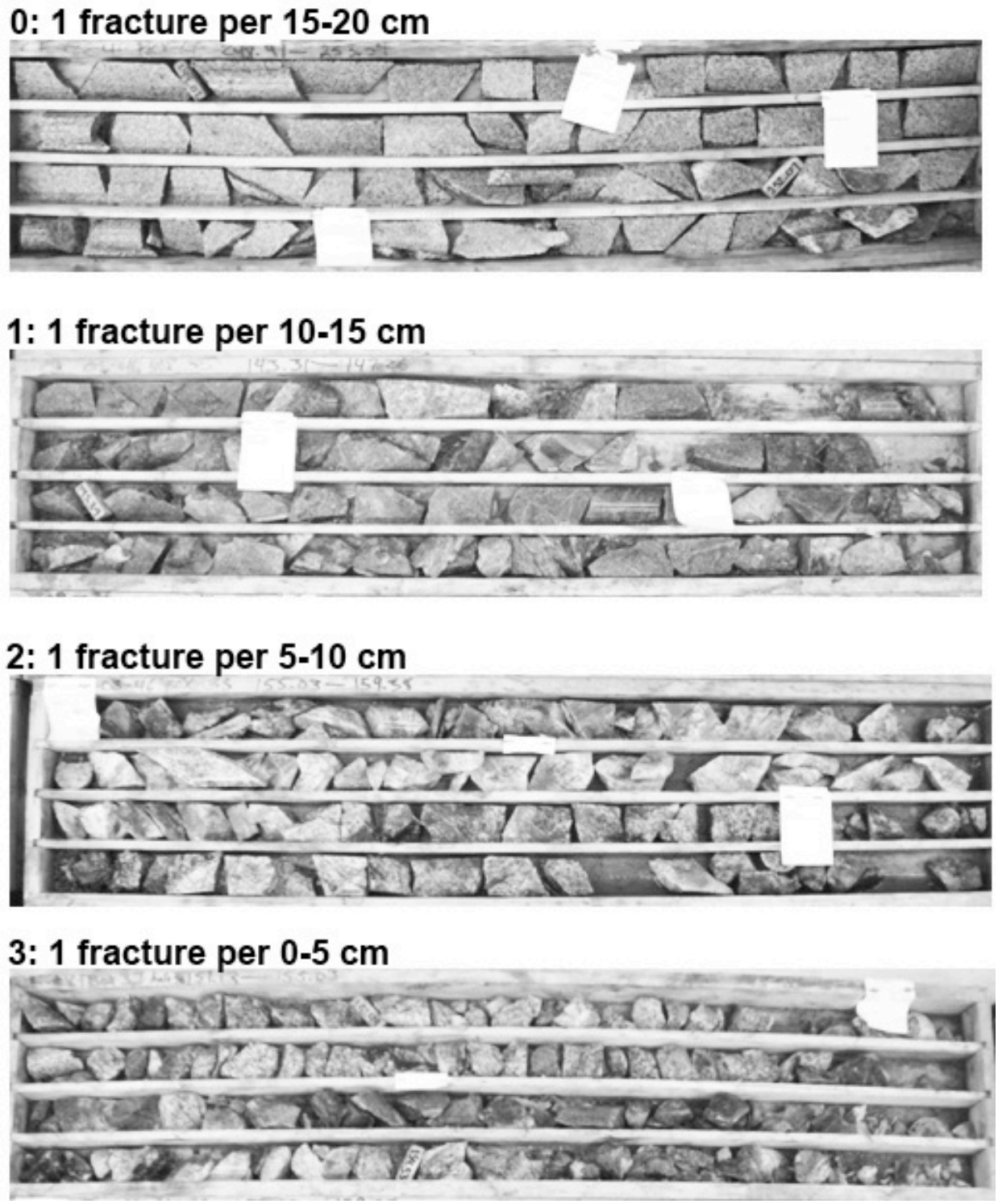

Figure 35: Boxes of core showing representative scale for relative fracture intensity based on number of fractures per unit length of drill core.

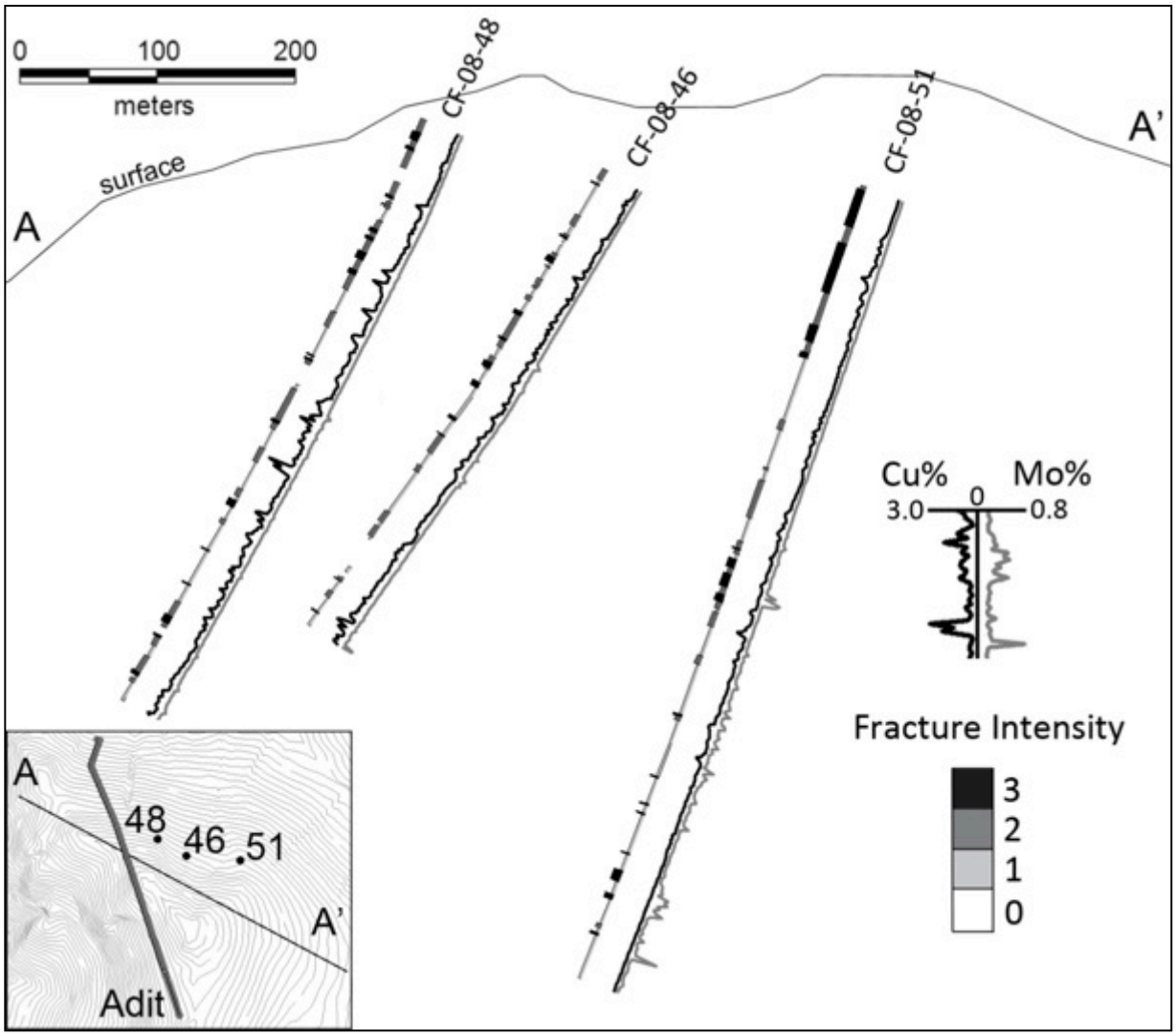

Figure 36: Cross-section of Catface porphyry deposit Cliff Zone showing Cu and Mo grades along drill cores and their association with a scale of fracture intensity.

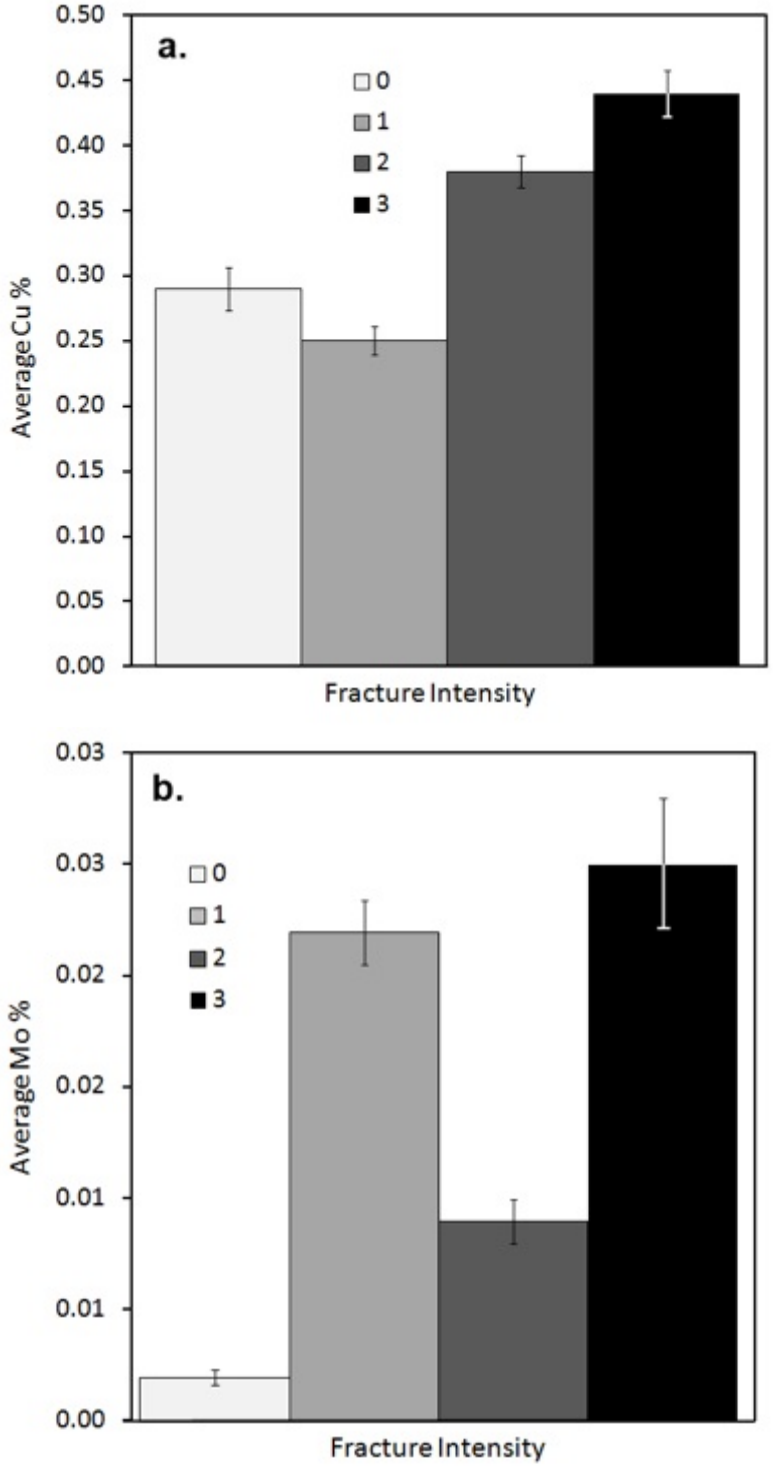

Figure 37: Average (a) Cu and (b) Mo grades versus relative fracture intensity for selected drill holes in the Catface porphyry deposit Cliff Zone.

structural emplacement of Catface are typical of porphyry deposits; however, the presence of hypogene pyrrhotite and absence of primary hematite and sulphate minerals suggest Catface was formed from reduced magmas. Mineralization and alteration paragenesis is summarized by four stages: progressing from main-stage quartz-albite-actinolite, quartz-actinolite-albite associated with Cu and Mo mineralization, to late-stage biotite-chlorite associated with Cu mineralization. A strong positive correlation between fracturing intensity and Cu grade is established.

Chapter 3
GEOCHRONOLOGY

3.1 Introduction

Geochronological studies of rock units and mineralization at the Catface deposit are completed to define the timing of magmatism and mineralization. The results will allow association of Catface magmas with one of the two suites of Paleogene magmatism on Vancouver Island defined by Madsen (2004) and further comparison with magmatic activity on nearby Vancouver Island and afar in the Cascade arc at North Fork. These geochronological data also test the validity of previous K-Ar ages reported by Muller and Carson (1969) and Muller (1974), and U-Pb, K-Ar, and Rb-Sr data reported by Isachsen (1987). Muller and Carson report a K-Ar age for the Hecate Bay quartz diorite of 48 ±12 Ma, and Muller reports an age of 192 ±9 Ma for Westcoast Complex elsewhere in the Alberni map area. The Richie Bay Pluton four km southeast of the Catface deposit on Meares Island has a U-Pb age of 41 ±1 Ma, and the Westcoast Complex Indian Island intrusion has a U-Pb age of 180 ±4 Ma (Isachsen, 1987).

Nine samples were selected for geochronology: seven for U-Pb in zircon, two Re-Os in molybdenite (Figure 5 and Figure 6). One of the Re-Os samples comprised vein-hosted massive molybdenite in Island Plutonic Suite, and the other comprised disseminated molybdenite in Catface Intrusion (Figure 38).

3.2 U-Pb Geochronology

U-Pb ages for zircons were determined at the University of British Columbia using methods described in Scoates and Friedman (2008). Concordia plots for U-Pb ages and errors for all analyses are reported at 2σ in (Figure 39). Five of the seven U-Pb samples were collected from NQ-sized drill core (in 1.5 m sections) and the remaining two samples were gathered from

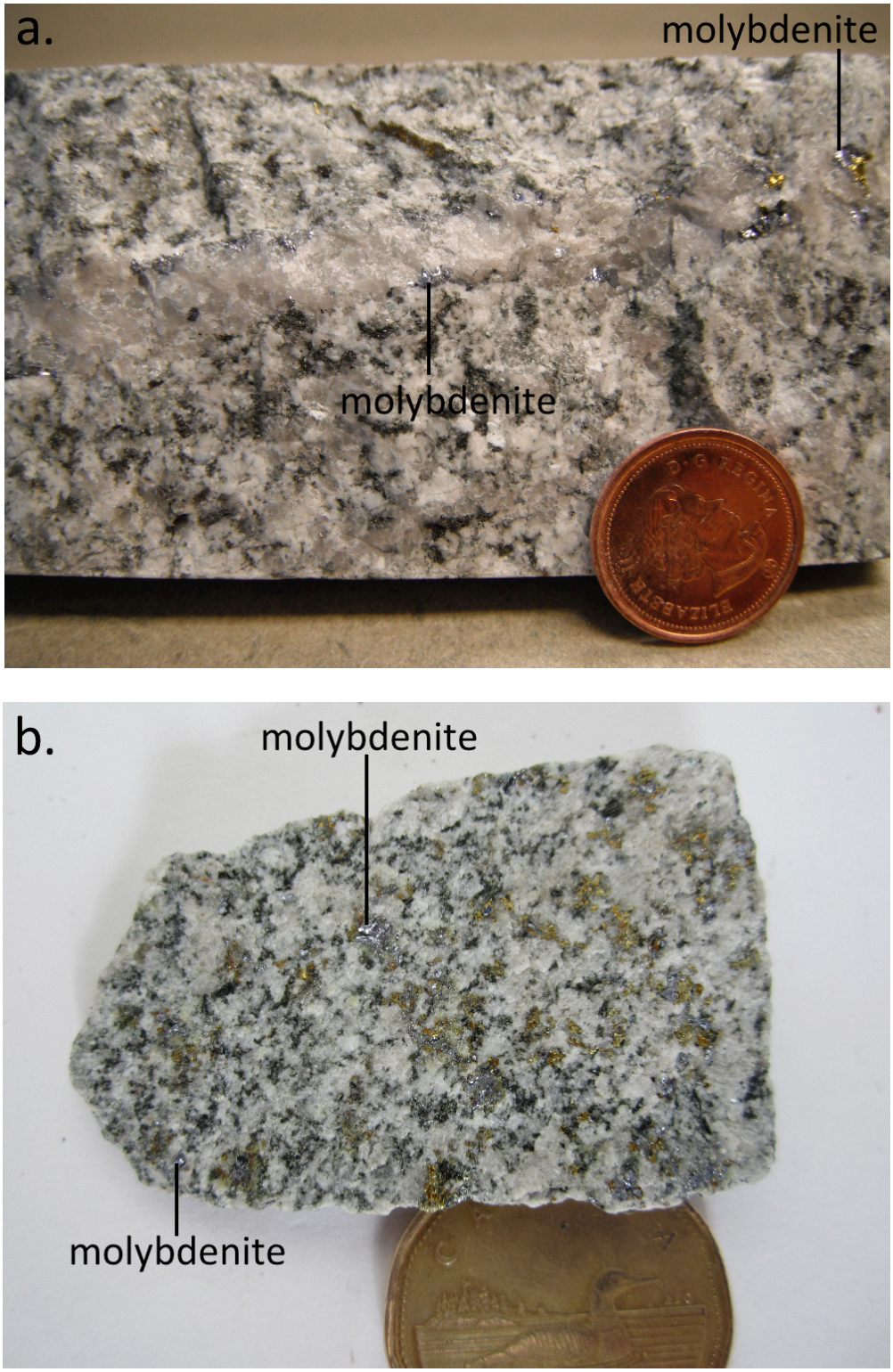

Figure 38: Hand samples showing two types of molybdenite mineralization dated using the Re-Os method: (a) 1 cm wide quartz-molybdenite-chalcopyrite vein in Island Plutonic Suite quartz diorite (CS10-108), (b) disseminated molybdenite in Catface Intrusion quartz diorite (CS10-119)

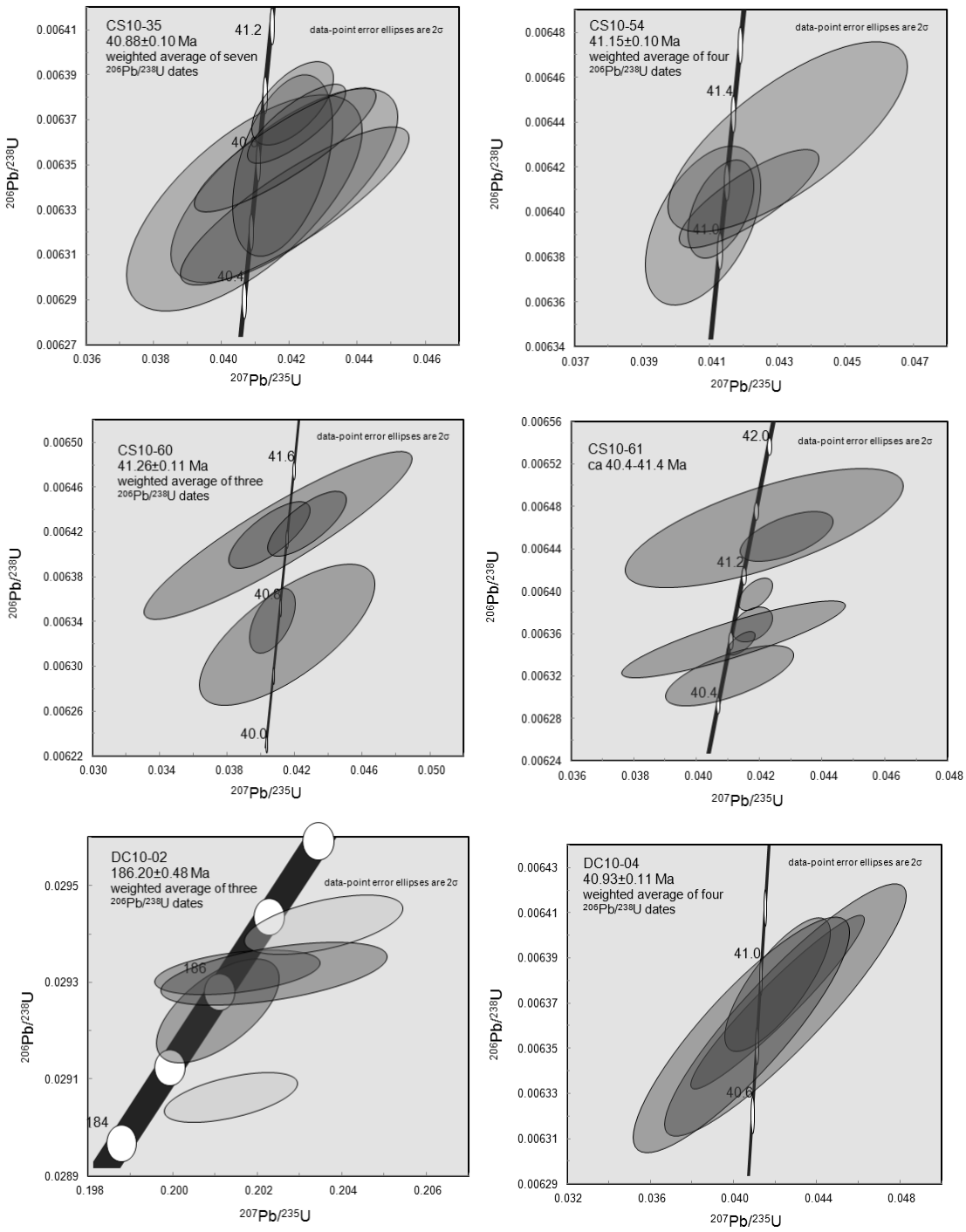

Figure 39: Concordia diagrams for U-Pb geochronology for samples from Catface deposit rocks, with error ellipses plotted at 2σ.

outcrop. All five different intrusive phases (Halo, Cliff, Catface, Hecate Bay, ADP Dykes) at the deposit were sampled (Appendix, Table A4 and A5). Five of the ages are within uncertainty of one another and suggest an age for all intrusive bodies of 41 Ma (Figure 40; Table 1). Sample CS10-61 was the only imprecise analysis, with a spread of data that ranged one million years. All interpreted ages, except for that of CS10-61, are based on weighted averages of $^{206}Pb/^{238}U$ dates for multiple concordant and age-equivalent zircon analyses from each sample.

Samples DC10-02 and CS10-109 returned unexpected ages of 186.20 ±0.48 and 184.46 ±0.41 Ma, respectively, and thus are unrelated to Paleogene intrusive activity of the Catface deposit, and belong to the Jurassic Island Plutonic Suite (Isachsen, 1987). The U-Pb ages at Catface of 40.4-41.4 Ma are identical to that of the Ritchie Bay Pluton, located four km SE of Catface on Meares Island (Isachsen, 1987). The ~41 Ma ages falls within the age range of the Mt. Washington Intrusive Suite defined by Madsen (2004) (Figure 41).

3.3 Re-Os Geochronology

Re-Os ages in molybdenite were determined by isotope dilution mass spectrometry at the University of Alberta using methods described by Selby and Creaser (2001), and Stein et al. (2007). Molybdenite (MoS_2) is naturally enriched in Re (^{187}Re) and contains insignificant nonradiogenic Os (^{188}Os) (Shelby and Creaser, 2001; after Morgan et al., 1968; Markey et al., 1998). As such, essentially all ^{187}Os in molybdenite is derived from the decay of ^{187}Re. Several studies have proven the Re-Os in molybdenite system to be resistant to hydrothermal, metamorphic, and/or tectonic resetting (i.e. Raith and Stein, 2000; Selby and Creaser, 2001; Bingen and Stein, 2003).

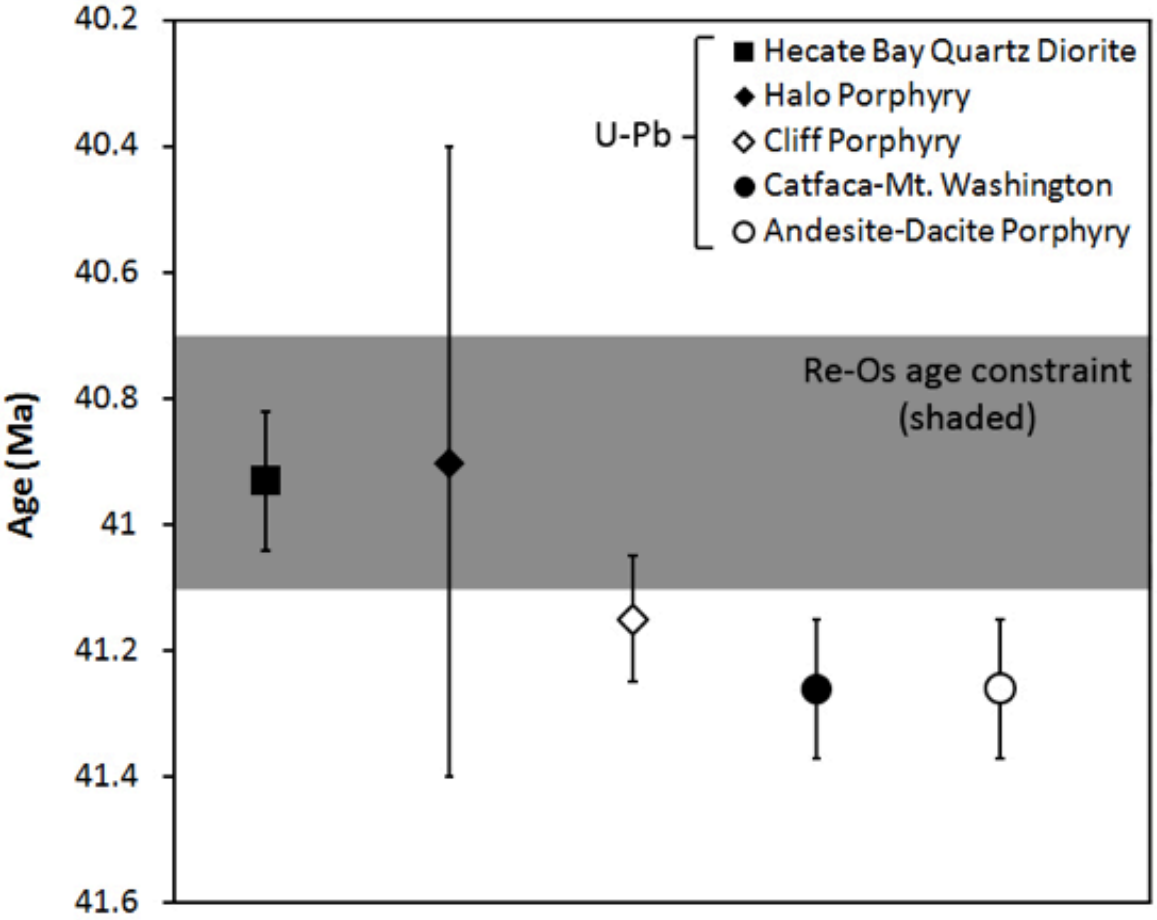

Figure 40: Summary of mean U-Pb and Re-Os ages for samples from the Catface Cu-Mo deposit with uncertainties.

Table 1: Summary of U-Pb and Re-Os Geochronological Results from the Catface Porphyry Deposit

Sample	Rock Name	Rock Type	Age (Ma)
DC10-04	Hecate Bay Quartz Diorite	Quartz Diorite	40.93 ±0.11
CS10-61	Halo Porphyry	Quartz Diorite	40.4-41.4
CS10-54	Cliff Porphyry	Quartz Diorite	41.15 ±0.10
CS10-35	Catface Intrusion	Quartz Diorite	41.26 ±0.11
CS10-60	ADP Dyke	Granodiorite	41.26 ±0.11
CS10-109	Island Plutonic Suite	Quartz Monzodiorite	184.46 ±0.41
DC10-02	Island Plutonic Suite	Quartz Diorite	186.20 ±0.48
CS10-108*	Island Plutonic Suite	Quartz Diorite	40.9 ±0.2
CS10-119*	Catface Intrusion	Quartz Diorite	40.9 ±0.2

*Re-Os in molybdenite date

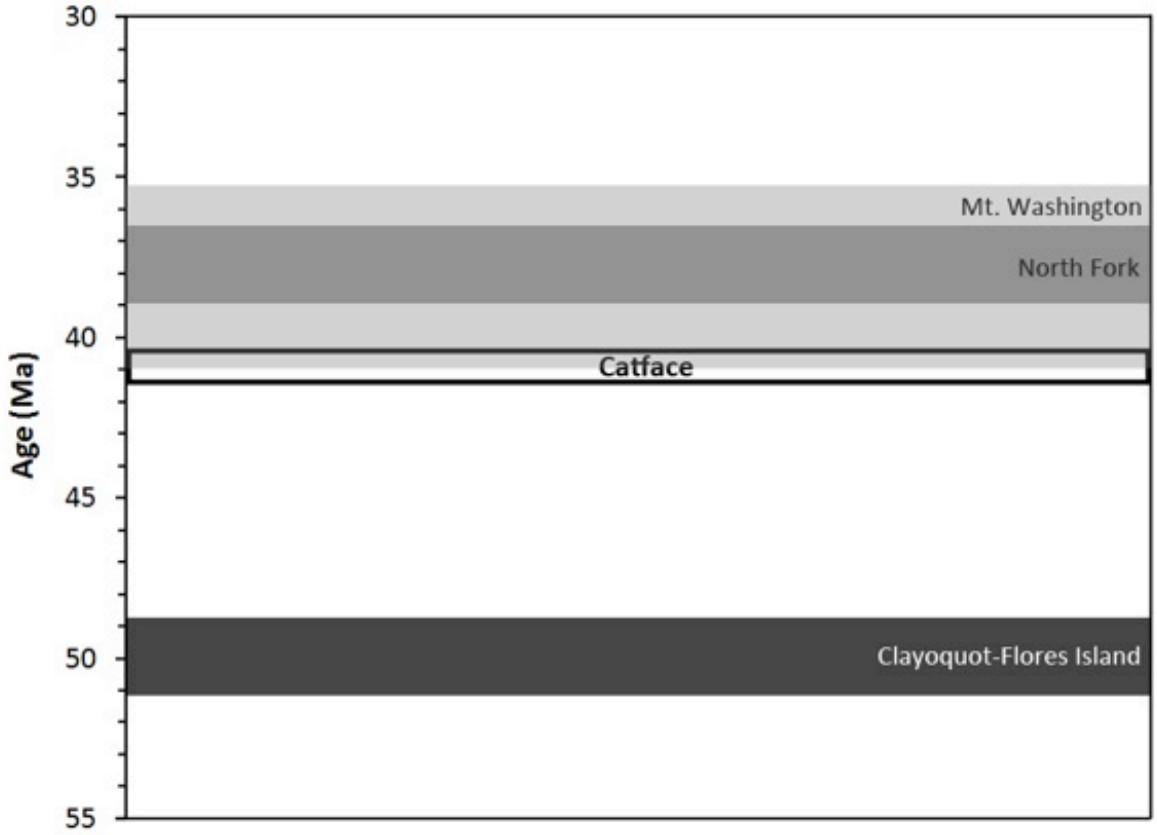

Figure 41: Comparison of ages for intrusive phases at the Catface porphyry deposit with the Mt. Washington and Clayoquot-Flores Island Suites, Vancouver island (Madsen, 2004; Madsen et al., 2006), and the North Fork porphyry deposit, Washington, USA (Smithson, 2004). Shaded regions represent age range including uncertainties.

Molybdenite in two samples from the Catface deposit was dated using the Re-Os method (Figure 38). One is a sample from Catface Intrusion (CF10-119) that hosts molybdenite as disseminated grains in a quartz-chalcopyrite-pyrite vein. The second sample (CS10-108) is from Jurassic Island Plutonic Suite country rock that hosts discrete blebs of molybdenite in a quartz-chalcopyrite-pyrite vein. The Re-Os ages for molybdenites in both samples were identical at 40.9 ±0.20 Ma (Figure 40; Table 1) and within error of U-Pb ages of all four intrusive phases at the Catface deposit.

3.4 Conclusions

U-Pb geochronological results from the Catface deposit confirm all four phases of intrusive activity are similar in age (~41 Ma) and belong to the Mt. Washington Intrusive Suite (Madsen, 2004). The results also confirm the presence of Jurassic Island Plutonic Suite country rock in the drill core. The Re-Os ages define a direct temporal correlation between magmatism and mineralization at 41 Ma. The Catface Intrusion and ADP Dykes were emplaced slightly before the onset of mineralization, indicating that the Halo Porphyry, Cliff Porphyry, or Hecate Bay quartz diorite is associated with mineralization at the Catface deposit.

Chapter 4
GEOCHEMISTRY AND MINERAL CHEMISTRY

4.1 Introduction

Whole rock geochemistry of Catface deposit rocks is assessed to characterize the composition of the intrusions and enable geochemical comparisons with other suites of Paleogene magmatism recognized in the Pacific Northwest. Trace element data is used to interpret petrogenesis of the magmas, and identify their possible source regions and affinity. Due to poor analytical quality, the data for precious and base metals (Au, Pb, Mo) was not used (Appendix, Figure A1 and A2). Mineral chemical data was collected in selected intrusive phases of Catface deposit rocks to (1) confirm the identity of mineral phases and (2) apply thermobarometers and oxybarometers for estimation of the pressure, temperature and fO_2 of the intrusions. Sulphate (SO_3) contents in apatites were analyzed to provide an independent study of magmatic oxidation state, as it has been shown that SO_3 in apatites increases with increasing fO_2 (Streck and Dilles, 1998; Peng et al., 1997; Parat et al., 2002; Imai 2002 and 2004).

Emplacement pressures, temperatures, and fO_2s for Paleogene Catface deposit rocks are estimated through Al-in-hornblende barometry, amphibole-plagioclase thermometry, and biotite-ilmenite oxybarometry, respectively. Thermobarometry of the Echo Lake intrusion (associated with the Mt. Washington Intrusive Suite) is assessed to allow for comparison with Catface deposit rocks. Oxybarometry of Paleogene Catface rocks serves to evaluate whether or not the Catface ore system is a reduced or oxidized porphyry copper deposit. Quantification of these intrinsic parameters enables a more thorough understanding of the geological conditions present during magmatism and mineralization, ultimately testing the affinity of Catface to the Cascade magmatic arc and associated porphyry deposits.

4.2 Geochemistry

Major and trace element abundances of 14 samples from the Catface porphyry deposit were determined at Acme Analytical Laboratories Ltd., Vancouver, British Columbia (Appendix, Table A6). Only the least-altered, homogeneous samples were selected. Samples were prepared by cutting away altered areas, crushing to pea-sized fragments in a jaw crusher, and then powdered using an agate mill. Major elements and loss on ignition (LOI) were obtained by XRF analysis of 12 g sample pulps. Trace element concentrations were determined by ICPMS on lithium metaborate and tetraborate fusion of 0.2 g samples followed by nitric acid digestion. A separate 0.5 g split sample was digested in aqua regia and analysed by ICP-MS to determine precious and base metal concentrations. Analytical precision was tested by submission of duplicate samples. Analytical accuracy was assessed by the comparison of values determined for rock standards. Results for precision and accuracy are illustrated in the Appendix (Figure A1 and Figure A2). Only elements that are reported in Figures were deemed to have precision or accuracy suitable for discussion.

4.2.1 Major Elements

All Paleogene intrusive phases at the Catface deposit are classified as quartz diorite or granodiorite when plotted on total alkali versus silica (TAS) plots (Figure 42). All rocks with the exception of the Cliff Porphyry are calc-alkaline (Low K) (Figure 43). The Catface rocks are weakly peraluminous (Andesite-Dacite Porphyry, Cliff Porphyry and Catface Intrusion) to moderately metaluminous (Halo Porphyry and Cliff Porphyry), with Aluminum Saturation Indexes (ASI) ranging 0.702-1.08 (Figure 44).

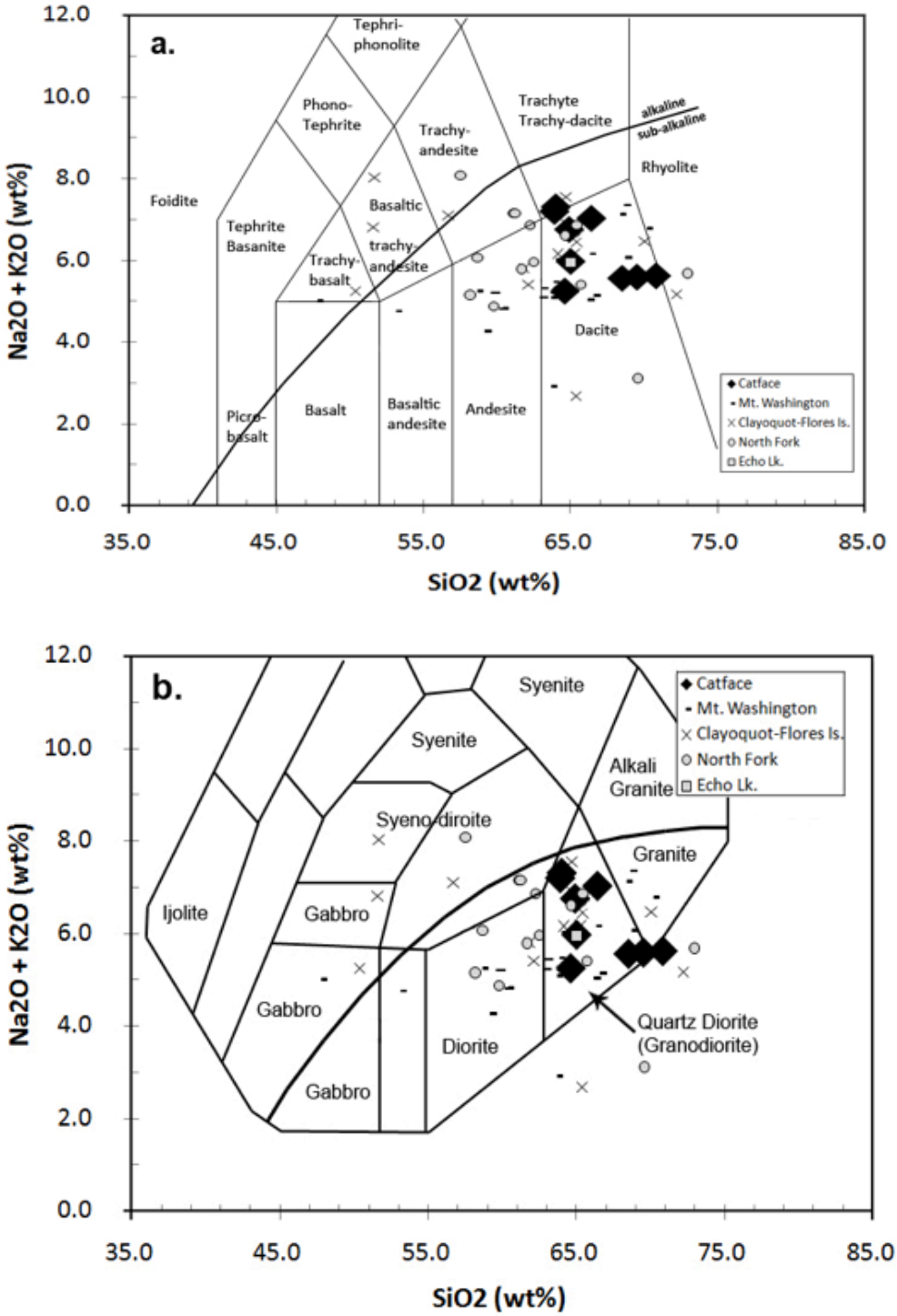

Figure 42: Total alkalis versus silica (TAS) plot for samples from Catface deposit compared with samples from North Fork, Echo Lake and other Vancouver Island samples (Madsen, 2004). Fields for rock classifications are for volcanic rocks in (a) (after Le Bas et al., 1986), and plutonic rocks in (b) (after Cox et al., 1979)

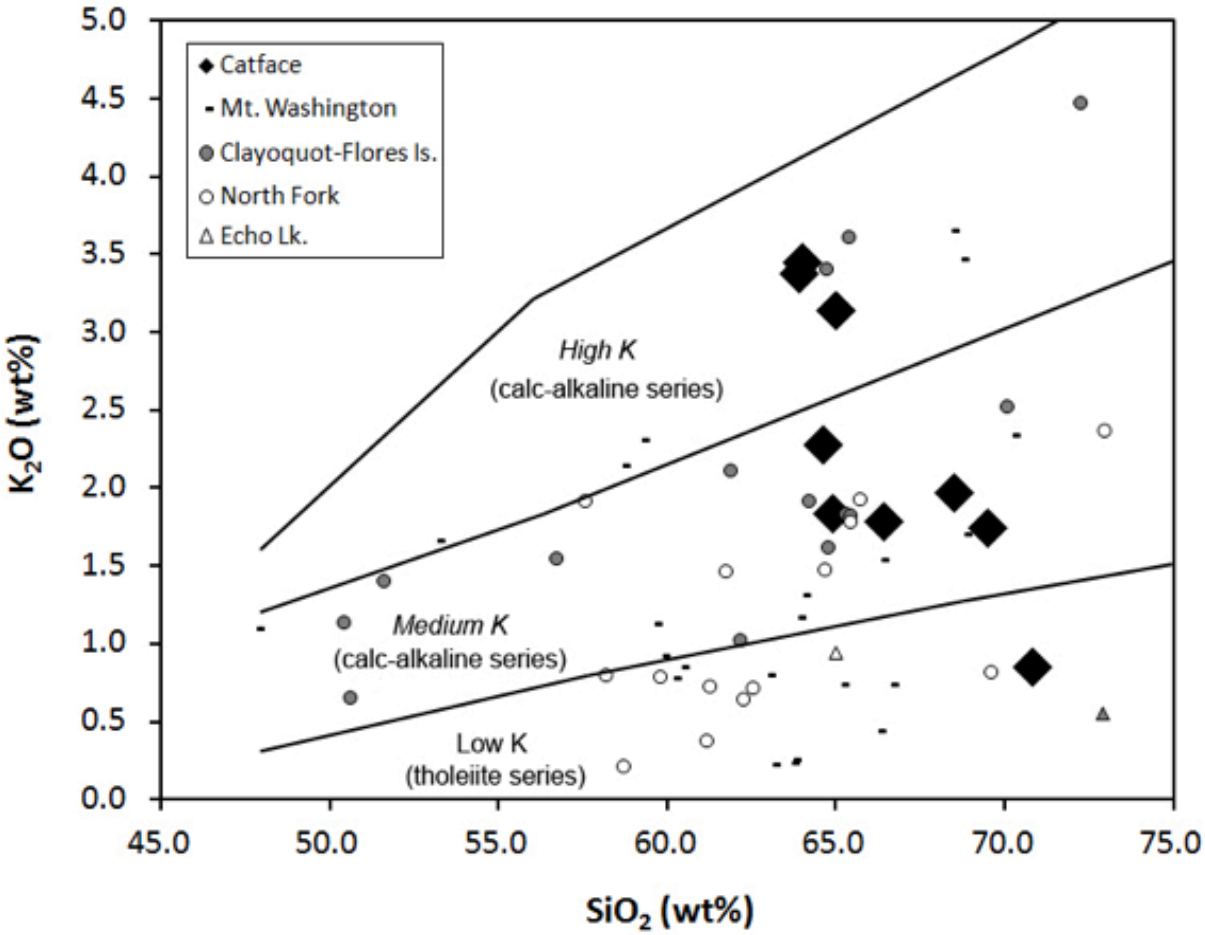

Figure 43: K_2O versus SiO_2 diagram showing samples of Paleogene Catface North Fork, Echo Lake and other Paleogene igneous rocks from Vancouver Island (Madsen) (fields after Gill, 1981).

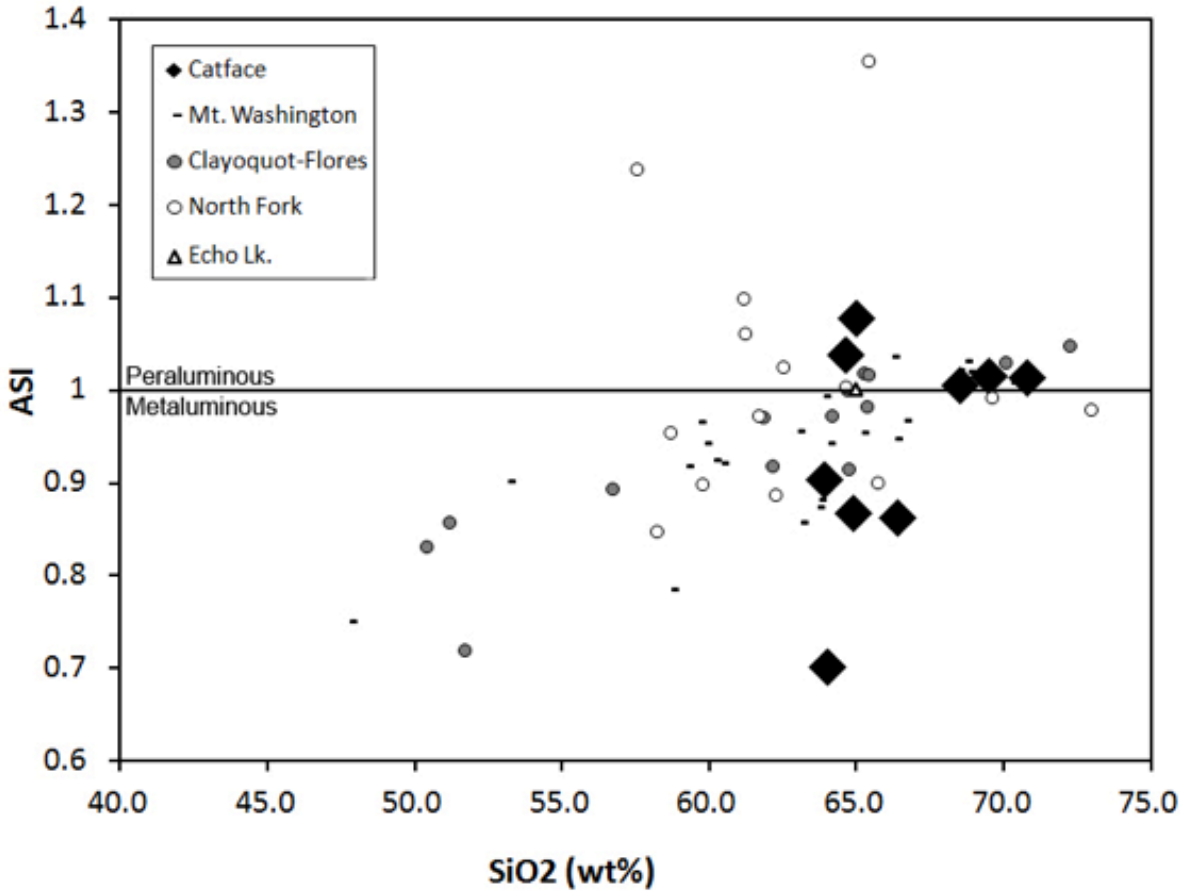

Figure 44: SiO_2 versus Alumina Saturation Index (ASI=molar Al/(Ca – 1·67P + Na + K))) for Catface, North Fork, Echo Lake and other Paleogene igneous rocks from Vancouver Island (Madsen) (Zen, 1986).

4.2.2 Trace Elements

On chondrite-normalized extended trace element diagrams, ("spidergrams"), Catface intrusions show patterns typical of arc magmas with negative Nb, Ti and P, anomalies and variable enrichments in Ba and Th (Figure 45; Nakamura, 1974; Thompson, 1982, Rock, 1987). There is considerable variation in K and Rb. On a Sr/Y versus Y (ppm) diagram, all but one sample plots in the (normal) calc-alkaline field, while the Cliff Porphyry (sample CS10-78) shows a weak association with the 'adakite' field (Figure 46, fields after Drummond and Defant, 1990).

4.3 Mineral Chemistry

Mineral chemistry was obtained for eight Paleogene samples from the Catface deposit and two samples from the Echo Lake intrusion for subsequent P-T-fO_2 calculations (Appendix, Table A7). The major and minor element mineral compositions were determined at the University of British Columbia, using a Cameca SX-50 Electron Microprobe. Operating conditions were 15 kV accelerating voltage, a beam current of 20 nA for amphibole and ilmenite, and a beam current of 10 nA for plagioclase feldspar, biotite, and apatite. All analyzed phases were primary and unaltered as confirmed from petrography. Only apatite grains greater than 70 microns in length were analyzed. Amphibole, plagioclase, and apatite were assessed for compositional zoning with core-to-rim analyses.

4.3.1 Amphibole

The majority of amphiboles at Catface are magnesiohornblendes, although one sample from the Halo Porphyry intrusion is tschermakite (Figure 47). Hornblendes in the Halo Porphyry intrusion have the lowest Fe# (Fe/Fe+Mg), and are enriched in Al, Mg and Na, relative to the other phases. Amphiboles vary in Al content from an average of 3.55-5.37 weight

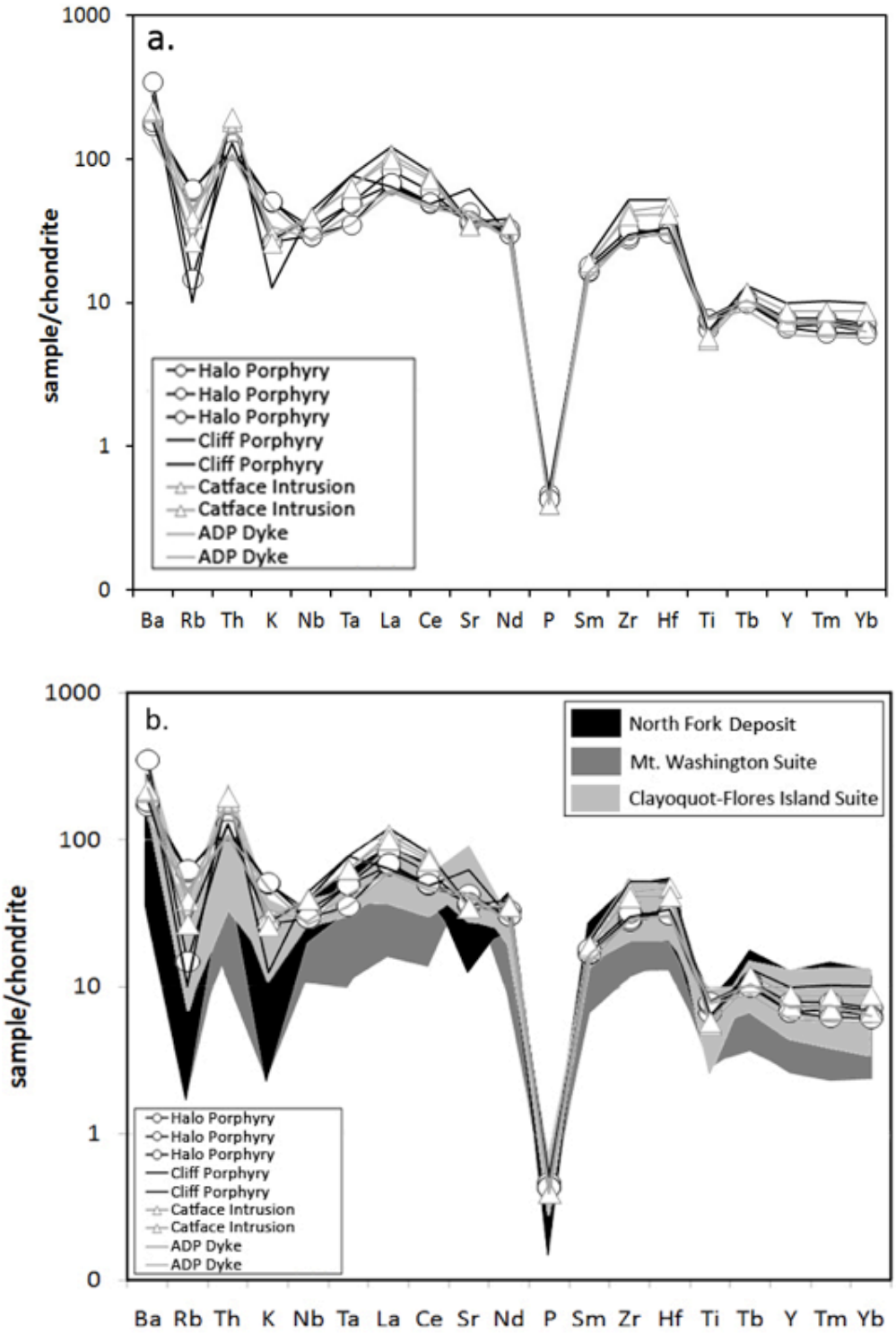

Figure 45: Chondrite-normalized spidergram plots for (a) Paleogene Catface deposit lithologies and comparison to (b) other Paleogene igneous rocks from North Fork, Washington and Vancouver Island (Madsen, 2004; Smithson, 2004).

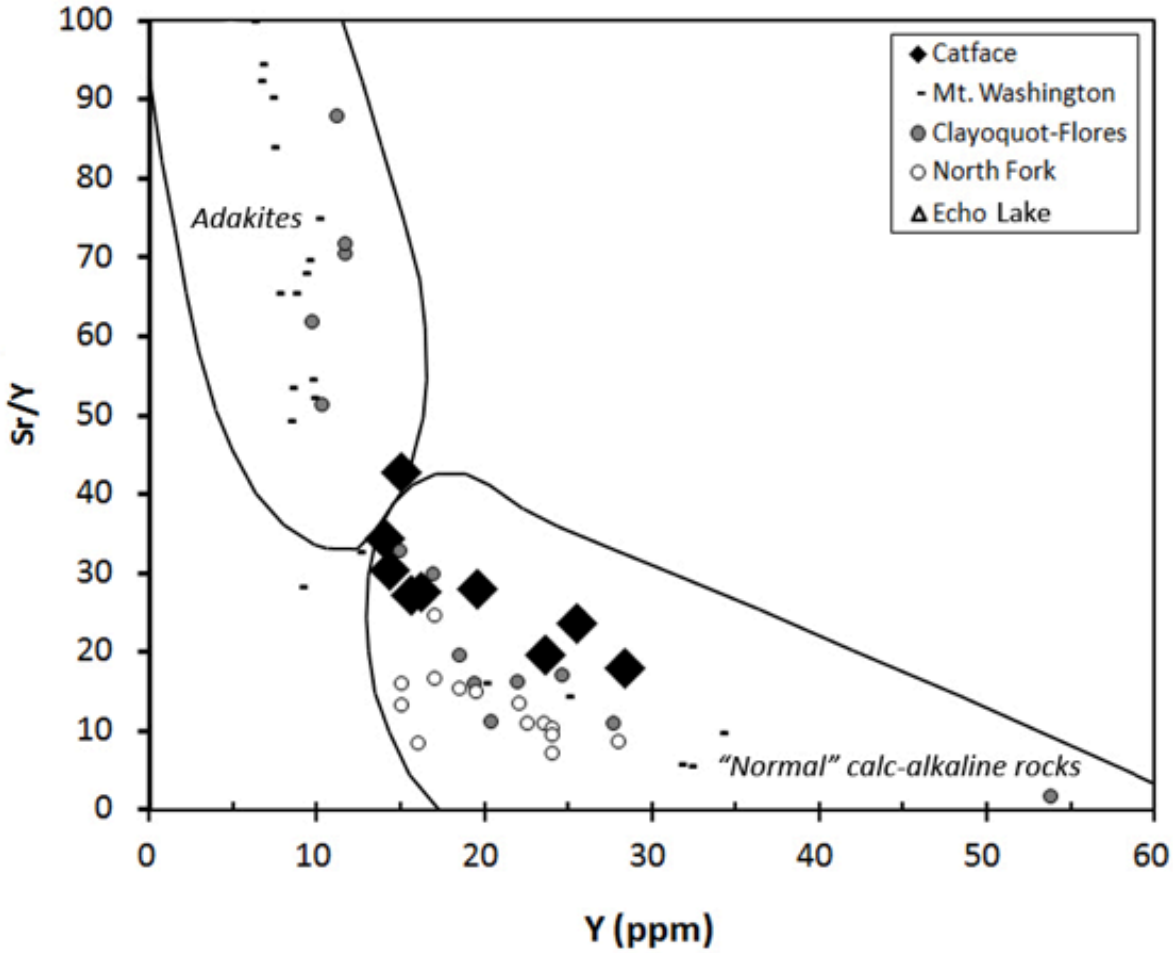

Figure 46: Sr/Y versus Y (ppm) diagram for Catface, North Fork, Echo Lake and other Paleogene igneous rocks from Vancouver Island (Madsen, 2004; Smithson, 2004) (fields after Drummond and Defant, 1990).

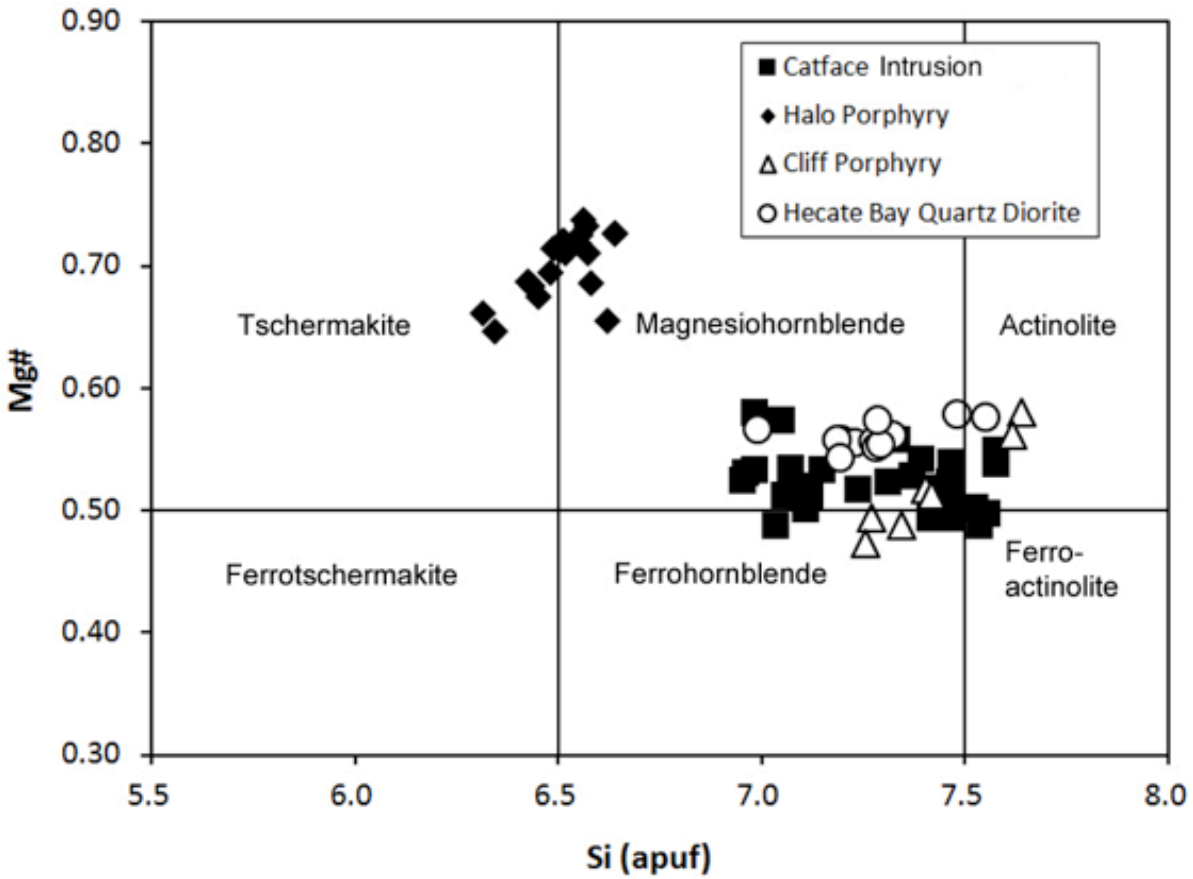

Figure 47: Amphibole classification diagram for intrusions from Catface deposit and Echo Lake (fields after Leake et al., 1997, Leake et al., 2004).

percent Al_2O_3 in the Catface Intrusion, Hecate Bay quartz diorite, and Cliff Porphyry, whereas the Halo Porphyry hosts Al-rich amphiboles that range 8.90-11.47 weight percent Al_2O_3. No significant intragrain compositional zonation in Mg# or Al is observed.

4.3.2 Plagioclase

Plagioclases from the Catface Intrusion have a wide range of anorthite content (X_{an}) from An_{61-18}, averaging An_{39}. The Cliff Porphyry and Hecate Bay quartz diorite have average anorthite components of An_{31-32}, and the Halo Porphyry is the most albitic with an average of An_{27}. The Halo Porphyry has the highest concentrations of Mg, Ca, Al, Mn and Fe and lowest concentrations of Na, Si and K of all samples. Plagioclase was altered and not analyzed in the ADP Dykes. Compositional zonation was subtle in most samples with increases (0.01-0.05) of anorthite content from core to rim (Figure 48).

4.3.3 K-Feldspar

K-feldspars were only analyzed in the Catface Intrusion and Cliff Porphyry lithologies, the orthoclase components (X_{or}) range is Or_{95-34} and Or_{94-93}, respectively.

4.3.4 Biotite

The Hecate Bay quartz diorite and Catface Intrusion samples have biotites with average Fe#'s of 0.56 and 0.57, respectively, whereas two analyses of Cliff Porphyry intrusion biotites yielded a higher average Fe# of 0.63. Average abundances of TiO_2 in the Hecate Bay quartz diorite, Catface Intrusion, and Cliff Porphyry are within 1 weight percent; however the largest range is observed in Catface Intrusion of 0.85-4.96 weight percent TiO_2. The Cliff Porphyry sample was an average of ~4 weight percent less siliceous (SiO_2) and ~2 weight percent less potassic (K_2O).

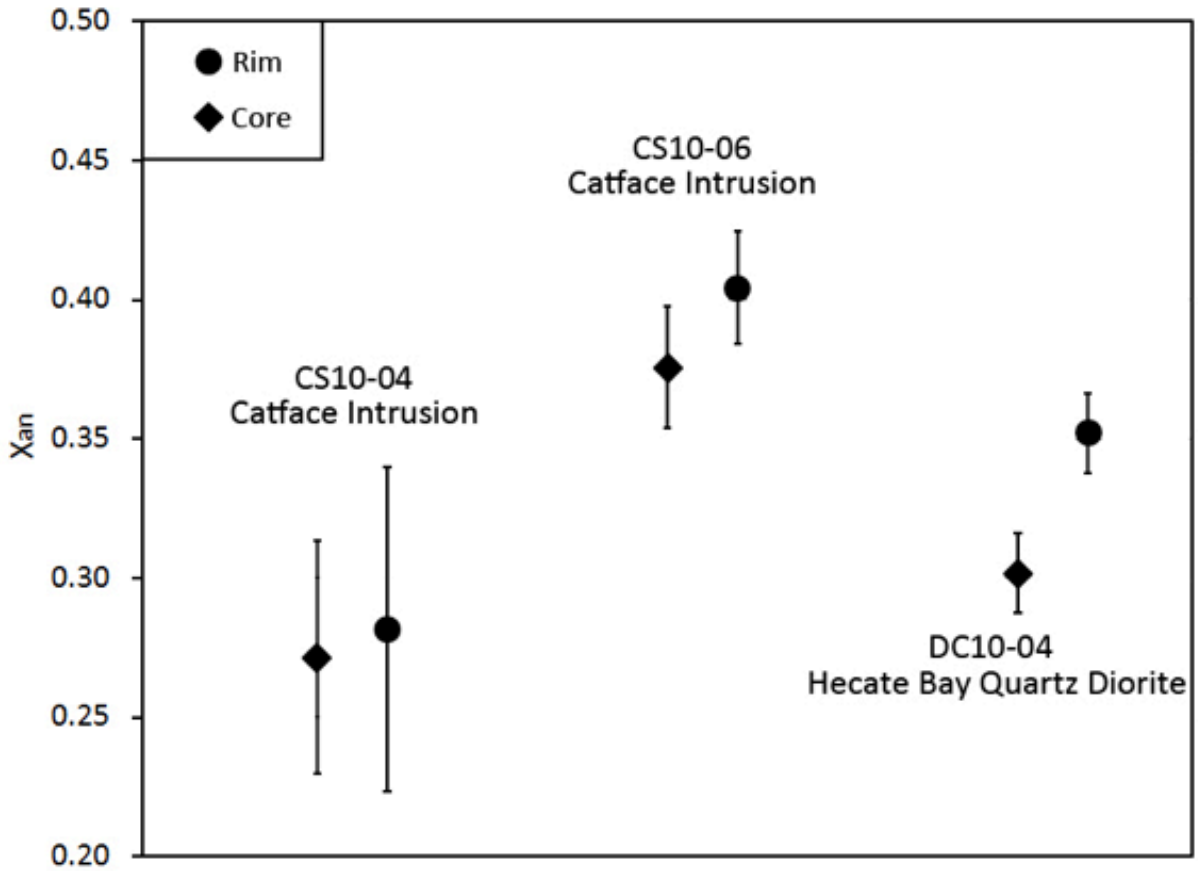

Figure 48: Comparison of core and rim compositions in plagioclase feldspars for intrusions from the Catface deposit.

4.3.5 Fe-Ti Oxides

Ilmenites are mostly hematite-ilmenite solid solutions. The hematite components (X_{hem}) of ilmenite grains were calculated according to stoichiometry using QUILF (Anderson, 1993). The Catface Intrusion ranges $X_{0.1-0.01}$ with an average of $X_{0.05}$ and the Hecate Bay quartz diorite ranges $X_{0.04-0.09}$, with an average of $X_{0.06}$.

Magnetite grains are Fe_3O_4 with less than 2% ulvospinel (Fe_2TiO_4) component.

4.3.6 Apatite

Analysis of apatite grains 70 to 200 µm in diameter examined the core-rim compositional zoning of SO_3 (e.g. Streck and Dilles, 1998; Peng et al., 1997; Parat et al., 2002). No systematic zonation is observed, and SO_3 concentrations were below detection limit (<450 ppm) in all analyses for the Paleogene Catface intrusives (Figure 49). Two samples (Catface Intrusion and ADP Dyke) yielded SO_3-depleted cores and the other two samples (Catface Intrusion and Hecate Bay quartz diorite) yielded SO_3-enriched core; however these estimations challenge analytical precision and should be considered with caution (detection limit ~450 ppm or 0.045 weight percent SO_3). In all four samples, an increase in Cl concentration is observed in the core of grains. In a plot of SO_3 versus Cl (in weight percent), the Catface samples are at the low end of a positive trend of data from the Imai sample suite (Figure 50; fields after Peng et al., 1997).

4.4 Thermobarometry

Mineral chemical data are used to estimate temperatures and pressures during emplacement of the Paleogene Catface intrusions. Pressures are calculated using the Al-in-hornblende geobarometer (Hammarstrom and Zen, 1986; Hollister et al., 1987; Schmidt, 1992; Anderson and Smith, 1995; Anderson, 1996; Anderson et al., 2008), and temperatures are

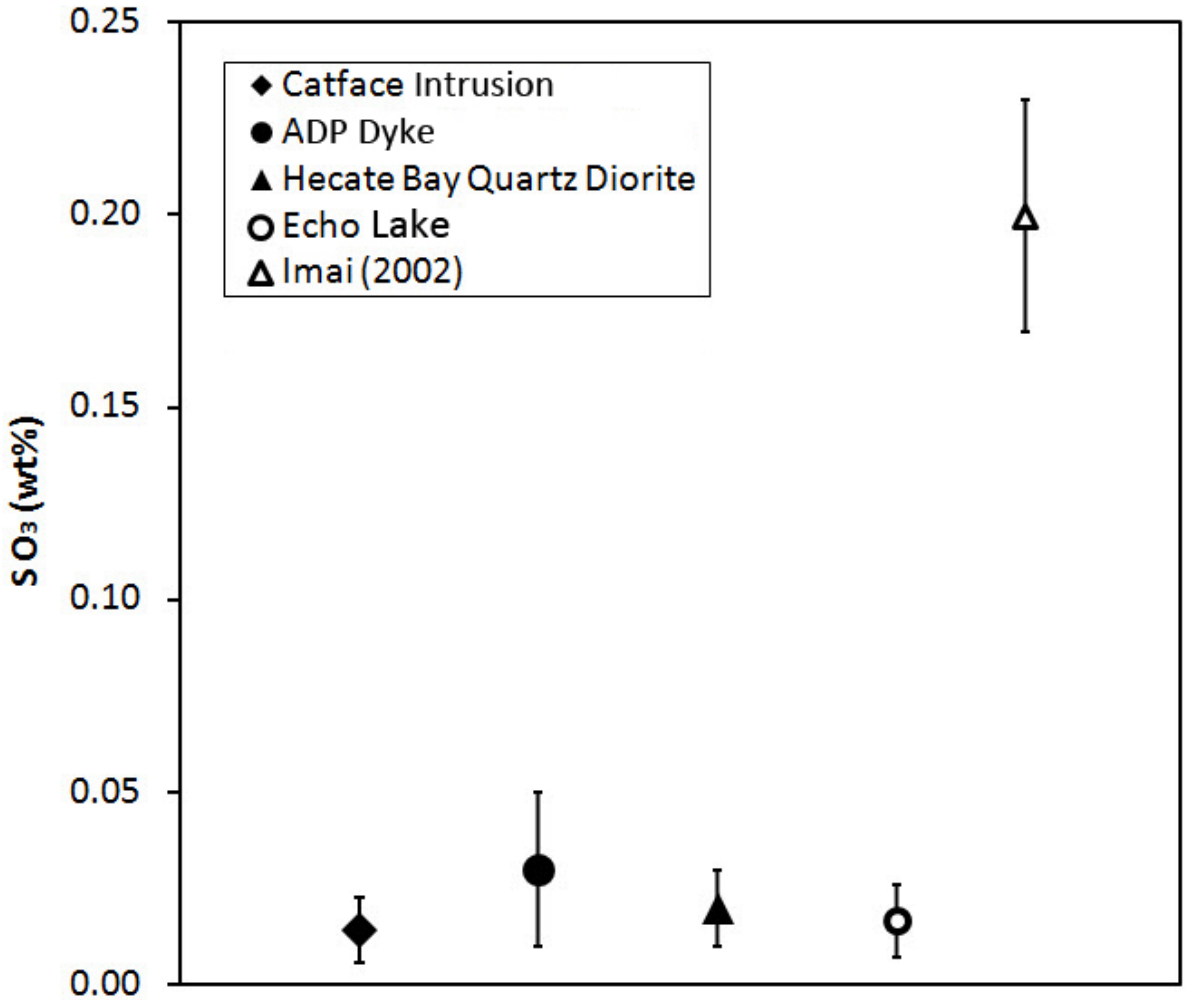

Figure 49: SO_3 concentrations in apatite for samples from Catface and the Echo Lake intrusion. Also shown are typical samples from porphyry copper deposits (Imai (2002)

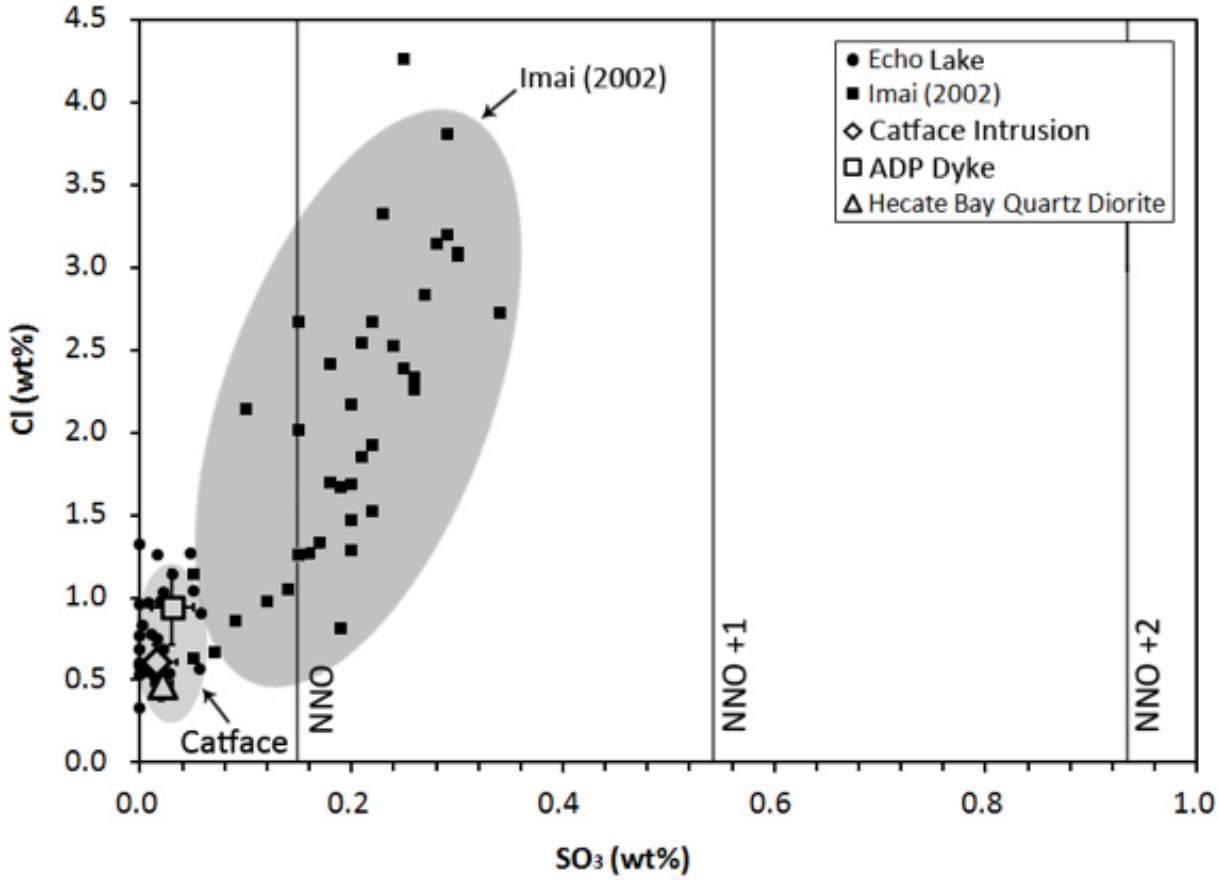

Figure 50: SO_3 verses Cl (weight percent) for apatites from Paleogene Catface rocks, compared to similar data from Echo Lake and a compilation in Imai (2002) fro other porphyry deposits. Vertical lines are minimum SO_3 thresholds for apatites in granitic liquids equilibrated at various oxygen fugacities (given in log units relative to the Nickel-Nickel-Oxide (NNO)) (Peng et al., 1997).

evaluated by application of the amphibole-plagioclase geothermometer (Blundy and Holland, 1990; Holland and Blundy, 1994). These two techniques are used simultaneously in the algorithm of Anderson et al (1996). Only lithologies that contain the required mineral assemblages (quartz-K-feldspar-plagioclase-biotite-hornblende-titanite-Fe Ti oxide) were selected for thermobarometry, as confirmed by thin section petrography.

4.4.1 Al-in-Hornblende Barometry

Total Al contents of hornblende in atoms per unit formula (Al^{tot}) increases linearly as a function of pressure. This barometer has been calibrated experimentally (Johnson and Rutherford, 1989; Thomas and Ernst, 1990; Schmidt, 1992) and empirically (Hammarstrom and Zen, 1986; Hollister et al., 1987) for the assemblage quartz + alkali feldspar + plagioclase + hornblende + biotite + Fe-Ti oxide + titanite + melt + fluid, at pressures of 2.5-13 kbar (250-1300 MPa) and temperatures of 655-700 °C (Anderson and Smith, 1995). As such, the Al-in-hornblende system offers a potential method for estimating crystallization pressures for granitic intrusions.

Potential pitfalls of this barometer include its dependence on plagioclase composition, temperature and oxygen fugacity (Poli and Schmidt, 1992; Rutherford and Johnson, 1992; Hammarstrom and Zen, 1992). Applying the Al-in-hornblende to plagioclase with anorthite contents higher then An_{35} can increase Al^{tot} independent of pressure, resulting in an overestimate of P. Consequently, Anderson recommends use of this barometer with plagioclase compositions within the range of An_{25-35}. Temperature can increase the Al content in hornblendes, and higher temperature plutons will host hornblendes with increased Al^{tot} (Anderson, 1995), an effect of up to 2 kbar per 100 °C. In low-fO_2 plutons, pressures can be overestimated by a factor of two or more (Anderson, 1995). Low-fO_2 granitoids have

hornblende Fe/(Fe+Mg) that exceed the 0.40-0.65 range used most experimental calibrations. Moreover, hornblendes in such reduced granitoids are enriched in Fe^{2+} versus Fe^{3+}, leading to anomalously Al-rich hornblendes and erroneously high pressures. It is therefore recommended that this barometer be only applied to granitoids with fO_2's above QFM oxygen buffer and Fe/(Fe + Mg) rations less than 0.65 (Anderson, 1995).

4.4.2 Amphibole-Plagioclase Thermometry

The exchange equilibrium of $(Na\square_{-1})^{A}(AlSi_{-1})^{T1}$ between amphibole and plagioclase is calibrated to estimate temperature using variations in the abundance of tetrahedral aluminum (Al^{IV}) in hornblende (Spears 1980, 1981; Nabelek and Lindsley, 1985; Blundy and Holland, 1990; Holland and Blundy, 1993). Tetrahedral aluminum is shown to constitute the majority of Al in synthetic and natural hornblendes, and linear correlation exists in plots of Al^{IV} versus temperature (Blundy and Holland, 1990). The coexistence of amphibole with plagioclase in silica-saturated rocks is required for amphibole-plagioclase thermometry, and Holland and Blundy (1993) recommend use of this system only with plagioclase less calcic than An_{92}, and with amphiboles with less than 7.8 Si atoms per unit formula. The calibration by Holland and Blundy (1993) takes into account non-ideal mixing in both plagioclase and amphibole, allowing for temperature estimates with an uncertainty of ±40 °C in the range of 400-1000 °C and 1-15 kbar.

4.4.3 Results

Pressures and temperatures estimated for the Catface intrusive phases are summarized in Figure 51 and Table 2. Only samples that meet the criteria detailed by Anderson (1995) are plotted, whereas the full dataset for other samples is included in the Appendix (Table A8). Results vary within the Paleogene Catface lithologies, and the validity of some of these

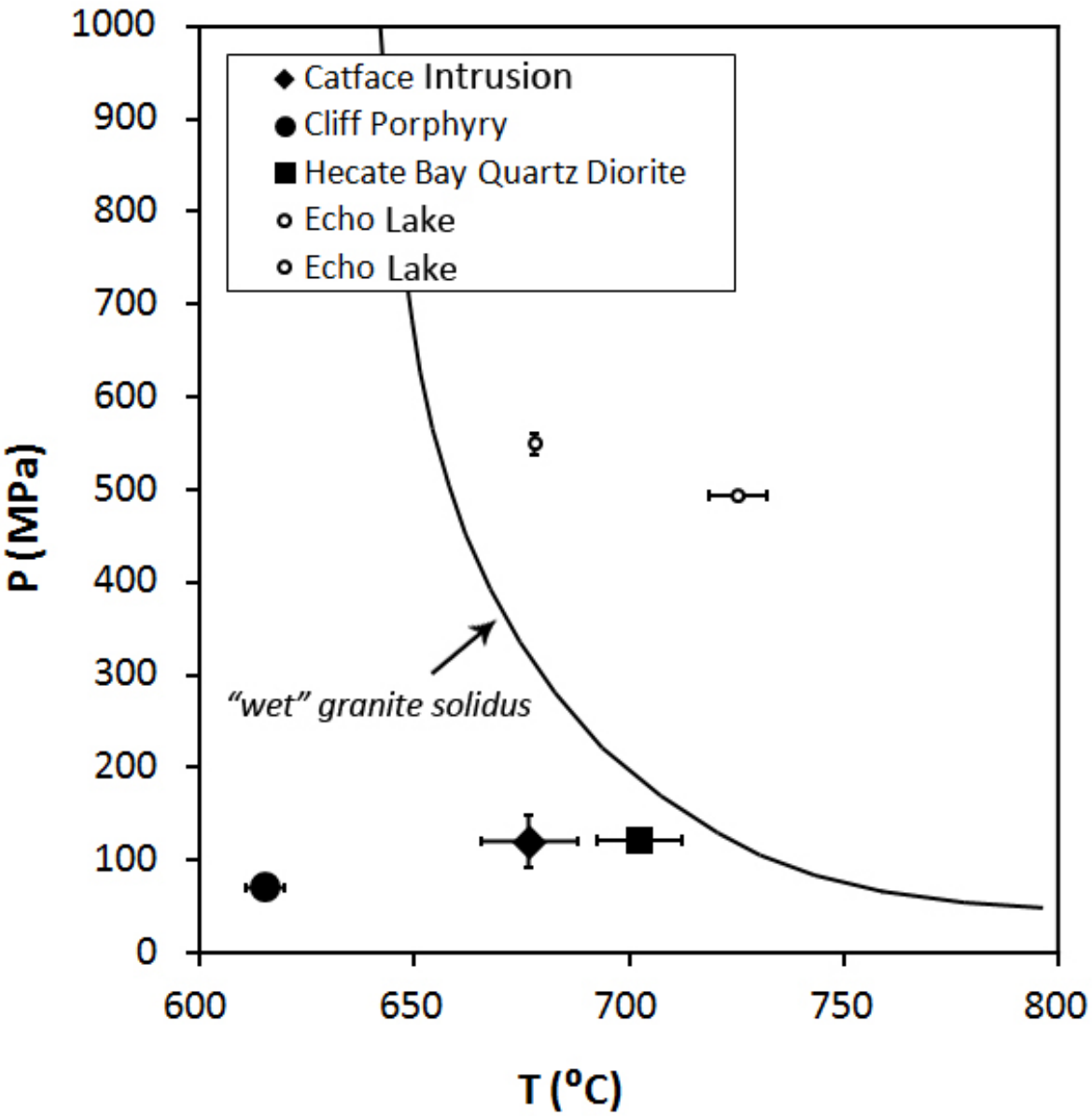

Figure 51: Pressures and temperatures estimated from Al-in-hornblende barometry and amphibole-plagioclase thermometry for samples from Catface and Echo Lake. Uncertainties are shown at 1 standard deviation. The "wet" granite solidus is after Naney (1983) and Piwinskii, (1968).

Table 2: Estimated Pressures and Temperatures for Catface and Echo Lake Samples from Al-in-Hornblende and Amphibole-Plagioclase Thermobarometry

Sample	**CS10-03 (Catface Intrusion)** *n = 6*		**CS10-31 (Cliff Porphyry)** *n = 2*		**DC10-04 (Hecate Bay quartz diorite)** *n = 3*		**Echo Lake (quartz diorite)** *n = 4*	
	AVG	ST DEV	AVG	ST DEV	AVG	ST DEV	AVG	ST DEV
T (°C)	677	22	615	9	702	20	702	29
P (Kb)	1.2	0.6	0.7	0.2	1.2	0.2	4	0
P (MPa)	120	58.5	70.6	16.4	121	22.6	400	35.1

Pressures (Anderson, 1995); Temperatures (Blundy and Holland, 1990; Holland and Blundy, 1994)

estimates can be questioned. Plagioclase compositions range An_{35-24}, and molar Fe/(Fe + Mg) ratios range 0.44-0.49, are consistent with recommendations of Anderson (1995). The calculated pressures for Catface intrusives are 70-120 ±60 MPa, and estimated temperatures vary 615-700 °C, with an average uncertainty in temperature is ±40 °C (Holland and Blundy, 1994; Anderson, 1995). Three samples plot below the water-saturated granite solidus. The Cliff Porphyry plots furthest from the solidus, and is likely untenable. Echo Lake samples yield a pressure range of 490-550 ±60 MPa and temperature range of 680-730 ±40 °C.

4.5 Oxybarometry

Qualitative assessment of the oxidation state of Catface intrusive phases can be made on the basis of Fe-Ti oxide mineralogy. The predominance of primary ilmenite over magnetite indicates a reduced oxidation state (Ishihara, 1977, 1981; Ague and Brimhall, 1988; Rowins, 2000a).

The magnetite-ilmenite oxybarometer developed by Buddington and Lindsley (1964) has proven problematic for plutonic rocks due to sub-solidus re-equilibration during slow cooling of magnetite (Wones, 1989). Wones and Eugster (1965) established that the annite (X_{Fe}) component in biotite is a function of fO_2 and temperature. Subsequent work developed the use of primary ilmenite-biotite pairs to estimate fO_2 conditions in reduced granitoids, demonstrating the resistance of ilmenite to change in composition upon cooling (Ague and Brimhall, 1988; Candela, 1989; McCoy et al.1997; Smithson, 2004). The compositions of coexisting primary biotites and ilmenites were applied to estimate T- fO_2 conditions of Paleogene Catface deposit rocks, using the equation:

$$\log fO_2 = 2 \log a^{ilm}_{hem} + {}^{4}/_{3}\log a^{feld}_{ksp} - {}^{4}/_{3}\log a^{biot}_{ann} - \log K + {}^{4}/_{3}\log a_{w}$$

of Ague and Brimhall (1988), where $a^{ilm}_{hem} = h\ X^{ilm}_{hem}$ and $\log h = (1332/T(K)) - 1.124$ (Nakada, 1983). Assumptions include: the activity of K-feldspar (a^{feld}_{ksp}) is 0.9 at 300 MPa (this is the pressure at which the equation was calibrated); the activity of water (a_w) is 1; and an ideal mixing model is used for calculating the activity of annite (Ague and Brimhall, 1988). Hematite components (X^{ilm}_{hem}) of ilmenites were calculated based on stoichiometry using QUILF (Anderson, 1993). The results are calculated at 300 MPa, and are plotted on a T-fO_2 diagram whereby the intersection with biotite and ilmenite isopleths defines the calculated T-fO_2 conditions of formation (Figure 38) (Candela, 1989).

4.5.1 Results

The K-feldspar-ilmenite-biotite assemblage coexists in the Catface Intrusion, Hecate Bay quartz diorite, and Cliff Porphyry intrusion. The Catface Intrusion and Hecate Bay quartz diorite have similar T-fO_2 results (QFM-2 at 900 °C), and the Cliff Porphyry is more reduced (QFM-3.5 at 900 °C). If one assumes the magmas crystallized at the temperatures estimated from amphibole-plagioclase thermometry (615-702 °C) the results range QFM-0.5 to QFM-1 (Figure 52, Table 3). The full list of oxybarometry calculations is included in the Appendix (Table A9).

4.6 Conclusions

Paleogene Catface intrusive rocks are calc-alkaline quartz diorite intrusions with trace-element patterns typical of arc magmas (Ti and Nb depletions). Catface deposit rocks display strong geochemical affinity to those associated with Paleogene magmatism on Vancouver Island (i.e. Mt. Washington Intrusive Suite) and in the Cascades (North Fork porphyry Cu-Au deposit). The ASI data show no affinity to S-type granitoids, and no slab melting or adakite signature is present in Sr/Y versus Y data for Catface rocks.

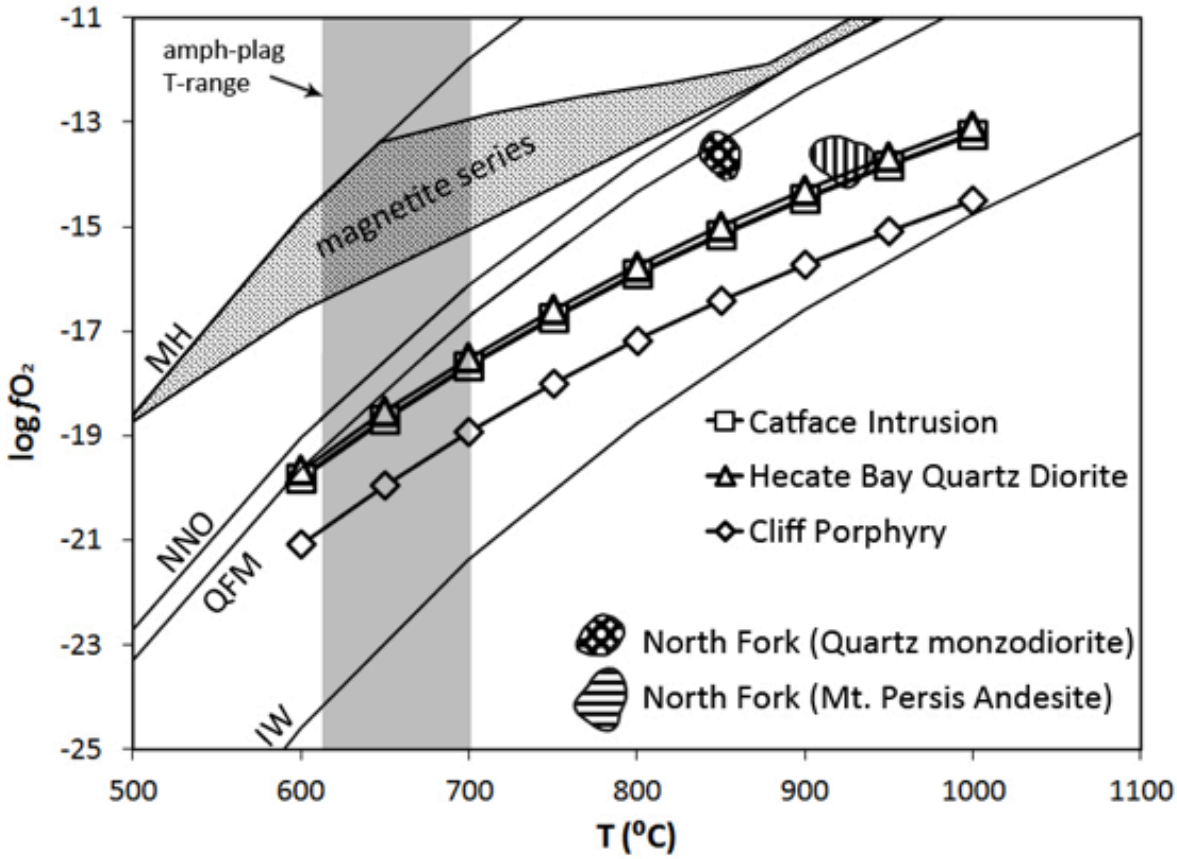

Figure 52: Temperature-fO_2 estimates at 300 MPa based on the assemblage Biot-Kspar-Ilm-Qz (Ague and Brimhall, 1988) for samples from three different intrusive phases of the Catface deposit. Shaded field is the range of temperatures from amphibole-plagioclase thermometry. Also shown for comparison are the fields for fO_2 estimates of magnetite-series granites (Ishihara, 1977; McCoy et al., 1997; Burnham et al., 1980) and the North Fork deposit (Smithson, 2004) Oxygen buffer abbreviations: MH (magnetite-hematite), NNO (nickel-nickel oxide), QFM (quartz-fayalite-magnetite), IW (iron-wustite).

Table 3: Calculated fO_2 at 300 MPa from Biotite-Ilmenite Assemblages in different intrusions at Catface Deposit

Temp (C)	**CS1001 (Catface Intrusion)** *n = 52*		**CS1031 (Cliff Porphyry)** *n = 2*		**DC1004 (Hecate Bay quartz diorite)** *n = 27*	
	AVG	ST DEV	AVG	ST DEV	AVG	ST DEV
600	-19.8	0.56	-21.0	0.28	-19.6	0.16
650	-18.6	0.56	-19.9	0.28	-18.5	0.16
700	-17.6	0.56	-18.9	0.28	-17.5	0.16
750	-16.7	0.56	-18.0	0.28	-16.5	0.16
800	-15.9	0.56	-17.1	0.28	-15.7	0.16
850	-15.1	0.56	-16.4	0.28	-15.0	0.16
900	-14.4	0.56	-15.7	0.28	-14.3	0.16
950	-13.8	0.56	-15.0	0.28	-13.6	0.16
1000	-13.2	0.56	-14.4	0.28	-13.0	0.16

(biotite-ilmenite oxybarometry after Ague and Brimhall, 1988; Candela, 1989)

Pressures and temperatures for Paleogene Catface rocks range 70-120 ±60 MPa and 615-700 ±40 ^{o}C, respectively, indicating emplacement conditions typical of porphyry deposits. Comparable temperatures are determined for the Echo Lake intrusion; however, pressures five times higher than Catface were evaluated for Echo Lake, suggesting the intrusion was potentially emplaced too deep to promote ore-forming hydrothermal circulation.

Oxygen fugacities from biotite-ilmenite oxybarometry for Paleogene Catface deposit rocks range QFM-0.5 to QFM-1, well below what is typical for oxidized porphyry copper deposits, and more reduced than the Cascadian North Fork deposit (Figure 48). These low fO_2's are in agreement with below detection limit contents of SO_3 in apatite, as well as the mineralogical presence of hypogene pyrrhotite and absence of primary hematite and sulphates. These results suggest that Catface a reduced porphyry copper deposit.

Chapter 5
DISCUSSION

5.1 Geology and Emplacement of the Catface Deposit

The four phases of Paleogene Catface magmatism are associated with the Mt. Washington Intrusive Suite, not the Clayoquot Intrusive Suite as previously suggested by Madsen (2004) and Madsen et al. (2006). Evidence includes the 40.4-41.4 Ma ages, the similar lithogeochemistry, and the identical age to the Ritchie Bay intrusion 41 ±1 Ma four km southeast of the Catface deposit (Figure 3). The presence of Jurassic Island Plutonic Suite in significant sections of the drill core was confirmed by geochronology, and a formerly unnamed 41.26 ±0.11 Ma intrusion, dissimilar in texture and morphology to other intrusions at Catface, is now termed the Catface Intrusion (Figure 6, Figure 19 and Figure 20).

The timing of ore deposition determined from Re-Os geochronology indicates a direct genetic tie between Paleogene magmatism and the main mineralizing event. The 40.9 ±0.2 Ma age of Mo mineralization establishes that, of the Eocene Catface intrusions, only the Hecate Bay quartz diorite, Cliff Porphyry, and Halo Porphyry units are potential mineralizing magmas (Figure 5 and Figure 6). The Hecate Bay quartz diorite is an unlikely candidate, given its distance from the main ore zones and weaker Cu grades, whereas the Cliff and Halo Porphyries are emplaced in the core of the Catface deposit. While the latter two phases are interpreted to be associated with the same pulse of magmatism, the presence of miarolitic cavities in the Halo Porphyry (Figure 17) is significant and distinct, and considered to represent direct evidence for volatile phase saturation in the magma (Richards, 1990; Frezzotti, 1992; Roedder, 1992; Candela, 1997; Kamenetsky 2002, Harris et al., 2004). Research has established that the compositions of minerals that grow in miarolitic cavities reflect the chemistry of the saturated

volatile phase, and in the case of the Halo Porphyry, the magmatic fluid phase was saturated in Cu and Fe sulphides (chalcopyrite and pyrite). For this reason, the Halo Porphyry intrusion is interpreted to be the mineralizing intrusion associated with the Catface ore system.

Pressures estimated from Al-in-hornblende barometry indicate a shallow plutonic setting of <4 km or <150 MPa (Figure 51). Epizonal emplacement of Catface is consistent with the presence of miarolitic cavities in the Halo Porphyry. This texture is restricted to epizonal granites intruded at less than 4 km depth and 100 MPa (Candela, 1997; Holm and Lux, 1998). Use of the Al-in-hornblende pressures to calculate depth results in over-estimates pressures for granitoids with fO_2 at or below QFM (Blundy and Holland, 1990; Poli and Schmidt, 1992; Hammarstrom and Zen, 1992; Rutherford and Johnson, 1992; Anderson, 1995). Paleogene Catface intrusives have *f*O2's less than QFM for the range in amphibole-plagioclase temperatures. The fO_2's and associated ferric to ferrous iron ratios in Catface rocks are lower than what is recommended for this barometer; however, results are broadly consistent with the presence of miarolitic cavities.

Temperatures estimated from amphibole-plagioclase thermometry are near the wet-granite solidus, but the Cliff Porphyry plots below that of the other rocks (Figure 51) (Naney, 1983; Piwinskii, 1968). Possible explanations for this result include sub-solidus re-equilibration of amphibole or plagioclase (Rutherford and Johnson, 1991).

The temporally related but barren Echo Lake (Mt. Washington Intrusive Suite) granodiorite intrusion, situated 120 km to the east of the Catface deposit, was sampled from outcrop for thermobarometric and geochemical analysis. The Echo Lake pluton intrudes the ~4 kilometer-thick Cretaceous Nanaimo Group sediments placing a geologic constraint on its maximum depth (Figure 3 and Figure 4) (Muller et al., 1974). Total Al in Echo Lake

hornblendes is on average two times that of Catface samples, producing an average pressure of 400 MPa indicating deeper emplacement (~12 km) (Figure 51). This depth of emplacement is likely over-estimated when considering the geological constraints of intrusion into the ~4 kilometer-thick Nanaimo Group. Consequently, the Echo Lake pluton may represent a dis-equilibrium plagioclase-hornblende assemblage. Despite the difference in calculated pressure the Echo Lake intrusion and Paleogene Catface deposit plutons are similar in terms of age and lithogeochemistry, further supporting consanguinity between Catface magmas and the Mt. Washington Intrusive Suite (Madsen, 2004; Madsen et al., 2006).

5.1.1 Alteration

Alteration associated with the Catface deposit is characterized by early potassic alteration, followed by sodic-calcic, calcic-sodic, and late potassic alteration (Figure 26). The latter three stages are associated with hydrothermal activity, whereas the initial potassic event is largely related to contact metamorphism. Further work is required to quantify P-T-x conditions of Catface-related fluids.

Early-stage potassic alteration at Catface is in mafic volcanics proximal to Paleogene intrusions (Figure 9). This biotite hornfels is commonly observed in porphyry copper deposits, and is normally overprinted by later stages of alteration (Carter, 1974; Seedorf et al., 2005; Sinclair, 2007). Potassium was introduced to the host rocks by intruding calc-alkaline magmas. The interaction of these fluids with Fe- and Mg-rich silicates in the mafic host-rocks resulted in recrystallization to fine-grained, shreddy, dark brown biotite and minor plagioclase and quartz.

Main-stage sodic-calcic and calcic-sodic alteration is associated with the bulk of Cu and Mo mineralization at Catface (Figures 27-30). Previous research on porphyry systems has lead to at least three models to explain the origin of sodic and calcic alteration in porphyry deposits

(e.g. Dilles et al., 1995; Lang et al., 1995; Barton and Johnson, 1996; Pollard, 2001). Work by Dilles et al. (1995) and Barton and Johnson (1996) suggest sodic-calcic alteration in a porphyry environment is derived from a non-magmatic evaporitic source (i.e., basinal brines). This is an unlikely possibility at the Catface deposit because there are no evaporitic rocks in the geological rock package hosting the deposit (Figure 4 and Figure 5). Pollard (2001) proposed that sodic-calcic alteration in some magmatic-hydrothermal iron oxide copper-gold (IOCG) deposits resulted from the unmixing of H_2O-CO_2-NaCl ± $CaCl_2$-KCl fluids derived from granitoid magmas. Although this option is consistent with the geological environment at Catface, the fluids forming porphyry copper deposits are typically saline and aqueous, and only rarely contain significant carbonic fluid species (i.e., CO_2 and CH_4). Fluid inclusion work would be required to test the fluid for carbonic species and determine if fluid unmixing had occurred. Finally, Lang et al. (1995) suggested that sodic-calcic alteration, which is common in many alkalic porphyry Cu-Au deposits and some calc-alkalic porphyries, is due to early magmatic fluid saturation at high temperatures. In this model, a direct relationship exists between the degree of pluton crystallization and the molar Na/K ratio of the magma and coexisting aqueous magmatic fluid (see Figure 11 in Lang et al., 1995). Successive pulses of magmatism with different Na/K ratios, crystallization paths, and fluid saturation temperatures, can lead to the development of extensive sodic-calcic alteration (i.e. Galore Creek, Mount Polley, Copper Mountain). This model accommodates the observed formation of late, fracture-controlled potassic alteration associated with Cu and Mo mineralization at Catface and elsewhere: as the magma cools and continues to crystallize, the magmatic Na/K ratio, and that in its exsolved fluid, decreases and potassic alteration minerals are stabilized (Figures 31-34) (Lang et al., 1995). In conclusion, the Lang et al. magmatic-hydrothermal model to explain

sodic-calcic alteration is most viable for Catface given the emplacement of numerous pulses of calc-alkaline magma and the transition from main-stage sodic-calcic to later potassic alteration.

5.2 Evidence for Reduced Magmas Forming the Catface Deposit

The Catface porphyry Cu-Mo deposit shows strong evidence of having formed from a reduced magma. Primary ilmenite is more abundant than magnetite in all studied samples, and ore mineralogy shows reduced characteristics. Typical oxidized porphyry copper deposits (i.e. Bingham Canyon, Chuquicamata, Highland Valley, Kemess South) precipitate hypogene sulphide minerals (such as chalcopyrite, pyrite and bornite) in equilibrium with primary hematite and anhydrite (Streck and Dilles, 1998; Rowins, 2000a; McCoy et al., 1997; Seedorf et al., 2005; Sinclair, 2007; Richards, 2009). Neither anhydrite nor hematite is identified at Catface, and the presence of abundant hypogene pyrrhotite demonstrates reducing magmatic-hydrothermal ore fluids.

In many oxidized porphyry copper deposits (i.e. Kemess South, Kemess North, Highland Valley, Pine…etc.), near-surface primary anhydrite hydrates to form secondary gypsum (Duuring et al., 2009). Volume expansions of up to 62.6% can occur during this hydration, which extensively fractures the country rock (Zanbak and Arthur, 1984). The gypsum is weathered away by meteoric waters, leaving behind an upper section of extensively fractured country rock, and the depth marking the base of this fractured ground is referred to as the "gypsum line" (Gustafson and Hunt, 1975; Olade, 1977; Duuring et al., 2009). No such feature is observed at the Catface deposit.

Primary mineralogical constraints on the redox conditions of the Catface magmas are confirmed by quantitative fO_2 estimates. Oxygen fugacities for the Catface Intrusion and Hecate Bay quartz diorite range QFM-0.5 to QFM-1, and the Cliff Porphyry intrusion is somewhat

more reducing, ranging QFM-2 to QFM-3 (Figure 52). These fO_2s are 2 to 4 log fO_2 units lower than those for typical arc magmas associated with oxidized porphyry copper deposits, which typically range from the NNO to HM oxygen buffer (i.e. magnetite-series, Figure 52**;** Burnham and Ohmoto, 1980; Burnham, 1981).

In calc-alkaline series granitoids similar in composition to those at Catface, apatite crystallizes at 850-950 ^{o}C (Green and Watson, 1982) suggesting this phase captures the high temperature portion of the liquid line of descent. Sulphur (SO_3) contents in experimental apatites increase with fO_2 from ≤0.04 weight percent SO_3 at the QFM buffer to > 1.0-2.6 weight percent SO_3 at the MH (magnetite-hematite) buffer (Peng et al., 1997). Furthermore, compositional zoning in primary apatite crystals can show an abrupt decrease in S from core to rim at the onset of anhydrite saturation in oxidized arc magmas (Peng et al., 1997; Streck and Dilles, 1998; Parat et al., 2002). Consequently, apatites from reduced magmas such as Catface should yield low SO_3 concentrations, and exhibit no compositional zonation given the absence of primary anhydrite.

The SO_3 contents in apatites from the Catface deposit are compared with those in apatites from suites of classic oxidized porphyry copper deposits studied by Imai (2002, 2004) (Figure 49 and Figure 50). The results confirm the expectation of low SO_3 concentration in apatites from Catface rocks (less than detection limit), with no SO_3 zonation. The lack of S content and zoning in Catface apatites is consistent with a reduced magma (fO_2 <QFM; Figure 49). Apatites from classic oxidized porphyry copper deposits average ~0.25 weight percent SO_3, markedly above Catface. The correlation between oxidation states estimated for Catface magmas from the apatite SO_3 concentrations (and the corresponding oxygen buffer shown in Figure 50) correspond well to those calculated from biotite-ilmenite oxybarometry in Figure 52.

This is independent confirmation of the validity of estimated magmatic oxidation states in this study. Higher levels of SO_3 in oxidized porphyry copper deposit apatites compiled by Imai (2002) are consistent with oxidized magmatic systems containing abundant SO_2. The small concentration of SO_3 in apatites from the Catface intrusives is consistent with reduced magmas having low SO_2/H_2S ratios (Ohmoto and Rye, 1979).

The recognition of an additional reduced Paleogene porphyry copper deposit of comparable age to the Cascadian North Fork deposit is favourable for regional mineral prospectivity. The petrochemical and temporal similarities between Catface and North Fork, in addition to the similar types of alteration (i.e., the predominance of the sodic-calcic alteration) and hypogene ore minerals (pyrite-chalcopyrite-pyrrhotite) support a northerly extension of the belt of reduced porphyry deposits from the Central Cascades of Washington (North Fork, Middle Fork, Quartz Creek) to Catface on Vancouver Island (e.g., Hollister, 1978; Rowins, 2000a, 2000b; Smithson, 2004).

5.3 Generation of Reduced Porphyry Copper Deposit Magma in an Arc Setting

It is accepted that arc-related magmas are more oxidized than other magmatic systems (Christie et al., 1986; Carmichael, 1991; Lange et al., 1993; Carmichael et al., 1996; Lange and Carmichael, 1996; Core, 2004; Lee et al., 2005). Redox conditions for terrestrial subduction zone magmas range from ~QFM-2.5 to +5.5 (NNO-3 to +5), whereas OIBs and MORBs range from ~QFM-2.5 to QFM (NNO-3 to-0.5). It is documented that mechanisms exist to oxidize magma during its ascent (Meuller, 1971; Candela, 1986; Ballhaus, 1992; Ballard et al., 2002; Lee et al., 2005). Fractional crystallization oxidizes magmas, as minerals species partition more ferrous than ferric iron (Meuller 1971, Ballard et al., 2002, Lee et al., 2005). Ballhaus (1992) describes how partial melts are more oxidized than crystalline mantle material, resulting in a

fundamental change in fO_2 buffering mechanism in magmas from graphite-CO_2 (CCO equilibrium) at the solidus to Fe^{3+}-Fe^{2+} equilibria after graphite has been eliminated by partial melting. Assimilation of oxidizing country rock or magma can also lead to increasing magma fO_2. Degassing of reduced volatile species (i.e. H_2, H_2S and CH_4) has been shown to increase the magmatic oxidation state (Mathez, 1984; Ballhaus et al., 1992; Ballard et al., 2002; Lee et al., 2005). Auto-oxidation reactions, whereby H_2O reacts with reduced species (i.e. Fe^{2+}) accompanied by preferential loss of H_2 from the system have been documented (Holloway, 2004; Lee et al., 2005).

Low fO_2 magmatic regimes are derived from a primary, reduced mantle source, or are reduced during ascent and emplacement. Similar processes can account for magma reduction, including assimilation, degassing, serpentinization, and depth of magma genesis (Frost, 1985; Ballhaus, 1993; Thompson et al. 1999, Takagi, 2004; Frost and Beard, 2007). The identification of reduced magmas at Catface with fO_2's of QFM -0.5 to -3 brings to light a conundrum concerning when and how the fO_2 was reduced: during formation or differentiation of granitic magmas in an arc setting.

Madsen (2004) and Madsen et al. (2006) suggest that Paleogene magmatism along coastal regions of Vancouver Island is emplaced in the forearc, from the subduction of a mid-ocean ridge and resultant formation of a slab window. The slab window setting could impart a pulse of primitive, lower-fO_2 source mantle into the overriding mantle wedge. The resulting magma would differentiate and interact with country rock, but would start at a lower fO_2 than arc magmas. However, the mineralogy and geochemistry of plutonic rocks at Catface and Echo Lake are indicative of intermediate to felsic calc-alkaline rocks formed in an arc setting, and show no geochemical evidence of derivation from a primitive mantle source (Figure 45).

The subduction of carbon and sulphide-rich sediments can lead to the production of reduced arc magmas and ilmenite-series plutonism (Frost et al., 1999; Takagi, 2004). Upon dehydration of the down-going plate, carbon from the sediments reacts with H_2O to produce CH_4 and CO_2 (Ballhaus, 1993; Takagi, 2004; Hayes and Waldbauer, 2006). Takagi explains that S isotope compositions of magnetite-series granites are heavier than those of ilmenite-series granites, and suggests that this distinction reflects different sources of S since there is only minor isotopic fractionation of sulfur at magmatic temperatures (Ohmoto and Goldhaber, 1997). Magnetite-series granitoids derive S from seawater as oxidized sulfate, whereas ilmenite-series granitoids derive S from reduced sulphide in metasedimentary rocks (Takagi, 2004). As such, it is conceivable that significant input of reducing sedimentary material to a subduction zone could reduce arc magmas at source. Takagi (2004) attributes the generation of low fO_2, ilmenite-series magmas in Japan to periodic changes in rate and amount of sediment subduction. Periodic increases in the flux of subducted carbon- and sulphide-rich sediments promoted extensive reduction of primary magmas to for ilmenite-series granitoids (Takagi, 2004). Nevertheless, $^{87}Sr/^{86}Sr$ ratios for Catface were much lower than Takagi's (<0.704 versus 0.705-0.709), indicating no sediment signature (Andrew et al., 1981; Andrew and Godwin, 1988; Isachsen, 1984).

Gastil et al. (1990) distinguished linear plutonic subprovinces of the Peninsular Ranges of southern and Baja California into an eastern magnetite-bearing and a western magnetite-free (ilmenite-bearing) granitic rocks. This geochemical zonation is interpreted to have resulted from the variable depth of magma generation along a subducting plate. In Gastil's model, ilmenite-series granitoids formed at depths where the down-going slab was dehydrating, and magnetite-series granitoids formed at either shallower or deeper levels (Gastil et al., 1990). The

depth at which a subducting slab can no longer support hydrous minerals determined by dehydration reactions (i.e. biotite + quartz = potassium feldspar + hypersthenes + water), in which hydroxyl groups are removed from the metamorphosed rock, and half the oxygen from the (OH) is retained to form new anhydrous minerals. Partial melts generated above where the slab dehydrates will be rich in H_2O, and will have high initial fH_2O and low fO_2 (Gastil et al., 1990). While Gastil's model cannot be ruled out at Catface, there is no geological evidence of linear ilmenite- and magnetite-series magmatic subprovinces.

Parental Catface magmas may have alternatively acquired a low fO_2 during their ascent through the mantle wedge and lithosphere. Interaction of a melt with reducing mantle or crust can lower its fO_2 (Ballhaus, 1993; Thompson et al. 1999, Takagi, 2004). Assimilation of graphite-bearing asthenosphere or country rock can change the systems main buffering mechanism from the Fe^{3+}-Fe^{2+} to CCO (graphite-CO-CO_2) equilibria (Ballhaus, 1993). The magma will then follow fO_2-presssure paths parallel to the graphite saturation surface as it rises, becoming reduced relative to QFM (Meuller, 1971; Ballhaus, 1993). The Mesozoic Pacific Rim Complex (Pacific Rim Terrane) lies structurally below Wrangellia and hosts carbonaceous mudstones and graphitic metasediments (Brandon, 1985 and 1989; Monger and Journeay, 1994; Groome et al., 2003). Paleogene Catface magmas may have ascended through and interacted with this reducing country rock. Metasedimentary rocks of the Pacific Rim Terrane have Sr^{87}/Sr^{86} ratios of 0.706 to 0.708, higher than those of Catface intrusions (<0.704) (Andrew et al., 1981; Andrew and Godwin, 1988; Isachsen, 1984). Strontium ratios for Catface intrusions indicate a pristine and juvenile source, suggesting little in any interaction or assimilation of the Pacific Rim Complex country rocks. Sr/Y ratios of Catface rocks show no adakite affinity, suggesting slab melting played no role (Figure 46).

Serpentinization and interaction with serpentine-bearing rocks can lower magmatic fO_2 (Frost, 1985; Frost and Beard, 2007). Fluids that evolve from serpentinites are reduced and alkaline with pH >10 (Barnes et al., 1978). The introduction of H_2O via slab dehydration to a mantle wedge composed of olivine and orthopyroxene can generate serpentine (Hyndman and Peacock, 2003). If temperatures remain less than 700 °C, and sufficient water and time is available, serpentinization of the entire forearc mantle wedge is possible (Hyndman and Peacock, 2003). Given the reducing nature of the fluids yielded by serpentines, these rocks have a high capacity to reduce magmas (Moody, 1976; Frost and Beard, 2007). Serpentine-rich shear zones are identified within the Pacific Rim Complex, and serpentine replaces enstatite and olivine in Westcoast Complex gabbro-peridotite (accounting for approximately 25-35% of whole rock modal abundance) in Lemmens Inlet, adjacent to Ritchie Bay on Meares Island (Isachsen, 1987; Brandon, 1989). Interaction of Catface magmas with either of these serpentine-bearing units may have induced reduction.

The preferred model for genesis of reduced Catface magmas is an association with inherently reduced primary magmas. The dominance of ilmenite over magnetite as a primary oxide suggests a reduced primary source, and subduction of sedimentary material shed off the Coast and Cascade Ranges during the Paleogene may have introduced reducing material into the mantle wedge. Reiners et al. (2002) report rapid Late Miocene exhumation and uplift rates of 0.5-1 km/my for the Washington Cascade Range; however more isotopic and geochemical work is required to fully evaluate this model.

Chapter 6
SUMMARY

6.1 Conclusions

The Catface porphyry Cu (Mo-Au) deposit is a reduced porphyry deposit on the basis of pluton mineralogy, ore mineral assemblage, SO_3 content in apatite, and fO_2 calculations. Magmas at Catface were emplaced at crustal depths of less than 4 km, as indicated by textural features (miarolitic cavities) and amphibole-plagioclase thermobarometry. Geochronology confirms a Paleogene age of intrusions, and demonstrates a direct temporal correlation between magmatism and mineralization. The Halo Porphyry intrusion is interpreted as the mineralizing intrusion due to its age, spatial association with the high-grade core of the system, and development of chalcopyrite- and pyrite-rich miarolitic cavities.

Magmas responsible for the generation of Catface were either derived from an inherently reduced source, or were reduced during ascent and emplacement. Strontium isotopes from Catface intrusives suggest a primitive source with no sedimentary assimilation, potentially fitting Madsen's slab-window model. However, geochemistry indicates a calc-alkaline, arc-related composition to Catface magmas. As such, it is unclear as to which specific process (or processes) contributed to the reduction of these magmas. The recognition of reduced, Paleogene, porphyry-generating magmatism on central Vancouver Island suggests that Catface and related intrusions are correlative with the more southerly Cascade arc porphyry systems.

6.2 Future Work

Analysis of more drill holes at the Catface deposit would allow for a more comprehensive assessment of the deposit geology and characteristics. Diamond drilling at Catface during the summer of 2010 focused on better-defining the Cliff Zone resource, and the

resulting drill core could yield more data. A review of the relationship between the Hecate Bay and Irishman Creek Zones and the main Catface ore system would enable a more thorough understanding of the ore system. Fluid inclusion studies of the Catface ores would enhance our understanding of the P-T-X conditions of the ore-forming event.

Calculation of intrinsic parameters (fO_2, P, T) for additional Mt. Washington Intrusive Suite plutons could determine if Catface is an exception within this suite, or part of a much larger reduced magmatic province. Further assessment of Paleogene reduced porphyry systems in the Cascade Range would broaden the scale of this evaluation, further testing the northerly extension of the Cascade reduced porphyry copper deposit belt.

What was the mechanism by which Catface magmas were reduced? The application of assimilation-fractional crystallization (AFC) equations developed by DePaolo (1981), and additional analysis of Sr and O isotopes at Catface could resolve this question.

Bibliography

Ague, J.J. and Brimhall, G.H., 1988, Magmatic arc asymmetry and distribution of anomalous plutonic belts in batholiths of California: effects of assimilation, cratonal thickness, and depth of crystallization, Geological Society of America Bulletin, Volume 100, p. 912-927

Anderson, J.L., 1996, Status of thermobarometry in granitic batholiths, Transactions of the Royal Society of Edinburgh, Earth Sciences, v. 87, p. 125-138

Anderson, J.L., Barth, A.P., Wooden, J.L., Mazdab, F., 2008, Thermometers and Thermobarometers in Granitic Systems, Reviews in Mineralogy & Geochemistry, v. 69, p. 121-142

Andersen, J.L., Lindsley, D.H., Davidson, P.M., 1993, QUILF - A Pascal program to assess equilibria among Fe-Mg-Mn-Ti oxides, pyroxenes, olivine, and quartz, Computers and Geosciences, Volume 19, p. 1333–1350

Anderson, J.L. and Smith, D.R., 1995, The effects of temperature and fO2 on the Al-in-hornblende barometer, American Mineralogist, v. 80, p, 549-559

Andrew, A., Armstrong, R.L., Runkle, D., 1991, Canadian Journal of Earth Science, Volume 28, p. 1744-1752

Ayers, J.C. and Watson, E.B., 1991, Solubility of Apatite, Monazite, Zircon, and Rutile in Supercritical Aqueous Fluids with Implications for Subduction Zone Geochemistry, Philosophical Transactions: Physical Sciences and Engineering, Vol. 335, No. 1638, p. 365-375

Ballhaus, C., 1993, Redox states of lithospheric and asthenospheric upper mantle, Contrib Mineral Petrol, Volume 114, p. 331-348

Barnes, I., O'Neil, J.R., Trescases, J.J., 1978, Present day Serpentinization in New Caledonia, Oman, and Yugoslavia. Geochimica et Cosmochimica Acta, Volume 42, p. 144-145

Barton, D.B., Johnson, D.A., 1996, Evaporitic-source model for igneous-related Fe oxide–(REE-Cu-Au-U) mineralization, Geology, Volume 24, Number 3, p. 259-263

Bingen, B. and Stein, H., 2003, Molybdenite Re–Os dating of biotite dehydration melting in the Rogaland high-temperature granulites, S Norway, Earth and Planetary Science Letters, Volume 208, Issues 3-4, p. 181-195

Blundy, J.D., and Holland, T.J.B., 1990, Calcic amphibole equilibria and a new amphibole-plagioclase geothermometer, Contributions to Mineralogy and Petrology, Volume 104, p. 208-224

Brandon, M.T., 1989, Deformational styles in a sequence of olistostromal melanges, Pacific Rim Complex, western Vancouver Island, Canada: Geological Society of America Bulletin, Volume 101, p. 1520–1542

Buddington, A.F. and Lindsley, D.H, 1964, Iron-titanium oxide minerals and synthetic equivalents, Journal of Petrology, Volume 5, Part 2, p. 310-357

Candela, P.A., 1989, Felsic magmas, volatiles, and metallogenesis, Society of Economic Geologists: Reviews in Economic Geology, Volume 4, p. 223-233

Candela, P.A., 1997, A Review of Shallow, Ore-related Granites: Textures, Volatiles, and Ore Metals, Journal of Petrology, Volume 38, Number 12, p. 1619-1633

Canil, D. and Larocque, J., 2010, The role of amphibole in the evolution of arc magmas and crust: the case from the Jurassic Bonanza arc section, Vancouver Island, Canada, Contributions to Mineralogy and Petrology, Volume 159, Number 4, p. 475-492

Canil, D., Styan, J., Laroque, J., Bonnet, E., Kyba, J., 2011, Thickness and composition of the Bonanza arc crustal section, Vancouver Island, Canada, GSA Bulletin; July/August 2010, Volume 122, Number 7/8, p. 1094–1105

Carter, N.C., 1974, Geology and geochronology of porphyry copper and molybdenum deposits in west-central British Columbia, PhD Thesis, University of British Columbia

Christie, D.M., Carmichael, I.S.E., Langmuir, C.H., 1986, Oxidation states of mid-ocean ridge basalt glasses, Earth and Planetary Sciences Letters, Volume 79, p. 397-411

Carmichael, I.S.E., 1991, The redox states of basic and silicic magmas: a reflection of their source regions?, Contributions to Mineralogy and Petrology, Volume 106, p. 129-141

Carmichael, I.S.E., Lange, R. A., and Luhr, J. F., 1996, Quaternary minettes and associated volcanic rocks of Mascota, western Mexico: a consequence of plate extension above a subduction modified mantle wedge: Contributions to Mineralogy and Petrology, Volume 124, p. 302-333

Christie, D.M., Carmichael, I.S.E., Langmuir, C.H., 1986, Oxidation states of mid0ocean ridge basalt glasses, Earth and Planetary Science Letter, Volume 79, p. 379-411

Core, D.P, 2004, Oxygen and Sulphur Fugacities of Granitoids: Implications for Ore-Forming Processes, PhD Thesis, University of Michigan

Cox, K.G., Bell, J.D., Pankhurst, R.J., 1979, The interpretation of Igneous Rocks, London, Allen & Unwin, p. 450

DePaolo, D.J., 1981, Trace element and isotopic effects of combined wallrock assimilation and fractional crystallization, Earth and Planetary Science Letters, Volume 53, p. 189-202

Dilles, J.H., Farmer, G.L., Field, C.W., 995, Sodium-calcium alteration by non-magmatic saline fluids in porphyry copper deposits: Results from Yerington, Nevada: Mineralogical Association of Canada short course series, Volume 23, p. 309-338

Drummond, M. S. and Defant, M. J., 1990, A model for trondhjemite-tonalite-dacite genesis and crustal growth via slab melting: Archean to modern comparisons. J. Geophys. Res., 95, B13, p. 21503-21521

Duuring, P., Rowins, S.M., McKinley, B., Orr, A.J., 2009, Porphyry cousins? Geological comparison of the Kemess South and Kemess North porphyry Au-Cu (Mo) deposits, Toodoggone District, British Columbia, Geological Society of America Abstracts with Programs, Volume 38, Number 5, p. 70

England, T.D.J. and Calon, T.J., 1991, The Cowichan fold and thrust system, Vancouver Island, southwestern British Columbia, Geological Society of America Bulletin 103, p. 336–362

Fairchild, L.H., Cowan, D.S., 1982, Structure, petrology, and tectonic history of the Leech River Complex northwest of Victoria, Vancouver Island, Canadian Journal of Earth Sciences, Volume 19, p. 1817-1835

Frezzotti, M.L., 1992, Magmatic immiscibility and fluid phase evolution in the Mount Genis granite (southeastern Sardinia, Italy), Geochemica et Cosmochemica Acta, Volume 56, p. 21-33

Frost, B. R., 1985, On the stability of sulfides, oxides, and native metals in serpentinite. Journal of Petrology, Volume 26, p. 31-63

Frost, C.D., Frost, B.R., Chamberlain, K.R., Edawrds, B.R., 1999, Petrogenesis of the 1·43 Ga Sherman Batholith, SE Wyoming, USA: a Reduced, Rapakivi-type Anorogenic Granite, Journal of Petrology, Volume 40, Number 12, p. 1771–1802

Frost, C.D., Beard, J.S., 2007, On Silica Activity and Serpentinization, Journal of Petrology, Volume 48, p 1351-1368

Gastil, G., Diamond, J., Knaack, C., Walawender, M., Marshall, M., Boyles, C., Chadwick, N., 1990, The problem of the magnetite/ilmenite boundary in southern and Baja Califorinia, Geological Society of America Memroir, Number 174, p. 19-32

Gill, J. B., 1981, Orogenic Andesites and Plate Tectonics, Volume 16, Minerals and Rocks, Springer-Verlag

Green, T.H. and Watson, E.B., 1979, Crystallization of Apatite in Natural Magmas Under High Pressure, Hydrous Conditions, with Particular Reference to 'Orogenic' Rock Series, Contributions to Mineralogy and Petrology, Volume 79, p. 96-105

Gustafson, L.B. and Hunt, J.P., 1975, The porphyry copper deposit at El Salvador, Chile, Economic Geology, Volume 70, Number 5, p. 857-912

Hammarstrom, J.M. and Zen, E., 1986, Aluminum in hornblende: An empirical igneous geobarometer, American Mineralogist, Volume 71, p. 1297-1313

Hammarstrom, J.M. and Zen, E., 1992, Discussion of "Calcic amphibole equilibria and a new amphibole-plagioclase geothermometer", Contributions to Mineralogy and Petrology, Volume 111, p. 264-266

Harris, A.C., Kamenetsky, V.S., White, N.C., Steele, D.A., 2004, Volatile phase separation in silicic magmas at Bajo de la Alumbrera porphyry Cu-Au deposit, NW Argentina. Resource Geology, Volume 54, Issue 3, p. 341-356

Hayes, J.M. and Waldbauer, J.R., 2006, The carbon cycle and associated redox processes through time, Philos Trans R Soc Lond B Biol Sci, Volume 361, p. 931–950

Holm, D. and Lux, D., 1998, Depth of emplacement and tilting of the Middle Proterozoic (1470 Ma) Wolf River batholith, Wisconsin: 40Ar/39Ar thermochronologic constraints, Canadian Journal of Earth Science, Volume 35, p. 1143–1151

Holland, T.J.B. and Blundy, J.D., 1994, Non-ideal interactions in calcic amphiboles and their bearing on amphibole-plagioclase thermometry, Contributions to Mineralogy and Petrology, Volume 116, p. 433-447

Holloway, J.R., 2004, Redox reactions in seafloor basalts: possible insights into silicic hydrothermal systems, Chemical Geology, Volume 210, p. 225-230

Hollister, L.S., Grissom, G.C., Peters, E.K., Stowell, H.H., Sisson, V.B., 1987, Confirmation of the empirical correlation of Al in hornblende with pressure of solidification of calc-alkaline plutons, American Mineralogist, v. 72, p. 231-239

Hyndman, R.D., Peacock, S.M., 2003, Serpentinization of the forearc mantle, Earth and Planetary Science Letters, Volume 212, p. 417-432

Imai, A., 2002, Metallogenesis of Porphyry Cu Deposits of the Western Luzon Arc, Philippines: K-Ar ages, SO3 Contents of Microphenocrystic Apatite and Significance of Intrusive Rocks, Resource Geology, Volume 52, Issue 2, p. 147–161

Imai, A., 2004, Variation of Cl and SO3 Contents of Microphenocrystic Apatite in Intermediate to Silicic Igneous Rocks of Cenozoic Japanese Island Arcs: Implications for Porphyry Cu Metallogenesis in the Western Pacific Island Arcs, Resource Geology, Volume 54, Number 3, p. 357-372

Isachsen, E.I., 1987, Geology, geochemistry, and cooling history of the Westcoast Crystalline Complex and related rocks, Meares Island and vicinity, Vancouver Island, British Columbia, Canadian Journal of Earth Sciences, Volume 24, Issue 10, p. 2047-2064

Ishihara, S., 1977, The magnetite-series and ilmenite-series granitic rocks, Mining Geology, Volume 27, p. 293-305

Ishihara, S., 1981, The granitoid series and mineralization: Economic Geology, 75th Anniversary Volume, p. 458–484

Johnson, M.E. and Rutherford, M.J., 1989, Experimental calibration of the aluminum-in-hornblende geobarometer with application to Long Valley caldera (California), Geology, Volume 17, p. 837-841

Johnston, S.T.J and Acton, S., 2003, The Eocene Southern Vancouver Island Orocline - a response to seamount accretion and the cause of fold-and-thrust belt and extensional basin formation, Tectonophysics, Volume 365, p. 165–183

Jones, D.L.; Silberling, N.J.; Hillhouse, J., 1977, Wrangellia-A displaced terrane in northwestern North America, Canadian Journal of Earth Sciences, vol. 14, issue 11, p. 2565-2577

Kamenetsky, V.S., Achterbergh, E., Ryan, C.G., Naumov, V.B., Mernagh, T.P.. Davidson, P., 2002, Extreme chemical heterogeneity of granite-derived hydrothermal fluids: An example from inclusions in a single crystal of miarolitic quartz, Geology, Volume 30, p. 459-462

Kretz, R., 1983, Symbols for rock-forming minerals, American Mineralogist, Volume 68, p. 277-279

Lalonde, A.E. and Bernard, P., 1993, Composition and color of biotite from granites: two useful properties in the characterization of plutonic suites from the Hepburn internal zone of Wopmay orogen, Northwest Territories. Canadian Mineralogist, Volume 31, p. 203-217

Lange, R.A., Carmichael, I.S.E., Renne, P. R., 1993, Potassic volcanism near Mono Basin, California: evidence for high water and oxygen fugacities inherited from subduction: Geology, Volume 21, p. 949-952

Lange, R.A., and Carmichael, I.S.E., 1996, The Aurora volcanic field, California-Nevada: oxygen fugacity constraints on the development of andesitic magma: Contributions to Mineralogy and Petrology, Volume 125, p. 167-185

Lang, J.R., Stanley, C.R., Thompson, J.F.H., Dunne, K.P.E., 1995, Na-K-Ca magmatic-hydrothermal alteration in alkalic porphyry Cu-Au deposits, British Columbia, in Magmas, Fluids and Ore Deposits, Mineralogical Association of Canada, Short Course Volume 23, p. 339-367

Le Bas, M.J., Le Maitre, R.W., Streckeisen, A., Zanettin, B., IUGS, 1986, A Chemical Classification of Volcanic Rocks Based on the Total Alkali-Silica Diagram, Journal of Petrology, Volume 27 (3), p. 745-750

Leake, B.E., Woolley, A.R., Arps, C.E.S., Birch, W.D., Gilbert, M.C., Grice, J.D., Hawthorne, F.C., Kato, A., Kisch, H.J., Krivovichev, V.G., Linthout, K., Laird, J., Mandarino, J.A., Maresch, W.V., Nickel, E.H., Rock, N.M.S., Schumacher, J.C., Smith, D.C., Stephenson, N.C.N., Ungaretti, L., Whittaker, E.J.W., and Youzhi, G., 1997, Nomenclature of amphiboles: Report of the Subcommittee on Amphiboles of the International Mineralogical Association, Commission on New Minerals and Mineral Names. American Mineralogist, Volume 82, p. 1019–1037

Leake, B.E., Woolley, A.R., Birch, W.D., Burke, A.J., Ferraris, G., Kisch, H.J., Hanan, J.D., Krivovichev, V.G., Schumacher, Stephenson, N.C.N., Whittaker, E.J.W., 2004, Nomenclature of amphiboles: Additions and revisions to the International Mineralogical Association's amphibole nomenclature, American Mineralogist, Volume 89, p. 883–887

Lee, A.C., Leeman, W.P., Canil, D., Li, Z.A, 2005, Similar V/Sc Systematics of MORB and Arc Basalts: Implications for the Oxygen Fugacities of their Mantle Source Regions, Journal of Petrology, Volume 46, Number 11, p. 2313-2336

Madsen, J., 2004, Geochemistry and geochronology of Eocene forearc magmatism on Vancouver Island: implications for Cenozoic to recent plate configurations in the Pacific basin, Masters Thesis, Simon Fraser University

Madsen, J., Thorkelson, J., Friedman, R., Marshall, D., 2006, Cenozoic to Recent plate configurations in the Pacific Basin: Ridge subduction and slab window magmatism in western North America, Geosphere, v. 2, no. 1, p. 11–34

Markey, R.J., Stein, H.J., Morgan, J. W., 1998, Highly precise Re-Os dating of molybdenite using alkaline fusion and NTIMS: Talanta, Volume 45, p. 935-946

Massey, N.W.D. and Friday, S.J., 1987, Geology of the Ministry of Energy, Mines and Petroleum Resources, Cowichan Lake Area, Vancouver Island (92C/16), B.C, Geological Fieldwork, 1986, Paper 1987-1, p. 223-229

Mathez, E.A., 1984, Influence of degassing on oxidation states of basaltic magmas, Nature, Volume 310, p. 371-375

McCoy, D., Newberry, R.J., Layer, P., DiMarchi, J.J., Bakke, A., Masterman, J.S., Minehane, D.L., 1997, Plutonic-Related Gold Deposits of Interior Alaska, Economic Geology, Monograph 9, p. 191-241

McDougall, J.J., 1976, Catface; In Porphyry Deposits of the Canadian Cordillera, Part B - Porphyry Copper and Copper-Molybdenum Deposits of the Calc-Alkalic Suite – Special Volume 15, Paper 29, p 299-310

McDougall, J.J. and Enns, S.G., 1995, Catface Copper Molybdenum Porphyry, West Central Vancouver Island, British Columbia: An Update. In Porphyry Deposits of the Northwestern

Cordillera of North America, The Canadian Institute of Mining and Metallurgy, Special Volume 46, pp. 322–326

Meuller, R.F., 1971, Oxidative capacity of magmatic components, American Journal of Science, Volume 270, p. 236-243

Meyer, W., Gale, R.E., Randall, A.W., 1976, O.K., Porphyry deposits of the Canadian Cordillera: Canadian Institute of Mining, Metallurgy, and Petroleum Special Volume 15, p. 311-316

MINFILE 092F 231, 1990, Hecate Bay, Catface, British Columbia Geological Survey, Ministry of Energy, Mines and Petroleum Resources

MINFILE 092F 120, 2008, Catface, British Columbia Geological Survey, Ministry of Energy, Mines and Petroleum Resources

Monger, J.W.H. 1997. Plate tectonics and Northern Cordilleran Geology: an unfinished revolution. Geoscience Canada, 24: 189–198

Monger, J.W.H., Journeay, J.M., 1994, Basement geology and tectonic evolution of the Vancouver region, Geological Survey of Canada, Bulletin 481, p. 3-25

Moody, J.B., 1976, Serpentinization: a review. Lithos, Volume 9, p. 125-138

Morgan, J.W., Lovering, J. F., Ford, R.J., 1968, Rhenium and non-radiogenic osmium in Australian molybdenites and other sulphide minerals by neutron activation analysis. Jour. Geol. Soc. Australia, 15, 189-194

Morton, J.W., 2008, OK Copper Property, Geological Survey of British Columbia Assessment Report #30, p. 301

Muller, J.E. and Carson, D.J., 1969, Geology and mineral deposits of Alberni map-area, British Columbia (92 F), Geological Survey of Canada, Paper 68-50

Muller, J.E., Northcote, K.E., and Carlisle, D., 1974, Geology and mineral deposits of the Nootka-Alert Bay-Cape Scott map area, Vancouver Island, British Columbia, Geological Survey of Canada, Paper 74-8, p. 77

Mustard, 1994, The Upper Cretaceous Nanaimo Group, Georgian Basin, in Geology and Geological Hazards of the Vancouver Region, Geological Survey of Canada Bulletin, Volume 481, p. 27-95

Nakada, S., 1983, Zoned Magma Chamber of the Osuzuyama Acid Rocks, Southwest Japan, J. Petrology, Volume 24, Issue 4, p. 471-494

Nakamura, N., 1974, Determination of REE, Ba, Fe, Mg, Na and K in carbonaceous and ordinary chondrites, Geochimica et Cosmochimica Acta, Volume 38, Issue 5, p. 757-775

Naney, M.T., 1983, Phase equilibria of rock-forming ferromagnesian silicates in granitic systems. American Journal of Science, Volume 283, p. 204-222

Nixon, G.T., Hammack, J.L., Hamilton, J. and Jennings, H., 1993, Preliminary geology of the Mahatta Creek area, northern Vancouver Island (92L/5); in Geological Fieldwork 1992, BC Ministry of Energy, Mines and Petroleum Resources, Paper 1993-1, p. 17–35

Nixon, G.T., Hammack, J.L., Payie, G.J., Snyder, L.D., Archibald, D.A. and Barron, D.J., 1995, Quatsino-San Josef map area, northern Vancouver Island: Geological overview (92L/12W, 1021/8,9); in Geological Fieldwork 1994, BC Ministry of Energy, Mines and Petroleum Resources, Paper 1995-1, p. 9–21

Nixon, G.T., Orr, A.J., 2007, Recent revisions to the Early Mesozoic stratigraphy of Northern Vancouver Island (NTS 102I; 092L) and metallogenic implicatinos, British Columbia, Geological Fieldwork 2006. British Columbia, Ministry of Energy, Mines and Petroleum Resources, Paper. Vol. 2007-1, p. 163-177

Ohmoto, H. and Goldhaber, M.B., 1997, Sulfur and carbon isotopes, in Barnes, ,H. L., editor, Geochemistry of hydrothermal ore deposits: New York, John Wiley & Sons, p. 517–611

Olade, M.A., 1977, Major element halos in granitic wall rocks of porphyry copper deposits, Guichon Creek batholith, British Columbia, Journal of Geochemical Exploration, Volume 7, p. 59-71

Oyarzun, R., Marquez, A., Lillo, J., Lopez, I., Rivera, S., 2001, Giant versus small porphyry copper deposits of Cenozoic age in northern Chile: adakitic versus normal calc-alkaline magmatism, Mineralium Deposita, Volume 36, p. 794-798

Panteleyev, A., 1981, Berg Porphyry Copper-Molybdenum Deposit: Geological Setting, Mineralization, Zoning, and Pyrite Geochemistry, Ministry of Energy, Mines and Petroleum Resources, Bulletin 66

Panteleyev, A., 1995, Porphyry Cu+/-Mo+/-Au, in Selected British Columbia Mineral Deposit Profiles, Volume 1 - Metallics and Coal, Lefebure, D.V. and Ray, G.E., Editors, British Columbia Ministry of Energy of Employment and Investment, Open File 1995-20, p. 87-92

Parat, F., Dungan, M.A., Streck, M.J., 2002, Anhydrite, pyrrhotite, and sulphur-rich apatite: tracing the sulphur evolution of an Oligocene andesite (Eagle Mountain, CO, USA), Lithos, Volume 64, p. 63-75

Pearce, T.H. and Kolisnik, A.M., 1989, Observations of plagioclase zoning using interference imaging, Earth-Science Reviews, Volume 29, p. 9-26

Peng, G., Luhn, J.F., McGee, J.J, 1997, Factors controlling sulphur concentrations in apatite, American Mineralogist, Volume 82, p. 1210-1224

Piwinskii, A.J., 1968, Experimental studies of igneous rock series: Central Sierra Nevada batholiths, California, Journal of Geology, Volume 76, p. 548-570

Poli, S., and Schmidt, M.W., 1992, A comment on "Calcic amphibole equilibria and a new amphibole-plagioclase geothermometer", Contributions to Mineralogy and Petrology, Volume 111, p. 273-278

Pollard, P.J., 2001, Sodic(-calcic) alteration in Fe-oxide-Cu-Au districts: an origin via unmixing of magmatic H2O-CO2-NaCl ± CaCl2-KCl fluids, Mineralium Deposita, Volume 36, p. 93-100

Raith, J.G. and Stein, H.J., 2000, Re–Os dating and sulfur isotope composition of molybdenite from tungsten deposits in western Namaqualand, South Africa: implications for ore genesis and the timing of metamorphism, Mineralium Deposita, Volume 35, Number 8, 741-753

Richards, J.P., 1990, Petrology and geochemistry of alkalic intrusives at the Porgera gold deposit, Papua New Guinea, Journal of Geochemical Exploration, Volume 35, p. 141-199

Reiners, P.W., Ehlers, T.A., Garver, J.I., Mitchell, S.G., Motgomery, D.R., Vance, J.A., Nicolesku, S., 2002, Late Miocene exhumation and uplift of the Washington Cascade Range.Geology, Volume 30, Number 9, p. 767-770

Roedder, E., 1992, Fluid inclusion evidence for immiscibility in magmatic differentiation, Geochemica et Cosmochimica Acta, Volume 56, p. 5-20

Rock, N.M.S., 1987, The need for standardization of normalized multi-element diagrams in geochemistry: a comment, Geochemical Journal, Volume 21, p. 75-84

Rowins, S.M., 2000a, Reduced porphyry copper-gold deposits: a new variation on an old theme: Geology, v. 28, p. 491-494

Rowins, S.M., 2000b, A model for the genesis of “reduced” porphyry copper-gold deposits, Geological Association of Canada, The Gangue, Number 67, p. 1-7

Rutherford, M.J. and Johnson, M.E., 1992, A comment on "Calcic amphibole equilibria and a new amphibole-plagioclase geothermometer", Contributions to Mineralogy and Petrology, Volume 111, p. 266-268

Seedorf, E., Dilles, J.H., Proffett, J.M., Einaudi, M.T., Zurcher, L., Stavast, W.J.A., Johnson, D.A., Barton, M.D., 2005, Porphyry deposits: Characteristics and origin of hypogene features: 100th Anniversary Volume of Economic Geology, p. 251-298

Schmidt, M.W., 1992, Amphibole composition in tonalite as a function of pressure: An experimental calibration of the Al-in-hornblende barometer, Contributions to Mineralogy and Petrology, Volume 110, p. 304-310

Schmidt, M.W., and Thompson, A.B., 1996, Epidote in calcalkaline magmas: An experimental study of stability, phase relationships and the role of epidote in magmatic evolution: American Mineralogist, Volume 81, p. 462–474

Scoates, J.S. and Friedman, R.M., 2008, Precise age of the platiniferous Merensky Reef, Bushveld Complex, South Africa, by the U-Pb zircon chemical abrasion ID-TIMS technique, Economic Geology, Volume 103, p. 465-471

Selby, D. and Creaser, R.A., 2001, Late and mid-Cretaceous mineralization in the northern Canadian Cordillera: Constraints from Re-Os molybdenite dates, Economic Geology, Volume. 96; no. 6, p. 1461-1467

Sillitoe, R.H., 1973, The Tops and Bottoms of Porphyry Deposits, Resource Geology, Volume 68, p. 799-815

Simpson, R.G. and Chapman, J., 2009, Mineral Resource Estimate Catface Copper, GeoSim Services Inc.

Sinclair, W.D., 2007, Porphyry deposits; in Mineral Deposits of Canada, A Synthesis of Major Deposit Types, District Metallogeny, the Evolution of Geological Provinces, and Exploration Methods, Geological Association of Canada, Mineral Deposits Division, Special Publication No. 5, p. 223-244

Smithson, D.M., 2004, Late Eocene tectono-magmatic evolution and genesis of reduced porphyry copper-gold mineralization at the North Fork deposit, Central Cascades Mountain Range, Washington, U.S.A., Master's Thesis, University of British Columbia

Stein, H.J., Markeya, R., Hannah, J.L., Zimmerman, A., Selby, D., Creaser, R.A., 2007, Standardizing Re–Os geochronology: A new molybdenite Reference Material (Henderson, USA) and the stoichiometry of Os salts, Chemical Geology, Volume 244, Issues 1-2, Pages 74-87

Takagi, T., Origin of magnetite- and ilmenite-series granitic rocks in the Japan Arc, American Journal of Science, Volume 34, p. 169-202

Thomas, W.M., and Ernst, W.G., 1990, The aluminum content of hornblende in calc-alkaline granitic rocks: A mineralogic barometer calibrated experimentally to 12 kbars, In R.J. Spencer and I-M. Chou, Eds., Fluid-mineral interactions: A tribute to H. P. Eugster, Geochemical Society Special Publication, Volume 2, p. 59-63

Thompson, R.N., 1982, Magmatism of the British Tertiary volcanic province, Journal of Geology, Volume 18, p, 49-107

Thompson, J.F.H., Sillitoe, R.H., Baker, T., Lang, J.R., and Mortenson, J.K., 1999, Intrusion-related gold deposits associated with tungsten-tin provinces: Mineralium Deposita, Volume 34, p. 323-334

Vance, J.A., 1962, Zoning in Igneous Plagioclase: Normal and Oscillatory Zoning, American Journal of Science, Volume 260, p. 746-760

Vance, J.A., 1965, Zoning in Igneous Plagioclase: Patchy Zoning, The Journal of Geology, Volume 73, No. 4, p. 636-651

Watson, E.B., 1979, Apatite saturation in basic to intermediate magmas. Geophys Res Lett, Volume 6, Number 12, p. 937-940

Watson, E.B. and Capobianco, C.J., 1981, Phosphorus and the rare earth elements in felsic magmas: an assessment of the role of apatite, Geochemica et Cosmochemica Acta, Volume 45, p. 2349-2358

Wones, D.R., 1989, Significance of the assemblage titanite + magnetite + quartz in granitic rocks, American Mineralogist, Volume 74, p. 744-749

Wones, D.R. and Eugster, H.P., 1964, Stability of biotite: experiment, theory, and application, The American Mineralogist, Volume 50, p. 1228-1271

Zanbak, C., Arthur, R.C., 1984, Rock Mechanics Aspects Of Volume Changes In Calcium Sulfate Bearing Rocks Due To Geochemical Phase Transitions, The 25th U.S. Symposium on Rock Mechanics (USRMS), American Institute of Mining, Metallurgical, and Petroleum Engineers Inc.

Zen, E., 1986, Aluminum Enrichment in Silicate Melts by Fractional Crystallization: Some Mineralogic and Petrographic Constraints, Journal of Petrology, Volume 27 (5), p. 1095-1117